

## Response to Editor (TC-2019-1)

Thank you for the handling of our manuscript. Below are private comments to you. We also include a response to A. Winstral. In addition, we include a 'track changes' and also a 'clean' version of our revision. We believe that we have handled all necessary revisions and that we have clearly demonstrated the improvement of our method. We hope to hear from you soon.

Comments to the Author:

Dear authors

Thanks for submitting the revised version of your manuscript. You have addressed all points in your replies raised by the reviewers. However, I believe you have failed to incorporate the arguments you bring forward to actually support your conclusions. I find it not sufficient to mention in the reply that you could have done this or that, or you would have even tried it, but it would not have changed the results.

In our first revision, we made numerous additions. Also, we tested several ways of building the regression model, and we found the results to be the same. So, perhaps there was a miscommunication. It was not that we could have tried a new approach. We actually did a new approach, but it did not make a difference. We state this explicitly in the revised paper.

I expect you to take the arguments by reviewer #2 more seriously and make the appropriate changes to the manuscript. I think it is not too difficult and you are actually close to a valuable contribution that includes a comprehensive, objective analysis with statistically supportable claims. If you are prepared to revise the manuscript accordingly I am happy to reconsider it for publication.

In the latest version you will find a side-by-side comparison of our model to three other widely used models. We apply all four models to three datasets:

1. The western North America snow pillow dataset (close to 2 million data points).
2. The complete western North America snow course / aerial marker data set (100,000+ data points).
3. The northeast USA collection of data sets (100,000+ measurements).

Our model has lower bias and RMSE in all cases, except for two very small northeast USA datasets (totaling about 1500 data points). We believe that this is a very convincing case that our approach is an improvement over existing methods.

Jürg Schweizer

## Response to A. Winstral Review of TC-2019-1

Thank you for the recent review of our manuscript. We appreciate the investment of time that you have made in improving our analysis. Below, we provide point-by-point responses to the May 2019 review of our second draft. Reviewer comments are in black. Our responses are indented and in blue. All references to table/figure/line numbers refer to the ‘clean’ version of revision #2. One notable change is that we have revised our regression analysis to use ‘winter precipitation’ and ‘winter temperature’ rather than mean annual precipitation and mean February temperature. This reduced our RMSE values.

Though I firmly stated that the authors had not presented convincing evidence to support their claims, they chose to not implement and include any of my major suggestions for revisions to make the work more convincing. Instead they have largely chosen to reason away my suggestions. I don’t wish to repeat my review nor get into a lengthy debate on the relevancy of my comments. Instead I’ll just go with what the presented data say to me. The authors have derived a method for estimating snow densities that includes climatological variables, which provide a means of capturing spatial heterogeneity. They developed and tested this method using data from snow pillows and snow courses. By the authors own admissions (lines 46-50) these data all come from “relatively simple topography”. Generally these are all located in flat, wind-sheltered locations. On the other hand the Sturm model, a well-regarded and oft-cited research piece, is based on similar data as well as data collected on manual traverses representing a range of topographic positions and snow deposition zones. The presented comparison with the Sturm model is conducted only at SNOTEL sites (i.e. flat, wind-sheltered). These same exact sites were used in both the calibration of the new model and for comparisons with the Sturm model. Results show that overall the new model performs better. However, if one were to eliminate taiga sites, which were not well represented in the Sturm data, the overall results are very similar (see table below).

We do not believe this to be an entirely correct statement. In Table 4 of the paper, we provide comparative results for ‘all data’ and also for the data broken out by snow class. In every row of this table, the results show that our model has a smaller bias and RMSE than Sturm’s model.

Note also that, in the revision, we now compare our model to Sturm at all of the northeastern USA data (nearly all snow course, not snow pillow). Our model has lower bias and RMSE than Sturm for all of these data sources. We also now compare our model to Sturm at all (100,000+ measurements) NRCS snow course sites in western North America. These sites are independent from the model training data and use a different method (snow coring instead of snow pillow). Our model has lower bias and RMSE than Sturm for this independent data set.

Though the authors acknowledged that I raised an important point regarding their splitting of data in which all stations were included in both training and validation sets they state only that a station-dependent splitting method produced “extremely close” results to the original without actually presenting those results.

Yes, this was a good point, and we tested it out after your first review. The results were the same. It felt redundant to us to present numeric data (identical) for both of these cases in the revised manuscript. In our new revision, we now explicitly state (beginning of section 2.2) that we did our model building / validation both ways, and that the results were the same.

Given how similar the provided results are for non-taiga performance of the two models, the only conclusion I can draw from the presented data is that at sheltered, taiga sites the new model performs better. At other sheltered locations, the new model might be better or worse.

Table 4 shows that the current model has smaller biases and RMSEs for all snow classes, not just Taiga. For the non-taiga sites, our RMSE is usually ~20% smaller than Sturm. And, our biases are much smaller than the biases of Sturm.

Additionally, the new application of our model, side-by-side with Sturm for two independent data sets shows that our model consistently has lower RMSE and bias.

The new method is trained in the same conditions and sites as the validation was conducted whereas the Sturm method is based on a greater diversity of data from independent sites. Given this unbalanced methodology and the closeness of the results, I find the comparative assessments of model performance at sheltered, non-taiga sites to be uncertain.

See our above remarks. We believe the modifications we have made alleviate this point, which is similar to several above points.

Results averaged over all snow classes except taiga (taken from snow class percentages provided in Section 3.1 and results in Table 4)

Sturm et al. Multi-variable two-equation

R2 0.97 0.97

rmse (mm) 72.1 67.8

bias (mm) 1.76 -2.26

Regarding the usefulness and accuracy of the new methodology at sites other than typical SNOTEL stations for estimating densities nothing has been shown (e.g. the manuscript-referenced crowd-sourced and Lidar data that are gathered in a variety of topographic settings). No data is presented for anything other than flat, wind-sheltered locations therefore conclusions on model performance in any other conditions are not possible.

We showed in our original paper our model applied a great variety of data (snow course, mostly) from the northeastern USA. The northeastern US snow courses (NY and ME Snow Survey sites) are not typical SNOTEL stations and include both forested and open sites in both flat and topographically complex settings. At Hubbard Brook, the snow courses are forested areas about ¼ hectare in size. Thompson Farm in Durham, NH, USA includes a forested site and open site. Sleeper's River in Vermont also includes forested and open field sites across a range of topographic classes.

In addition to this, we have now included all western North America snow course data (100,000+ measurements). These are completely different data from the SNOTEL snow pillow data.

So, we have great confidence in the ability of our model to perform in a wide variety of environments.

Yes, the maps look pretty and capture greater heterogeneity but how accurate are they? A theoretical argument can easily be made that the Sturm method – based on a more diverse set of data – would actually be better.

I would be remiss if I didn't further comment on one of my major suggested revisions that wasn't followed up on: direct comparisons to the Jonas et al. method. Rather than including direct comparisons to the Jonas method (based on over 11,000 observations and cited over 140 times) as suggested, the authors have chosen to make comparisons to the simple Pistocchi method that is solely a function of day-of-year (based on 206 observations and cited 5 times). According to the authors this was necessary because the Jonas method is dependent on month of year, elevation, and a geographic "offset" term. Certainly the former two variables are available to the authors. The presence of the offset term however leads the authors to conclude that the Jonas model cannot be applied to other regions while implying that Jonas et al. did not "construct" their model for such applications. Yet in referring to the importance of the offset term Jonas et al. state, "However, the minor importance of regional effects suggests that the model may also be applicable in other regions with similar snow climatologic conditions." In fact, if one averaged the regional offset term over all the data records in the Jonas application it comes to a mere 3 kg/m<sup>3</sup>. One could in fact, easily optimize the Jonas "offset" term to the data presented here in the calibration set. (It is my personal belief that any comprehensive analysis should include this). Yet even a straight-out-of-the-box Jonas application using the average offset or none at all would be insightful. If, in fact, the presented model performs better than the Jonas model at the tested sites then this would show that there are indeed regional constraints present in the Jonas model that must be accounted for. On its own, these insights on regionality for one of the most widely cited density parameterizations would be relevant. Of course, this would also lend greater credence to the model presented in this work as well. This entire analysis including optimization could probably be done in less than a day. Without optimizing the offset term, this is about 5 lines of code that could even be handled in a spreadsheet. I truly don't understand why this revision wasn't undertaken.

We now present results for the Jonas model applied to (1) the SNOTEL data, (2) the northeastern USA data, and (3) all NRCS snow course data. Please see sections 3.3, 3.4, and 3.5. The present model has lower bias and RMSE than Jonas for (1), for four out of 6 datasets in (2) and for (3). The two datasets for (2) where Jonas has lower RMSE and bias are the smallest datasets by 1-2 orders of magnitude.

Unfortunately, save for the inclusion of the Pistocchi model comparison, the authors have presented no new data. It is my opinion that the presented work still does not compellingly support the stated conclusions, particularly this one (lines 432-33), "The results presented in this

study show that the regression equation described by equations (5, 7-8) is an improvement (lower bias and RMSE) over other widely used bulk density equations.”

The present model is now compared against three others (Sturm, Jonas, and Pistocchi) for many different datasets from different regions and different methodologies. The results objectively show that the present model has lower values for bias and RMSE.

The authors have the data available to make this a much more extensive and scientifically supportable work (e.g. significance tests would be a nice touch).

We are not 100% sure which specific tests you are asking for. We have provided metrics such as RMSE, R2, and bias. If you are referring to significance tests related to the linear regression analysis, the p values for each variable were 0, and we have now stated that in the manuscript. We also (this was discussed in the original paper and the discussion remains) indicate the use of adjusted R2 values in the construction of the model. This is important since one can always add more predictors and improve the R2. The adjusted R2 ensures that we are only adding in more predictors that produce enough of an improvement in R2 to justify the inclusion.

I think I have provided several constructive ideas on how to go about this. At the very least, if they weren't to follow up on these suggestions they need to objectively evaluate their results and in my opinion, substantially scale back their claims.

In summary, our model is compared to three others for three different datasets, representing a wide variety of methodologies (for measuring SWE) and physical locations.

1. Western North America snow pillow data
2. Western North America snow course data
3. Northeast USA data (mostly snow course, some snow pillow)

For all three of these datasets, our model had the smallest errors and biases.

# 1 **Converting Snow Depth to Snow Water Equivalent Using** 2 **Climatological Variables**

3  
4 David F. Hill<sup>1</sup>, Elizabeth A. Burakowski<sup>2</sup>, Ryan L. Crumley<sup>3</sup>, Julia Keon<sup>4</sup>, J. Michelle Hu<sup>5</sup>,  
5 Anthony A. Arendt<sup>6</sup>, Katreen Wikstrom Jones<sup>7</sup>, Gabriel J. Wolken<sup>8</sup>

6  
7 <sup>1</sup>Civil and Construction Engineering, Oregon State University, OR, USA

8 <sup>2</sup>Institute for the Study of Earth, Oceans, and Space, University of New Hampshire, NH, USA

9 <sup>3</sup>Water Resources Graduate Program, Oregon State University, OR, USA

10 <sup>4</sup>Civil and Construction Engineering, Oregon State University, OR, USA

11 <sup>5</sup>Civil and Environmental Engineering, University of Washington

12 <sup>6</sup>Applied Physics Laboratory, University of Washington

13 <sup>7</sup>Alaska Division of Geological & Geophysical Surveys, Fairbanks, AK, USA

14 <sup>8</sup>Alaska Division of Geological & Geophysical Surveys, Fairbanks, AK, USA; International Arctic Research Center,  
15 University of Alaska Fairbanks, Fairbanks, AK, USA

16 *Correspondence to:* David F. Hill (david.hill@oregonstate.edu)

17  
18  
19 **Abstract.** We present a simple method that allows snow depth measurements to be converted to snow water  
20 equivalent (SWE) estimates. These estimates are useful to individuals interested in water resources, ecological  
21 function, and avalanche forecasting. They can also be assimilated into models to help improve predictions of total  
22 water volumes over large regions. The conversion of depth to SWE is particularly valuable since snow depth  
23 measurements are far more numerous than costlier and more complex SWE measurements. Our model regresses  
24 SWE against snow depth ( $h$ ), day of water year ( $DOY$ ) and climatological (30-year normal) values for winter  
25 (December, January, February) precipitation ( $PPTWT$ ) and the difference ( $TD$ ) between mean temperature of the  
26 warmest month and mean temperature of the coldest month, producing a power-law relationship. Relying on  
27 climatological normals rather than weather data for a given year allows our model to be applied at measurement  
28 sites lacking a weather station. Separate equations are obtained for the accumulation and the ablation phases of the  
29 snowpack. The model is validated against a large database of snow pillow measurements and yields a bias in SWE  
30 of less than 2 mm and a root-mean-squared-error (RMSE) in SWE of less than 60 mm. The model is additionally  
31 validated against two completely independent sets of data; one from western North America, and one from the  
32 northeast United States. Finally, the results are compared with three other models for bulk density that have varying  
33 degrees of complexity and that were built in multiple geographic regions. The results show that the model described  
34 in this paper has the best performance for the validation data sets.

35 **1 Introduction**

36 In many parts of the world, snow plays a leading-order role in the hydrological cycle (USACE, 1956; Mote et al.,  
37 2018). Accurate information about the spatial and temporal distribution of snow water equivalent (SWE) is useful to  
38 many stakeholders (water resource planners, avalanche forecasters, aquatic ecologists, etc.), but can be time  
39 consuming and expensive to obtain.

40  
41 Snow pillows (Beaumont, 1965) are a well-established tool for measuring SWE at fixed locations. Figure 1 provides  
42 a conceptual sketch of the variation of SWE with time over a typical water year. A comparatively long accumulation  
43 phase is followed by a short ablation phase. While simple in operation, snow pillows are relatively large in size and  
44 they need to be installed prior to the onset of the season's snowfall. This limits their ability to be rapidly or  
45 opportunistically deployed. Additionally, snow pillow installations tend to require vehicular access, limiting their  
46 locations to relatively simple topography. Finally, snow pillow sites are not representative of the lowest or highest  
47 elevation bands within mountainous regions (Molotch and Bales, 2005). In the western United States (USA), the  
48 Natural Resources Conservation Service (NRCS) operates a large network of Snow Telemetry (SNOTEL) sites,  
49 featuring snow pillows. The NRCS also operates the smaller Soil Climate Analysis Network (SCAN) which  
50 provides the only, and very limited, snow pillow SWE measurements in the eastern USA.

51  
52 SWE can also be measured manually, using a snow coring device that measures the weight of a known volume of  
53 snow to determine snow density (Church, 1933). These measurements are often one-off measurements, or in the  
54 case of 'snow courses' they are repeated weekly or monthly as a transect of measurements at a given location. The  
55 simplicity and portability of coring devices expand the range over which measurements can be collected, but it can  
56 be challenging to apply these methods to deep snowpacks due to the limited length of standard coring devices. Note  
57 that there are numerous different styles of coring devices, including the Adirondack sampler and the Mt. Rose /  
58 Federal sampler (Church and Marr, 1937). The NRCS operates a large network of snow course sites (USDA, 2011)  
59 in the western United States.

60  
61 There are a number of issues that affect the accuracy of both snow pillow and snow coring measurements. With  
62 coring measurements, if the coring device is not carefully extracted, a portion of the core may fall out of the device.  
63 Or, snow may become compressed in the coring device during insertion. These effects have led to varying  
64 conclusions, with some studies (e.g., Sturm et al., 2010) showing a low SWE bias and other studies (e.g., Goodison,  
65 1978) showing a high SWE bias. As noted by Johnson et al. (2015) a good rule of thumb is that coring devices are  
66 accurate to around  $\pm 10\%$ . Also, studies comparing different styles of snow samplers report statistically different  
67 results, suggesting that SWE measurements are sensitive to the design of the specific coring device, such as the  
68 presence of holes or slots, the device material, etc. (Beaumont and Work, 1963; Dixon and Boon, 2012). With snow  
69 pillows, some studies (e.g., Goodison et al., 1981) note that ice bridging can lead to low biases in measured SWE,  
70 with the snow surrounding the pillow partly supporting the snow over the pillow. Other studies (Johnson and Marks,  
71 2004; Dressler et al., 2006; Johnson et al., 2015) note a more complex situation with SWE under-reported at times,

72 but over-reported at other times. Note that when snow pillow data are evaluated, they are most commonly compared  
73 to coring measurements at the same location.

74  
75 All methods of measuring SWE are challenged by the fact that SWE is a depth-integrated property of a snowpack.  
76 This is why the snowpack must be weighed, in the case of a snow pillow, or a core must be extracted from the  
77 surface to the ground. This measurement complexity makes it difficult to obtain SWE information with the spatial  
78 and temporal resolution desired for watershed-scale studies. Other snowpack properties, such as the depth  $h$ , are  
79 much easier to measure. For example, using a graduated device such as a meterstick or an avalanche probe to  
80 measure the depth takes only seconds. Automating depth measurements at a fixed location can easily be done using  
81 low-cost ultrasonic devices (Goodison et al., 1984; Ryan et al., 2008). High-spatial-resolution measurements of  
82 snowpack depth are commonly made with Light Detection and Ranging (LIDAR). One example of this is the  
83 Airborne Snow Observatory program (ASO; Painter et al., 2016). The comparatively high expense of airborne  
84 LIDAR surveys typical limits measurements geographically (to a few basins) and temporally (weekly to monthly  
85 interval).

86  
87 Given the relative ease in obtaining depth measurements, it is common to use  $h$  as a proxy for SWE. Figure 1 shows  
88 a conceptual sketch of the variation of SWE with  $h$  over a typical water year. Noting the arrows on the curve, we see  
89 that SWE is multi-valued for each  $h$ . This is due to the fact that the snowpack increases in density throughout the  
90 water year, producing a hysteresis loop in the curve. A large body of literature exists on the topic of how to convert  
91  $h$  to SWE. It is beyond the scope of this paper to provide a full review of these ‘bulk density equations,’ where the  
92 density is given by  $\rho_b = SWE/h$ . Instead, we refer readers to the useful comparative review by Avanzi et al. (2015).  
93 Here, we prefer to discuss a limited number of previous studies that illustrate the spectrum of methodologies and  
94 complexities that can be used to determine  $\rho_b$  or SWE.

95  
96 Many studies express  $\rho_b$  as an increasing function (often linear) of  $h$ . In some cases (e.g., Lundberg et al., 2006) a  
97 second equation is added where  $\rho_b$  attains a constant value when a threshold  $h$  is exceeded. A single linear equation  
98 captures the process of densification of the snowpack during the accumulation phase, but performs poorly during the  
99 ablation phase, where depths are decreasing but densities continue to increase or approach a constant value.

100 Other approaches choose to parameterize  $\rho_b$  in terms of time, rather than  $h$ . Pistocchi (2016) provides a single  
101 equation while Mizukami and Perica (2008) provide two sets of equations, one set each for early and late season.  
102 Each set contains four equations, each of which is applicable to a particular ‘cluster’ of stations. This clustering was  
103 driven by observed densification characteristics and the resulting clusters are relatively spatially discontinuous.  
104 Jonas et al. (2009) take the idea of region- (or cluster-) specific equations and extend it further to provide  
105 coefficients that depend on time and elevation as well. They use a simple linear equation for  $\rho_b$  in terms of  $h$  and the  
106 slope and intercept of the equation are given as monthly values, with three elevation bins for each month (36 pairs of  
107 coefficients). There is an additional contribution to the intercept (or ‘offset’) which is region-specific (one of 7  
108 regions).



109

110 These classifications, whether based on region, elevation, or season, are valuable since they acknowledge that all  
111 snow is not equal. McKay and Findlay (1971) discuss the controls that climate and vegetation exert on snow density,  
112 and Sturm et al. (2010) address this directly by developing a snow density equation where the coefficients depend  
113 upon the ‘snow class’ (5 classes). Sturm et al. (1995) explain the decision tree, based on temperature, precipitation,  
114 and wind speed, that leads to the classification. The temperature metric is the ‘cooling degree month’ calculated  
115 during winter months only. Similarly, only precipitation falling during winter months was used in the classification.  
116 Finally, given the challenges in obtaining high quality, high-spatial-resolution wind information, vegetation  
117 classification was used as a proxy. Using climatological values (rather than values for a given year), Sturm et al.  
118 (1995) were able to develop a global map of snow classification.

119

120 There are many other formulations for snow density that increase in complexity and data requirements. Meloyund  
121 et al. (2007) express  $\rho_b$  in terms of sub-daily measurements of relative humidity, wind characteristics, air pressure,  
122 and rainfall, as well as  $h$  and estimates of solar exposure (‘sun hours’). McCreight and Small (2014) use daily snow  
123 depth measurements to develop their regression equation. They demonstrate improved performance over both Sturm  
124 et al. (2010) and Jonas et al. (2009). However, a key difference between the McCreight and Small (2014) model and  
125 the others listed above is that the former cannot be applied to a single snow depth measurement. Instead, it requires a  
126 continuous time series of depth measurements at a fixed location. Further increases in complexity are found in  
127 energy-balance snowpack models (SnowModel, Liston and Elder, 2006; VIC, Liang et al., 1994, DHSVM,  
128 Wigmosta et al., 1994, others), many of which use multi-layer models to capture the vertical structure of the  
129 snowpack. While the particular details vary, these models generally require high temporal-resolution time series of  
130 many meteorological variables as input.

131

132 Despite the development of multi-layer energy-balance snow models, there is still a demonstrated need for bulk  
133 density formulations and for vertically integrated data products like SWE. Pagano et al. (2009) review the  
134 advantages and disadvantages of energy-balance models and statistical models and describe how the NRCS uses  
135 SWE (from SNOTEL stations) and accumulated precipitation in their statistical models to make daily water supply  
136 forecasts. If SWE information is desired at a location that does not have a SNOTEL station, and is not part of a  
137 modeling effort, then bulk density equations and depth measurements are an excellent choice.

138

139 The present paper seeks to generalize the ideas of Mizukami and Perica (2008), Jonas et al. (2009), and Sturm et al.,  
140 (2010). Specifically, our goal is to regress physical and environmental variables directly into the equations. In this  
141 way, environmental variability is handled in a continuous fashion rather than in a discrete way (model coefficients  
142 based on classes). The main motivation for this comes from evidence (e.g., Fig. 3 of Alford, 1967) that density can  
143 vary significantly over short distances on a given day. Bulk density equations that rely solely on time completely  
144 miss this variability and equations that have coarse (model coefficients varying over either vertical bins or horizontal  
145 grids) spatial resolution may not fully capture it either.

146

147 Our approach is most similar to Mizukami and Perica (2008), Jonas et al. (2009), and Sturm et al., (2010) in that a  
148 minimum of information is needed for the calculations; we intentionally avoid approaches like Meloysund et al.  
149 (2007) and McCreight and Small (2014). This is because our interests are in converting  $h$  measurements to SWE  
150 estimates in areas lacking weather instrumentation. The following sections introduce the numerous data sets that  
151 were used in this study, outline the regression model adopted, and assess the performance of the model.

## 152 **2 Methods**

153

### 154 **2.1 Data**

155

#### 156 **2.1.1 Snow Depth and Snow Water Equivalent**

157 In this section, we list sources of 1970-present snow data utilized for this study (Table 1). With regards to snow  
158 coring devices, we refer to them using the terminology preferred in the references describing the datasets.

159

##### 160 **2.1.1.1 USA NRCS Snow Telemetry and Soil Climate Analysis Networks**

161 SNOTEL (Serreze et al., 1999; Dressler et al., 2006) and SCAN (Schaefer et al. 2007) stations in the contiguous  
162 United States (CONUS) and Alaska typically record sub-daily observations of  $h$ , SWE, and a variety of weather  
163 variables (Figure 2a). The periods of record are variable, but the vast majority of stations have a period of record in  
164 excess of 30 years. For this study, data from all SNOTEL sites in CONUS and Alaska and northeast USA SCAN  
165 sites (Figure 2b) were obtained with the exception of sites whose period of record data were unavailable online.  
166 Only stations with both SWE and  $h$  data were retained.

167

##### 168 **2.1.1.2 Canada (British Columbia) Snow Survey Data**

169 Goodison et al. (1987) note that Canada has no national digital archive of snow observations from the many  
170 independent agencies that collect snow data and that snow data are instead managed provincially. The quantity and  
171 availability of the data vary considerably among the provinces. The Water Management Branch of the British  
172 Columbia (BC) Ministry of the Environment manages a comparatively dense network of Automated Snow Weather  
173 Stations (ASWS) that measure SWE,  $h$ , accumulated precipitation, and other weather variables (Figure 2a). For this  
174 study, data from all British Columbia ASWS sites were initially obtained. As with the NRCS stations, only ASWS  
175 stations with both SWE and  $h$  data were retained.

176

##### 177 **2.1.1.3 USA NRCS Snow Course / Aerial Marker Data**

178 The snow survey program (USDA, 2008) dates to the 1930s and includes a large number of snow course and aerial  
179 marker sites (Figure 2c) in western North America. While the measurement frequency is variable, it is most  
180 commonly monthly. To generate a dataset for this study, data were extracted using the National Water and Climate

181 Center Report Generator 2.0. This allows filtering by time period, elevation band, and other elements. All sites with  
182 data between 1980-2018 were included (Figure 2c).

183

#### 184 **2.1.1.4 Northeast USA Data**

185 In addition to the data from the SCAN sites, snow data for this project from the northeast US come from two  
186 networks and three research sites (Figure 2b). The Maine Cooperative Snow Survey (MCSS, 2018) network  
187 includes  $h$  and SWE data collected by the Maine Geological Survey, the United States Geological Survey, and  
188 numerous private contributors and contractors. MCSS snow data are collected using the Standard Federal or  
189 Adirondack snow sampling tubes typically on a weekly to bi-weekly schedule throughout the winter and spring,  
190 1951-present. The New York Snow Survey network data were obtained from the National Oceanic and Atmospheric  
191 Administration's Northeast Regional Climate Center at Cornell University (NYSS, 2018). Similar to the MCSS,  
192 NYSS data are collected using Standard Federal or Adirondack snow sampling tubes on weekly to bi-weekly  
193 schedules, 1938-present.

194

195 The Sleepers River, Vermont Research Watershed in Danville, Vermont (Shanley and Chalmers, 1999) is a USGS  
196 site that includes 15 stations with long-term weekly records of  $h$  and SWE collected using Adirondack snow tubes.  
197 Most of the periods of record are 1981-present, with a few stations going back to the 1960s. The sites include  
198 topographically flat openings in conifer stands, old fields with shrub and grass, a hayfield, a pasture, and openings in  
199 mixed softwood-hardwood forests. The Hubbard Brook Experiment Forest (Campbell et al., 2010) has collected  
200 weekly snow observations at the Station 2 rain gauge site, 1959-present. Measurement protocol collects ten samples  
201 2 m apart along a 20 m transect in a hardwood forest opening about  $\frac{1}{4}$  hectare in size. At each sample location along  
202 the transect,  $h$  and SWE are measured using a Mt. Rose snow tube and the ten samples are averaged for each  
203 transect. Finally, the Thompson Farm Research site includes a mixed hardwood forest site and an open pasture site  
204 (Burakowski et al. 2013; Burakowski et al. 2015). Daily (from 2011-2018), at each site, a snow core is extracted  
205 with an aluminum tube and weighed (tube + snow) using a digital hanging scale. The net weight of the snow is  
206 combined with the depth and the tube diameter to determine  $\rho_b$ , similar to a Federal or Adirondack sampler.

207

#### 208 **2.1.1.5 Chugach Mountains (Alaska) Data**

209 In the spring of 2018, we conducted three weeks of fieldwork in the Chugach mountains in coastal Alaska, near the  
210 city of Valdez (Figure 2d-e). We measured  $h$  using an avalanche probe at 71 sites along elevational transects during  
211 March, April, and May. The elevational transects ranged between 250 and 1100 m (net change along transect) and  
212 were accessible by ski and snowshoe travel. At each site, we measured  $h$  in 8 locations within the surrounding 10  
213  $\text{m}^2$ , resulting in a total of 550+ snow depth measurements. These 71 sites were scattered across 8 regions in order to  
214 capture spatial gradients that exist in the Chugach mountains as the wetter, more-dense maritime snow near the coast  
215 gradually changes to drier, less dense snow on the interior side.

216

### 217 2.1.1.5 Data Pre-Processing

218 Figure 3 demonstrates that it is not uncommon for automated snow pillow measurements to become noisy or non-  
219 physical, at times reporting large depths when there is no SWE reported. This is different from instances when  
220 physically plausible, but very low densities might be reported; say in response to early season dry, light snowfalls. It  
221 was therefore desirable to apply some objective, uniform procedure to each station's dataset in order to remove clear  
222 outlier points, while minimizing the removal of valid data points. We recognize that there is no accepted  
223 standardized method for cleaning bivariate SWE-*h* data sets. While Serreze et al. (1999) offer a procedure for  
224 SNOTEL data in their appendix, it is relevant only for precipitation and SWE values, not *h*. Given the strong  
225 correlation between *h* and SWE, we instead choose to use common outlier detection techniques for bivariate data.

226  
227 The Mahalanobis distance (MD; Maesschalck et al., 2000) quantifies how far a point lies from the mean of a  
228 bivariate distribution. The distances are in terms of the number of standard deviations along the respective principal  
229 component axes of the distribution. For highly correlated bivariate data, the MD can be qualitatively thought of as a  
230 measure of how far a given point deviates from an ellipse enclosing the bulk of the data. One problem is that the MD  
231 is based on the statistical properties of the bivariate data (mean, covariance) and these properties can be adversely  
232 affected by outlier values. Therefore, it has been suggested (e.g., Leys et al., 2018) that a 'robust' MD (RMD) be  
233 calculated. The RMD is essentially the MD calculated based on statistical properties of the distribution unaffected  
234 by the outliers. This can be done using the Minimum Covariance Determinant (MCD) method as first introduced by  
235 Rousseeuw (1984).

236  
237 Once RMDs have been calculated for a bivariate data set, there is the question of how large an RMD must be in  
238 order for the data point to be considered an outlier. For bivariate normal data, the distribution of the square of the  
239 RMD is  $\chi^2$  (Gnanadesikan and Kettenring, 1972), with *p* (the dimension of the dataset) degrees of freedom. So, a  
240 rule for identifying outliers could be implemented by selecting as a threshold some arbitrary quantile (say 0.99) of  
241  $\chi_p^2$ . For the current study, a threshold quantile of 0.999 was determined to be an appropriate compromise in terms of  
242 removing obviously outlier points, yet retaining physically plausible results.

243  
244 A scatter plot of SWE vs. *h* for the SNOTEL dataset from CONUS and AK reveals many non-physical points,  
245 mostly when a very large *h* is reported for a very low SWE (Figure 4a). Approximately 0.7% of the original data  
246 points were removed in the pre-processing described above, creating a more physically plausible scatter plot (Figure  
247 4b). Note that the outlier detection process was applied to each station individually. The distribution of 'day of year'  
248 (*DOY*) values of removed data points was broad, with a mean of 160 and a standard deviation of 65. Note that the  
249 *DOY* origin is 1 October. The same procedure was applied to the BC snow pillow, NRCS snow course, and  
250 northeast USA data sets as well (not shown). Table 1 summarizes useful information about the numerous data sets  
251 described above and indicates the final number of data points retained for each. We acknowledge that our process  
252 inevitably removes some valid data points, but, as a small percentage of an already small 0.7% removal rate, we  
253 judged this to be acceptable.

254

255 Table 1: Summary of information about the datasets used in this study. Datasets in bold font were used to construct  
 256 the regression model. The numbers of stations and data points reflect the post-processed data.

Dataset Name	Dataset Type	Number of retained stations	Number and percentage of retained data points	Precision ( $h$ / SWE)
<b>NRCS SNOTEL</b>	<b>Snow pillow (SWE), ultrasonic (<math>h</math>)</b>	<b>791</b>	<b>1,900,000 (99.3%)</b>	<b>(0.5 in / 0.1 in)</b>
NRCS SCAN	Snow pillow (SWE), ultrasonic ( $h$ )	5	7094 (97.8%)	(0.5 in / 0.1 in)
<b>British Columbia Snow Survey</b>	<b>Snow pillow (SWE), ultrasonic (<math>h</math>)</b>	<b>31</b>	<b>61,000 (97.5%)</b>	<b>(1 cm / 1 mm)</b>
NRCS Snow Survey	Federal sampler / Aerial marker	1085	116,000 (99.6%)	(0.5 in / 0.1 in) for manual sampler (2 in / n/a) for aerial marker
Maine Geological Survey	Adirondack or Federal sampler (SWE and $h$ )	431	28,000 (99.3%)	(0.5 in / 0.5 in)
Hubbard Brook (Station 2), NH	Mount Rose sampler (SWE and $h$ )	1	704 (99.4%)	(0.1 in / 0.1 in)
Thompson Farm, NH	Snow core (SWE and $h$ )	2	988 (99.4%)	0.5 in / 0.5 in)
Sleepers River, VT	Adirondack sampler	14	7214 (99.4%)	(0.5 in / 0.5 in)
New York Snow Survey	Adirondack or Federal sampler (SWE and $h$ )	523	44,614 (98.2%)	(0.5 in / 0.5 in)
Chugach Mountains, AK	Avalanche probe ( $h$ )	71	71 (100%)	(1 cm)

257

### 258 2.1.2 Climatological Variables

259 30-year climate normals at 1 km resolution for North America were obtained from the ClimateNA project (Wang et  
 260 al., 2016). This project provides grids for minimum, maximum, and mean temperature, and total precipitation for a  
 261 given month. These grids are based on the PRISM normals (Daly et al., 1994) and are available for the periods  
 262 1961-1990 and 1981-2010. For this study, the more recent climatology was used. The ClimateNA project also  
 263 provides a wide array of derived bioclimatic variables, such as precipitation as snow ( $PAS$ ), frost-free-period ( $FFP$ ),  
 264 mean annual relative humidity ( $RH$ ) and others. Wang et al. (2012) summarize these additional variables and how  
 265 they are derived. Figure 5 shows gridded maps of winter (sum of December, January, February) precipitation  
 266 ( $PPTWT$ ) and the temperature difference ( $TD$ ) between the mean temperature of the warmest month and the mean  
 267 temperature of the coldest month. The latter variable ( $TD$ ) is a measure of continentality.

268

### 269 2.2 Regression Model

270 In order to demonstrate the varying degrees of influence of explanatory variables, several regression models were  
 271 constructed. In each case, the model was built by randomly selecting 50% of the paired SWE- $h$  measurements from  
 272 the aggregated CONUS, AK, and BC snow pillow datasets. The model was then validated by applying it to the

273 remaining 50% of the dataset and comparing the modeled SWE to the observed SWE for those points. We  
274 constructed a second version of the regression models by randomly selecting 50% of the snow pillow stations and  
275 using all of the data from those stations. The model was then validated by applying it to the data from the remaining  
276 50% of the stations. These two methods provided identical results, likely due to the very large sample size (N) of our  
277 dataset. In all cases, the p values from the linear regression were 0, again due to the large sample size. Additional  
278 validation was done with the northeast USA datasets (SCAN snow pillow and various snow coring datasets) and the  
279 NRCS snow course dataset, which were completely left out of the model building process.

280

### 281 **2.2.1 One-Equation Model**

282 The simplest equation, and one that is supported by the strong correlation seen in the portions of Figure 3 when  
283 SWE is present, is one that expresses SWE as a function of  $h$ . A linear model is attractive in terms of simplicity, but  
284 this limits the snowpack to a constant density. An alternative is to express SWE as a power law, i.e.,

285

$$286 \quad (1) \quad SWE = Ah^{a_1}.$$

287

288 This equation can be log-transformed into

289

$$290 \quad (2) \quad \log_{10}(SWE) = \log_{10}(A) + a_1 \log_{10}(h)$$

291

292 which immediately allows for simple linear regression methods to be applied. With both  $h$  and SWE expressed in  
293 units of mm, the obtained coefficients are  $(A, a_1) = (0.146, 1.102)$ . Information on the performance of the model  
294 will be deferred until the results section.

295

### 296 **2.2.2 Two-Equation Model**

297 Recall from Figures 1 and 4 that there is a hysteresis loop in the SWE- $h$  relationship. During the accumulation  
298 phase, snow densities are relatively low. During the ablation phase, the densities are relatively high. So, the same  
299 snowpack depth is associated with two different SWEs, depending upon the time of year. The regression equation  
300 given above does not resolve this difference. This can be addressed by developing two separate regression  
301 equations, one for the accumulation (*acc*) and one for the ablation (*abl*) phase. This approach takes the form

302

$$303 \quad (3) \quad SWE_{acc} = Ah^{a_1}; \quad DOY < DOY^*$$

304

$$305 \quad (4) \quad SWE_{abl} = Bh^{b_1}; \quad DOY \geq DOY^*$$

306

307 where  $DOY$  is the number of days from the start of the water-year, and  $DOY^*$  is the critical or dividing day-of-water-  
308 year separating the two phases. Put another way,  $DOY^*$  is the day of peak SWE. Interannual variability results in a  
309 range of  $DOY^*$  for a given site. Additionally, some sites, particularly the SCAN sites in the northeast USA,

310 demonstrate multi-peak SWE profiles in some years. To reduce model complexity, however, we investigated the use  
 311 of a simple climatological (long term average) value of  $DOY^*$  at each site. For each snow pillow station, the average  
 312  $DOY^*$  was computed over the period of record of that station. Analysis of all of the stations revealed that this  
 313 average  $DOY^*$  was relatively well correlated with the climatological mean April maximum temperature (the average  
 314 of the daily maximums recorded in April;  $R^2 = 0.7$ ). However, subsequent regression analysis demonstrated that the  
 315 SWE estimates were relatively insensitive to  $DOY^*$  and the best results were actually obtained when  $DOY^*$  was  
 316 uniformly set to 180 for all stations. Again, with both SWE and  $h$  in units of mm, the regression coefficients turn out  
 317 to be  $(A, a_1) = (0.150, 1.082)$  and  $(B, b_1) = (0.239, 1.069)$ .

318  
 319 As these two equations are discontinuous at  $DOY^*$ , they are blended smoothly together to produce the final two-  
 320 equation model

321  
 322 (5) 
$$SWE = SWE_{acc} \frac{1}{2} (1 - \tanh[0.01\{DOY - DOY^*\}]) +$$
  
 323 
$$SWE_{abl} \frac{1}{2} (1 + \tanh[0.01\{DOY - DOY^*\}])$$

324  
 325 The coefficient 0.01 in the tanh function controls the width of the blending window and was selected to minimize  
 326 the root mean square error of the model estimates.

327  
 328 **2.2.3 Two-Equation Model with Climate Parameters**

329 A final model was constructed by incorporating climatological variables. Again, the emphasis in this study is on  
 330 methods that can be implemented at locations lacking the time series of weather variables that might be available at  
 331 a weather or SNOTEL station. Climatological normals are unable to account for interannual variability, but they do  
 332 preserve the high spatial gradients in climate that can lead to spatial gradients in snowpack characteristics. Stepwise  
 333 linear regression was used to determine which variables to include in the regression. The initial list of potential  
 334 variables included was

335  
 336 (6) 
$$SWE = f(h, z, PPTWT, PAS, TWT, TD, DOY, RH)$$

337  
 338 where  $z$  is the elevation (m),  $PPTWT$  is the winter (sum of December, January, February) precipitation (mm),  $PAS$  is  
 339 mean annual precipitation as snow (mm),  $TWT$  is the winter (December, January, February) mean temperature ( $^{\circ}C$ ),  
 340  $TD$  is the difference between the mean temperature of the warmest month and the mean temperature of the coldest  
 341 month ( $^{\circ}C$ ),  $DOY$  is the day of water year, and  $RH$  is the relative humidity (%). In the stepwise regression,  
 342 explanatory variables were accepted only if they improved the adjusted  $R^2$  value by 0.001. The result of the  
 343 regression yielded

344  
 345 (7) 
$$SWE_{acc} = Ah^{a_1} PPTWT^{a_2} TD^{a_3} DOY^{a_4}; \quad DOY < DOY^*$$

346

347 (8)  $SWE_{abl} = Bh^{b_1}PPTWT^{b_2}TD^{b_3}DOY^{b_4}; \quad DOY \geq DOY^*$

348

349 or, in log-transformed format,

350

351 (9)  $\log_{10}(SWE_{acc}) = \log_{10}(A) + a_1\log_{10}(h) + a_2\log_{10}(PPTWT) +$   
352  $a_3\log_{10}(TD) + a_4\log_{10}(DOY); \quad DOY < DOY^*$

353

354 (10)  $\log_{10}(SWE_{abl}) = \log_{10}(B) + b_1\log_{10}(h) + b_2\log_{10}(PPTWT) +$   
355  $b_3\log_{10}(TD) + b_4\log_{10}(DOY); \quad DOY \geq DOY^*$

356

357 indicating that only snow depth, winter precipitation, temperature difference, and day of water year were relevant.

358 Manual tests of model construction with other variables included confirmed that Eqns. (7-8) yielded the best results.

359 These two SWE estimates for the individual (*acc* and *abl*) phases of the snowpack were then blended with Eqn. (5)

360 to produce a single equation for SWE spanning the entire water year. The obtained regression coefficients were

361  $(A, a_1, a_2, a_3, a_4) = (0.0533, 0.9480, 0.1701, -0.1314, 0.2922)$  and  $(B, b_1, b_2, b_3, b_4) = (0.0481, 1.0395,$

362  $0.1699, -0.0461, 0.1804)$ . The physical interpretation of these coefficients is straightforward. For example, both  $a_2$

363 and  $b_2$  are greater than zero. So, for two locations with equal  $h$ ,  $DOY$ , and  $TD$ , the location with greater  $PPTWT$  will

364 have a greater SWE and therefore density. These locations are typically maritime climates with wetter, denser snow.

365 In contrast, both  $a_3$  and  $b_3$  are less than zero. Therefore, for two locations with equal  $h$ ,  $DOY$ , and  $PPTWT$ , the

366 location with greater  $TD$  (a more continental climate) will have a lower density, which is again an expected result.

367 These trends are similar in concept to Sturm et al. (2010), whose discrete snow classes (based on climate classes)

368 indicate which snow will densify more rapidly.

### 369 **3 Results**

370 A comparison of the three regression models (one-equation model, Eq. (2); two-equation model, Eqs. (3-5); multi-

371 variable two-equation model, Eqs. (5, 7-8)) is provided in Figure 6. The left column shows scatter plots of modeled

372 SWE to observed SWE for the validation data set with the 1:1 line shown in black. The right column shows

373 distributions of the model residuals. The vertical lines in the right column show the mean error, or model bias.

374 Visually, it is clear that the one-equation model performs relatively poorly with a large negative bias. This large

375 negative bias is partially overcome by the two-equation model (middle row, Figure 6). The cloud of points is closer

376 to the 1:1 line and the vertical black line indicating the mean error is closer to zero. In the final row of Figure 6, we

377 see that the multi-variable two-equation model yields the best result by far. The residuals are now evenly distributed

378 with a small bias. Several metrics of performance for the three models, including  $R^2$  (Pearson coefficient), bias, and

379 root-mean-square-error (RMSE), are provided in Table 2. Figure 7 shows the distribution of model residuals for the

380 multi-variable two-equation model as a function of  $DOY$ .

381



382 Table 2: Summary of performance metrics for the three regression models presented in Section 2.2.

Model	R <sup>2</sup>	Bias (mm)	RMSE (mm)
One-equation	0.946	-19.5	102
Two-equation	0.962	-5.1	81
Multi-variable two-equation	0.978	-1.2	59

383

384 It is useful to also consider the model errors in a non-dimensional way. Therefore, an RMSE was computed at each  
 385 station location and normalized by the winter precipitation (*PPTWT*) at that location. Figure 8 shows the probability  
 386 density function of these normalized errors. The average RMSE is approximately 15% of *PPTWT* with most values  
 387 falling into the range of 5-30%. The spatial distribution of these normalized errors is shown in Figure 9. For the  
 388 SNOTEL stations, it appears there is a slight regional trend, in terms of stations in continental climates (Rockies)  
 389 having larger relative errors than stations in maritime climates (Cascades). The British Columbia stations also show  
 390 higher relative errors.

391

### 392 3.1 Results for Snow Classes

393 A key objective of this study is to regress climatological information in a continuous rather than a discrete way. The  
 394 work by Sturm et al. (2010) therefore provides a valuable point of comparison. In that study, the authors developed  
 395 the following equation for density  $\rho_b$

396

$$397 (11) \quad \rho_b = (\rho_{max} - \rho_0)[1 - e^{(-k_1 h - k_2 DOY)}] + \rho_0$$

398

399 where  $\rho_0$  is the initial density,  $\rho_{max}$  is the maximum or ‘final’ density (end of water year),  $k_1$  and  $k_2$  are coefficients,  
 400 and *DOY* in this case begins on January 1. This means that their *DOY* for October 1 is -92. The coefficients vary  
 401 with snow class and the values determined by Sturm et al. (2010) are shown in Table 3.

402

403 Table 3: Model parameters by snow class for Sturm et al. (2010).

Snow Class	$\rho_{max}$	$\rho_0$	$k_1$	$k_2$
Alpine	0.5975	0.2237	0.0012	0.0038
Maritime	0.5979	0.2578	0.0010	0.0038
Prairie	0.5941	0.2332	0.0016	0.0031
Tundra	0.3630	0.2425	0.0029	0.0049
Taiga	0.2170	0.2170	0.0000	0.0000

404

405 To make a comparison, the snow class for each SNOTEL and British Columbia snow survey (Rows 1 and 3 of Table  
 406 1) site was determined using a 1-km snow class grid (Sturm et al., 2010). The aggregated dataset from these stations  
 407 was made up of 27% Alpine, 14% Maritime, 10% Prairie, 11% Tundra, and 38% Taiga data points. Equation (11)  
 408 was then used to estimate snow density (and then SWE) for every point in the validation dataset described in Section  
 409 2.2. Figure 10 compares the SWE estimates from the Sturm model and from the current multi-variable, two-equation  
 410 model (Equations 5, 7-8). The upper left panel of Figure 10 shows all of the data, and the remaining panels show the  
 411 results for each snow class. In all cases, the current model provides better estimates (narrow cloud of points; closer  
 412 to the 1:1 line). Plots of the residuals by snow class are provided in Figure 11, giving an indication of the bias of

413 each model for each snow class. Summaries of the model performance, broken out by snow class, are given in Table  
 414 4. The current model has smaller biases and RMSEs for each snow class.

415

416 Table 4: Comparison of model performance by Sturm et al. (2010) and the current study.

Model	Sturm et al. (2010)			Multi-variable two-equation model		
Snow Class	R <sup>2</sup>	Bias (mm)	RMSE (mm)	R <sup>2</sup>	Bias (mm)	RMSE (mm)
All Data	0.928	-29.2	111	0.978	-1.2	59
Alpine	0.973	10.1	55	0.978	-2.7	48
Maritime	0.968	-16.8	109	0.975	-7.8	95
Prairie	0.967	18.7	56	0.971	-0.7	45
Tundra	0.956	-10.5	82	0.974	-2.9	59
Taiga	0.943	-80.0	151	0.978	2.6	54

417

### 418 3.2 Comparison to Pistocchi (2016)

419 In order to provide an additional comparison, the simple model of Pistocchi (2016) was also applied to the validation  
 420 dataset. His model calculates the bulk density as

421

$$422 \quad (12) \quad \rho_b = \rho_0 + K(DOY + 61),$$

423

424 where  $\rho_0$  has a value of 200 kg m<sup>-3</sup> and  $K$  has a value of 1 kg m<sup>-3</sup>. The  $DOY$  for this model has its origin at  
 425 November 1. Application of this model to the validation dataset yields a bias of 55 mm and an RMSE of 94 mm.  
 426 These results are comparable to the Sturm et al. (2010) model, with a larger bias but smaller RMSE.

427

### 428 3.3 Comparison to Jonas et al. (2009)

429 A final point of comparison can be provided by the model of Jonas et al. (2009). The full version of that model  
 430 contains region-specific offset parameters that are not relevant to North America, so the following partial version of  
 431 the model is used (their Eq. 4):

432

$$433 \quad (13) \quad \rho_b = ah + b,$$

434

435 where the parameters  $(a, b)$  vary with elevation and month, as given by Table 5. Note that coefficients are not given  
 436 for every month. Application of the Jonas et al. (2009) model to the snow pillow dataset yields a bias of -5 mm and  
 437 an RMSE of 69 mm. These results are not directly comparable to those of the current model (Table 2, row 3) since  
 438 the Jonas et al. (2009) model is unable to compute results for several months of the year. To make a direct  
 439 comparison to the current model, it is necessary to first remove those data points (about 5%). When this is done, the  
 440 current model yields a bias of -0.3 mm and an RMSE of 59 mm.

441

442 Table 5: Model coefficients  $(a, b)$  for the Jonas et al. (2009) model.

Month	$z > 2000 \text{ m}$	$2000 \text{ m} > z > 1400 \text{ m}$	$1400 \text{ m} > z$
January	(206, 52)	(208, 47)	(235, 31)

February	(217, 46)	(218, 52)	(279, 9)
March	(272, 26)	(281, 31)	(333, 3)
April	(331, 9)	(354, 15)	(347, 25)
May	(378, 21)	(409, 29)	(413, 19)
June	(452, 8)	n/a	n/a
July	(470, 15)	n/a	n/a
August	n/a	n/a	n/a
September	n/a	n/a	n/a
October	n/a	n/a	n/a
November	(206, 47)	(183, 35)	(149, 37)
December	(203, 52)	(190, 47)	(201, 26)

443

### 444 3.4 Results for Northeast USA

445 The regression equations in this study were developed using a large collection of snow pillow sites in CONUS, AK,  
446 and BC. The snow pillow sites are limited to locations west of approximately W 105° (Figure 2a). By design, the  
447 data sets from the northeastern USA (Section 2.1.1.3) were left as an entirely independent validation set. These  
448 northeastern sites are geographically distant from the training data sets, subject to a very different climate, largely  
449 use different methods (snow coring, with the exception of the SCAN network) and are generally at much lower  
450 elevations than the western sites, providing an interesting opportunity to test how robust the current model is.

451

452 Figure 12 graphically summarizes the datasets and the performance of the multi-variable two-equation model of the  
453 current study. The RMSE values are comparable to those found for the western stations, but, given the  
454 comparatively thinner snowpacks in the northeast, represent a larger relative error (Table 5). The bias of the model  
455 is consistently positive, in contrast to the western stations where the bias was negligible. Note that Table 5 also  
456 includes results from the application of the other three models discussed. Sturm et al. (2010) cannot be applied to  
457 several of the datasets since their available 1 km snowclass dataset cuts off at -71.6° longitude. The current model  
458 and the Jonas et al. (2009) model perform better than the other two models, with the current model generally  
459 outperforming the Jonas et al. (2009) model. The two datasets where the Jonas et al. (2009) model has a slightly  
460 better performance are the two smallest datasets (less than 1000 measurements; see Table 1).

461

462 Table 5: Performance metrics for various models applied to the northeastern USA datasets. Bold font is used to  
463 highlight the model with the best performance for each dataset.

Dataset Name	Multi-variable, two-equation model		Sturm et al. (2010)		Jonas et al. (2009)		Pistocchi (2015)	
	Bias (mm)	RMSE (mm)	Bias (mm)	RMSE (mm)	Bias (mm)	RMSE (mm)	Bias (mm)	RMSE (mm)
Maine Geological Survey, ME	<b>13.1</b>	<b>34.0</b>	n/a	n/a	25.1	46.0	59.2	77.1
Hubbard Brook (Station 2), NH	21.8	66.6	34.2	76.9	<b>19.4</b>	<b>65.4</b>	52.0	90.8
Thompson Farm, NH	7.1	20.2	n/a	n/a	<b>5.6</b>	<b>19.9</b>	20.4	32.3
NRCS SCAN	<b>-1.2</b>	<b>39.2</b>	8.4	45.0	-2.8	40.6	23.4	56.9
Sleepers River, VT	<b>14.4</b>	<b>28.2</b>	36.5	48.9	20.4	33.5	55.8	67.1
New York Snow Survey	<b>14.8</b>	<b>31.2</b>	21.0	49.3	16.3	33.0	41.3	56.1

464

465 **3.5 Results for NRCS Snow Course / Aerial Marker Data**

466 The NRCS snow course and aerial marker data were also left out of the model building process so they provide an  
 467 additional and completely independent comparison of the various models considered. Recall that these data come  
 468 from snow course (coring measurements) and aerial surveys, which are different measurement methods than the  
 469 snow pillows which provided the data for construction of the current regression model. Table 6 shows the results  
 470 and demonstrates that the current model has the best performance.

471  
 472 Table 6: Performance metrics for various models applied to the NRCS snow course and aerial marker dataset. Bold  
 473 font is used to highlight the model with the best performance.

	Multi-variable, two-equation model		Sturm et al. (2010)		Jonas et al. (2009)		Pistocchi (2015)	
Dataset Name	Bias (mm)	RMSE (mm)	Bias (mm)	RMSE (mm)	Bias (mm)	RMSE (mm)	Bias (mm)	RMSE (mm)
NRCS Snow Course / Aerial Marker	<b>0</b>	<b>59</b>	-24	123	24	72	71	99

474 **4 Discussion**

475 The results presented in this study show that the regression equation described by equations (5, 7-8) is an  
 476 improvement (lower bias and RMSE) over other widely used bulk density equations. The key advantage is that the  
 477 current method regresses in relevant parameters directly, rather than using discrete bins (for snow class, elevation,  
 478 month of year, etc.), each with its own set of model coefficients. The comparison (Figs. 10-11; Table 4) to the model  
 479 of Sturm et al. (2010) reveals a peculiar behavior of that model for the Taiga snow class, with a large negative bias  
 480 in the Sturm estimates. Inspection of the coefficients provided for that class (Table 3) shows that the model simply  
 481 predicts that  $\rho_b = \rho_{max} = 0.217$  for all conditions.

482  
 483 When our multi-variable two-equation model, developed solely from western North American data, is applied to  
 484 northeast USA locations, it produces SWE estimates with smaller RSME values and larger biases than the western  
 485 stations. When comparing the SWE-*h* scatter plots of the SNOTEL data (Figure 4b) to those of the east coast data  
 486 sets (left column; Figure 12), it is clear that the northeast data generally have more scatter. This is confirmed by  
 487 computing the correlation coefficients between SWE and *h* for each dataset. It is unclear if this disparity in  
 488 correlation is related to measurement methodology or is instead a ‘signal to noise’ issue. Comparing Figures 4 and  
 489 12 shows the considerable difference in snowpack depth between the western and northeastern data sets. When the  
 490 western dataset is filtered to include only measurement pairs where *h* < 1.5 m, the correlation coefficient is reduced  
 491 to a value consistent with the northeast datasets. This suggests that the performance of the current (or other)  
 492 regression model is not as good at shallow snowpack depths. This is also suggested upon examination of the time  
 493 series of observed  $\rho_b = SWE/h$  for a given season at a snow pillow site. Very early in the season, when the depths  
 494 are small, the density curve has a lot of variability. Later in the season, when depths are greater, the density curve  
 495 becomes much smoother. Very late in the season, when depths are low again, the density curve becomes highly  
 496 variable again.

497

498 Measurement precision and accuracy affect the construction and use of a regression model. Upon inspection of the  
499 snow pillow data, it was observed that the precision of the depth measurements was approximately 25 mm and that  
500 of the SWE measurements was approximately 2.5 mm. To test the sensitivity of the model coefficients to the  
501 measurement precision, the depth values in the training dataset were randomly perturbed by  $\pm 25$  mm and the SWE  
502 values were randomly perturbed by  $\pm 2.5$  mm and the regression coefficients were recomputed. This process was  
503 repeated numerous times and the mean values of the perturbed coefficients were obtained. These adjusted  
504 coefficients were then used to recompute the SWE values for the validation data set and the bias and RMSE were  
505 found to be -10.5 mm and 72.7 mm. This represents a roughly 10% increase in RMSE, but a considerable increase in  
506 bias magnitude (see Table 4 for the original values). This sensitivity of the regression analysis to measurement  
507 precision underscores the need to have high-precision measurements for the training data set. Regarding accuracy,  
508 random and systematic errors in the paired SWE -  $h$  data used to construct the regression model will lead to  
509 uncertainties in SWE values predicted by the model. As noted in the introduction, snow pillow errors in SWE  
510 estimates do not follow a simple pattern. Additionally, they are complicated by the fact that the errors are often  
511 computed by comparing snow pillow data to coring data, which itself is subject to error. Lacking quantitative  
512 information on the distribution of snow pillow errors, we are unable to quantify the uncertainty in the SWE  
513 estimates.

514  
515 Another important consideration has to do with the uncertainty of depth measurements that the model is applied to.  
516 For context, one application of this study is to crowd-sourced, opportunistic snow depth measurements from  
517 programs like the Community Snow Observations (CSO; Hill et al., 2018) project. In the CSO program,  
518 backcountry recreational users submit depth measurements, typically taken with an avalanche probe, using a  
519 smartphone in the field. The measurements are then converted to SWE estimates which are assimilated into  
520 snowpack models. These depth measurements are ‘any time, any place’ in contrast to repeated measurements from  
521 the same location, like snow pillows or snow courses. Most avalanche probes have cm-scale graduated markings, so  
522 measurement precision is not a major issue. A larger problem is the considerable variability in snowpack depth that  
523 can exist over short (meter scale) distances. The variability of the Chugach avalanche probe measurements was  
524 assessed by taking the standard deviation of 8  $h$  measurements per site. The average of this standard deviation over  
525 the sites was 22 cm and the average coefficient of variation (standard deviation normalized by the mean) over the  
526 sites was 15%. This variability is a function of the surface roughness of the underlying terrain, and also a function of  
527 wind redistribution of snow. Propagating this uncertainty through the regression equations yields a slightly higher  
528 (16%) uncertainty in the SWE estimates. CSO participants can do three things to ensure that their recorded depth  
529 measurements are as representative as possible. First, avoid measurements in areas of significant wind scour or  
530 deposition. Second, avoid measurements in terrain likely to have significant surface roughness (rocks, fallen logs,  
531 etc.). Third, take several measurements and average them.

532  
533 Expansion of CSO measurements in areas lacking SWE measurements can increase our understanding of the  
534 extreme spatial variability in snow distribution and the inherent uncertainties associated with modeling SWE in

535 these regions. It could also prove useful for estimating watershed-scale SWE in regions like the northeastern USA,  
536 which is currently limited to five automated SCAN sites with historical SWE measurements for only the past two  
537 decades. Additionally, historical snow depth measurements are more widely available in the Global Historical  
538 Climatology Network (GHCN-Daily; Menne et al. 2012), with several records extending back to the late 1800s.  
539 While many of the GHCN stations are confined to lower elevations with shallower snow depths, the broader  
540 network of quality-controlled snow depth data paired with daily GHCN temperature and precipitation measurements  
541 could potentially be used to reconstruct SWE in the eastern US given additional model development and refinement.

## 542 **5 Conclusions**

543 We have developed a new, easy to use method for converting snow depth measurements to snow water equivalent  
544 estimates. The key difference between our approach and previous approaches is that we directly regress in  
545 climatological variables in a continuous fashion, rather than a discrete one. Given the abundance of freely available  
546 climatological norms, a depth measurement tagged with coordinates (latitude and longitude) and a time stamp is  
547 easily and immediately converted into SWE.

548  
549 We developed this model with data from paired SWE-*h* measurements from the western United States and British  
550 Columbia. The model was tested against entirely independent data (primarily snow course; some snow pillow) from  
551 the northeastern United States and was found to perform well, albeit with larger biases and root-mean-squared-  
552 errors. The model was tested against other well-known regression equations and was found to perform better. The  
553 model was also tested against a large dataset of independent snow course and aerial marker measurements from  
554 western North America. For this second independent test, the current model outperformed the other models  
555 considered.

556  
557 This model is not a replacement for more sophisticated snow models that evolve the snowpack based on high  
558 frequency (e.g., daily or sub-daily) weather data inputs. The intended purpose of this model is to constrain SWE  
559 estimates in circumstances where snow depth is known, but weather variables are not, a common issue in sparsely  
560 instrumented areas in North America.

## 561 **6 Acknowledgements**

562 Support for this project was provided by NASA (NNX17AG67A). R. Crumley acknowledges support from the  
563 CUAHSI Pathfinder Fellowship. E. Burakowski acknowledges support from NSF (MSB-ECA #1802726). We thank  
564 M. Sturm, A. Winstral and a third anonymous referee for their careful and thoughtful reviews of this manuscript.

## 565 **7 Data Access**

566 Numerous online datasets were used for this project and were obtained from the following locations:

- 567 1. NRCS Snow Telemetry: <https://www.wcc.nrcs.usda.gov/snow/SNOTEL-wedata.html>
- 568 2. NRCS Soil Climate Analysis Network: <https://www.wcc.nrcs.usda.gov/scan/>

- 569 3. British Columbia Automated Snow Weather Stations:  
570 [https://www2.gov.bc.ca/gov/content/environment/air-land-water/water/water-science-data/water-data-  
572 tools/snow-survey-data/automated-snow-weather-station-data](https://www2.gov.bc.ca/gov/content/environment/air-land-water/water/water-science-data/water-data-<br/>571 tools/snow-survey-data/automated-snow-weather-station-data)  
573 4. Maine Cooperative Snow Survey: <https://mgs-maine.opendata.arcgis.com/datasets/maine-snow-survey-data>  
574 5. New York Snow Survey: <http://www.nrcc.cornell.edu/regional/snowsurvey/snowsurvey.html>  
575 6. Sleepers River Research Watershed. Snow data not available online; request data from contact at:  
576 <https://nh.water.usgs.gov/project/sleepers/index.htm>  
577 7. Hubbard Brook Experimental Forest: <https://hubbardbrook.org/d/hubbard-brook-data-catalog>  
578 8. Climatological Data: <https://adaptwest.databasin.org/pages/adaptwest-climatena>  
579 9. NRCS Snow Course / Aerial Marker Data: <https://wcc.sc.egov.usda.gov/reportGenerator/>

580 A Matlab function for calculating SWE based on the results in this paper has been made publicly available at Github  
581 (<https://github.com/communitysnowobs/snowdensity>).  
582  
583

584 **References**

585

586 Alford, D.: Density variations in alpine snow, *J. Glaciol.*, 6(46), 495-503,  
587 <https://doi.org/10.3189/S0022143000019717>, 1967.

588

589 Avanzi, F., De Michele, C., and Ghezzi, A.: On the performances of empirical regressions for the estimation of bulk  
590 snow density, *Geogr. Fis. Dinam. Quat.*, 38, 105-112, doi:10.4461/GFDQ.2015.38.10, 2015.

591

592 Beaumont, R.: Mt. Hood pressure pillow snow gage, *J. Appl. Meteorol.*, 4, 626-631, [https://doi.org/10.1175/1520-0450\(1965\)004<0626:MHPPSG>2.0.CO;2](https://doi.org/10.1175/1520-0450(1965)004<0626:MHPPSG>2.0.CO;2) 1965.

594

595 Beaumont, R., and Work, R.: Snow sampling results from three samplers, *Hydrol. Sci. J.*, 8(4), 74-78,  
596 <https://doi.org/10.1080/02626666309493359>, 1963.

597

598 Burakowski, E.A., Ollinger, S., Lepine, L., Schaaf, C.B., Wang, Z., Dibb, J.E., Hollinger, D.Y., Kim, J.-H., Erb, A.,  
599 and Martin, M.E.: Spatial scaling of reflectance and surface albedo over a mixed-use, temperate forest landscape  
600 during snow-covered periods, *Remote Sens. Environ.*, 158, 465-477, <https://doi.org/10.1016/j.rse.2014.11.023>,  
601 2015.

602

603 Burakowski, E.A., Wake, C.P., Stampone, M., and Dibb, J.: Putting the Capital 'A' in CoCoRAHS: An  
604 Experimental Program to Measure Albedo using the Community Collaborative Rain Hail and Snow (CoCoRaHS)  
605 Network, *Hydrol. Process.*, 27(21), 3024-3034, <https://doi.org/10.1002/hyp.9825>, 2013.

606

607 Campbell, J., Ollinger, S., Flerchinger, G., Wicklein, H., Hayhoe, K., and Bailey, A.: Past and projected future  
608 changes in snowpack and soil frost at the Hubbard Brook Experimental Forest, New Hampshire, USA, *Hydrol.*  
609 *Process.*, 24, 2465-2480, <https://doi.org/10.1002/hyp.7666>, 2010.

610

611 Church, J.E.: Snow surveying: its principles and possibilities, *Geogr. Rev.*, 23(4), 529-563, DOI: 10.2307/209242,  
612 1933.

613

614 Church, J.E., and Marr, J.C.: Further improvement of snow-survey apparatus, *Transactions of the American*  
615 *Geophysical Union*, 18(2), 607-617, [10.1029/TR018i002p00607](https://doi.org/10.1029/TR018i002p00607), 1937.

616

617 Daly, C., Neilson, R., and Phillips, D.: A statistical-topographic model for mapping climatological precipitation over  
618 mountainous terrain, *J. Appl. Meteorol.*, 33, 140-158, [https://doi.org/10.1175/1520-0450\(1994\)033<0140:ASTMFM>2.0.CO;2](https://doi.org/10.1175/1520-0450(1994)033<0140:ASTMFM>2.0.CO;2), 1994.

620



621 Dixon, D., and Boon, S.: Comparison of the SnowHydro sampler with existing snow tube designs, *Hydrol. Process.*,  
622 26(17), 2555-2562, <https://doi.org/10.1002/hyp.9317>, 2012.

623

624 Dressler, K., Fassnacht, S., and Bales, R.: A comparison of snow telemetry and snow course measurements in the  
625 Colorado River basin, *J. Hydrometeorol.*, 7, 705-712, <https://doi.org/10.1175/JHM506.1>, 2006.

626

627 Goodison, B.: Accuracy of snow samplers for measuring shallow snowpacks: An update, *Proceedings of the 35<sup>th</sup>*  
628 *Annual Eastern Snow Conference*, Hanover, NH, 36-49, 1978.

629

630 Goodison, B., Ferguson, H., and McKay, G.: Measurement and data analysis. *The Handbook of Snow: Principles,*  
631 *Processes, Management, and Use*, D. Gray and D. Male, Eds., Pergamon Press, 191-274, 1981.

632

633 Goodison, B., Wilson, B., Wu., K. and Metcalfe, J.: An inexpensive remote snow-depth gauge: An assessment,  
634 *Proceedings of the 52<sup>nd</sup> Annual Western Snow Conference*, Sun Valley, ID, 188-191, 1984.

635

636 Goodison, B., Glynn, J., Harvey, K., and Slater, J.: Snow Surveying in Canada: A Perspective, *Can. Water Resour.*  
637 *J.*, 12(2), 27-42, <https://doi.org/10.4296/cwrj1202027>, 1987.

638

639 Gnanadesikan, R., and Kettenring, J.: Robust estimates, residuals, and outlier detection with multiresponse data,  
640 *Biometrics*, 28, 81-124, DOI: 10.2307/2528963, 1972.

641

642 Hill, D.F., Wolken, G. J., Wikstrom Jones, K., Crumley, R., and Arendt, A.: Crowdsourcing snow depth data with  
643 citizen scientists, *Eos*, 99, <https://doi.org/10.1029/2018EO108991>, 2018.

644

645 Johnson, J., and Marks, D.: The detection and correction of snow water equivalent pressure sensor errors, *Hydrol.*  
646 *Proc.*, <https://doi.org/10.1002/hyp.5795>, 2004.

647

648 Johnson, J., Gelvin, A., Duvoy, P., Schaefer G., Poole, G., and Horton, G.: Performance characteristics of a new  
649 electronic snow water equivalent sensor in different climates, *Hydrol. Proc.*, DOI: 10.1002/hyp.10211, 2015.

650

651 Jonas, T., Marty, C., and Magnusson, M.: Estimating the snow water equivalent from snow depth measurements, *J.*  
652 *Hydrol.*, 378, 161-167, <https://doi.org/10.1016/j.jhydrol.2009.09.021>, 2009.

653

654 Leys, C., Klein, O., Dominicy, Y., and Ley, C.: Detecting multivariate outliers: use a robust variant of the  
655 Mahalanobis distance, *J. Exp. Soc. Psychol.*, 74, 150-156, <https://doi.org/10.1016/j.jesp.2017.09.011>, 2018.

656

657 Liang, X., Lettermaier, D., Wood, E., and Burges, S.: A simple hydrologically based model of land surface water  
658 and energy fluxes for general circulation models, *J. Geophys. Res. Atmos.*, 99(D7), 14,415-14,428,  
659 <https://doi.org/10.1029/94JD00483>, 1994.  
660

661 Liston, G., and Elder, K.: A distributed snow evolution modeling system (SnowModel), *J. Hydrometeorol.*, 7, 1259-  
662 1276, <https://doi.org/10.1175/JHM548.1>, 2006.  
663

664 Lundberg, A., Richardson-Naslund, C., and Andersson, C.: Snow density variations: consequences for ground  
665 penetrating radar, *Hydrol. Process.*, 20, 1483-1495, <https://doi.org/10.1002/hyp.5944>, 2006.  
666

667 Maine Geological Survey: Maine Cooperative Snow Survey Dataset,  
668 [https://www.maine.gov/dacf/mgs/hazards/snow\\_survey/](https://www.maine.gov/dacf/mgs/hazards/snow_survey/), 2018.  
669

670 McKay, G., and Findlay, B., 1971: Variation of snow resources with climate and vegetation in Canada, *Proceedings*  
671 *of the 39<sup>th</sup> Western Snow Conference*, Billings, MT, 17-26, 1971.  
672

673 De Maesschalck, R., Jouan-Rimbaud, D., and Massart, D.: The Mahalanobis distance, *Chemometr. Intell. Lab. Syst.*,  
674 50(1), 1-18, [https://doi.org/10.1016/S0169-7439\(99\)00047-7](https://doi.org/10.1016/S0169-7439(99)00047-7), 2000.  
675

676 McCreight, J., and Small, E.: Modeling bulk density and snow water equivalent using daily snow depth  
677 observations, *The Cryosphere*, 8, 521-536, <https://doi.org/10.5194/tc-8-521-2014>, 2014.  
678

679 Meloyund, V., Leira, B., Hoiseth, K., and Liso, K.: Predicting snow density using meteorological data, *Meteorol.*  
680 *Appl.*, 14, 413-423, <https://doi.org/10.1002/met.40>, 2007.  
681

682 Menne, M.J., I. Durre, R.S. Vose, B.E. Gleason, and Houston, T.G.: An overview  
683 of the Global Historical Climatology Network-Daily Database, *J. Atmos. Ocean. Technol.*, 29, 97-910,  
684 [doi:10.1175/JTECH-D-11-00103.1](https://doi.org/10.1175/JTECH-D-11-00103.1), 2012.  
685

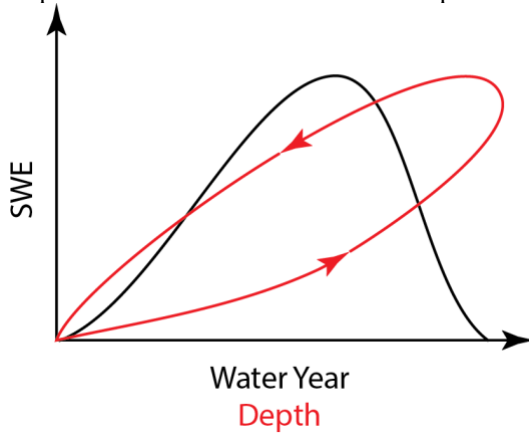
686 Molotch, N.P., and Bales, R.C.: SNOTEL representativeness in the Rio Grande headwaters on the basis of  
687 physiographics and remotely sensed snow cover persistence, *Hydrol. Process.*, 20(4), 723-739,  
688 <https://doi.org/10.1002/hyp.6128>, 2006.  
689

690 Mote, P., Li, S., Lettermaier, D., Xiao, M., and Engel, R.: Dramatic declines in snowpack in the western US,” *npj*  
691 *Clim. Atmos. Sci.*, 1(2), 1-6, [doi:10.1038/s41612-018-0012-1](https://doi.org/10.1038/s41612-018-0012-1), 2018.  
692

693 Mizukami, N., and Perica, S.: Spatiotemporal characteristics of snowpack density in the mountainous regions of the  
694 western United States, *J. Hydrometeorol.*, 9, 1416-1426, <https://doi.org/10.1175/2008JHM981.1>, 2008.  
695  
696 New York Snow Survey, NOAA, Northeast Regional Climate Center at Cornell University, 2018.  
697  
698 Pagano, T., Garen, D., Perkins, T., and Pasteris, P.: Daily updating of operational statistical seasonal water supply  
699 forecasts for the western U.S., *J. Am. Water Resour. Assoc.*, 45(3), 767-778, <https://doi.org/10.1111/j.1752->  
700 1688.2009.00321.x, 2009.  
701  
702 Painter, T., Berisford, D., Boardman, J., Bormann, K., Deems, J., Gehrke, F., Hedrick, A., Joyce, M., Laidlaw, R.,  
703 Marks, D., Mattmann, C., Mcgurk, B., Ramirez, P., Richardson, M., Skiles, S., Seidel, F., and Winstral, A.: The  
704 Airborne Snow Observatory: fusion of scanning lidar, imaging spectrometer, and physically-based modeling for  
705 mapping snow water equivalent and snow albedo, *Remote Sens. Environ.*, 184, 139-152,  
706 [doi:10.1016/j.rse.2016.06.018](https://doi.org/10.1016/j.rse.2016.06.018), 2016.  
707  
708 Pistocchi, A.: Simple estimation of snow density in an Alpine region, *J. Hydrol. Reg. Stud.*, 6, 82-89,  
709 <http://dx.doi.org/10.1016/j.ejrh.2016.03.004>, 2016.  
710  
711 Rousseeuw, P.: Least Median of Squares Regression, *J. Am. Stat. Assoc.*, 79, 871-880, DOI:  
712 10.1080/01621459.1984.10477105, 1984.  
713  
714 Ryan, W., Doesken, N., and Fassnacht, S.: Evaluation of Ultrasonic Snow Depth Sensors for U.S. Snow  
715 Measurements, *J. Atmos. Ocean. Technol.*, 25, 667-684, <https://doi.org/10.1175/2007JTECHA947.1>, 2008.  
716  
717 Schaefer, G., Cosh, M., and Jackson, T.: The USDA Natural Resources Conservation Service Soil Climate Analysis  
718 Network (SCAN), *J. Atmos. Ocean. Technol.*, 24, 2073-2077, <https://doi.org/10.1175/2007JTECHA930.1>, 2007.  
719  
720 Serreze, M., Clark, M., Armstrong, R., McGinnis, D., and Pulwarty, R.: Characteristics of the western United States  
721 snowpack from snowpack telemetry (SNOTEL) data, *Water Resour. Res.*, 35(7), 2145-2160,  
722 <https://doi.org/10.1029/1999WR900090>, 1999.  
723  
724 Shanley, J., and Chalmers, A.: The effect of frozen soil on snowmelt runoff at Sleepers River, Vermont, *Hydrol.*  
725 *Process.*, 13(12-13), 1843-1857, [https://doi.org/10.1002/\(SICI\)1099-1085\(199909\)13:12/13<1843::AID-](https://doi.org/10.1002/(SICI)1099-1085(199909)13:12/13<1843::AID-)  
726 [HYP879>3.0.CO;2-G](https://doi.org/10.1002/(SICI)1099-1085(199909)13:12/13<1843::AID-HYP879>3.0.CO;2-G), 1999.  
727  
728 Sturm, M., Holmgren, J., and Liston, G.: A seasonal snow cover classification system for local to global  
729 applications, *J. Clim.*, 8, 1261-1283, [https://doi.org/10.1175/1520-0442\(1995\)008<1261:ASSCCS>2.0.CO;2](https://doi.org/10.1175/1520-0442(1995)008<1261:ASSCCS>2.0.CO;2), 1995.

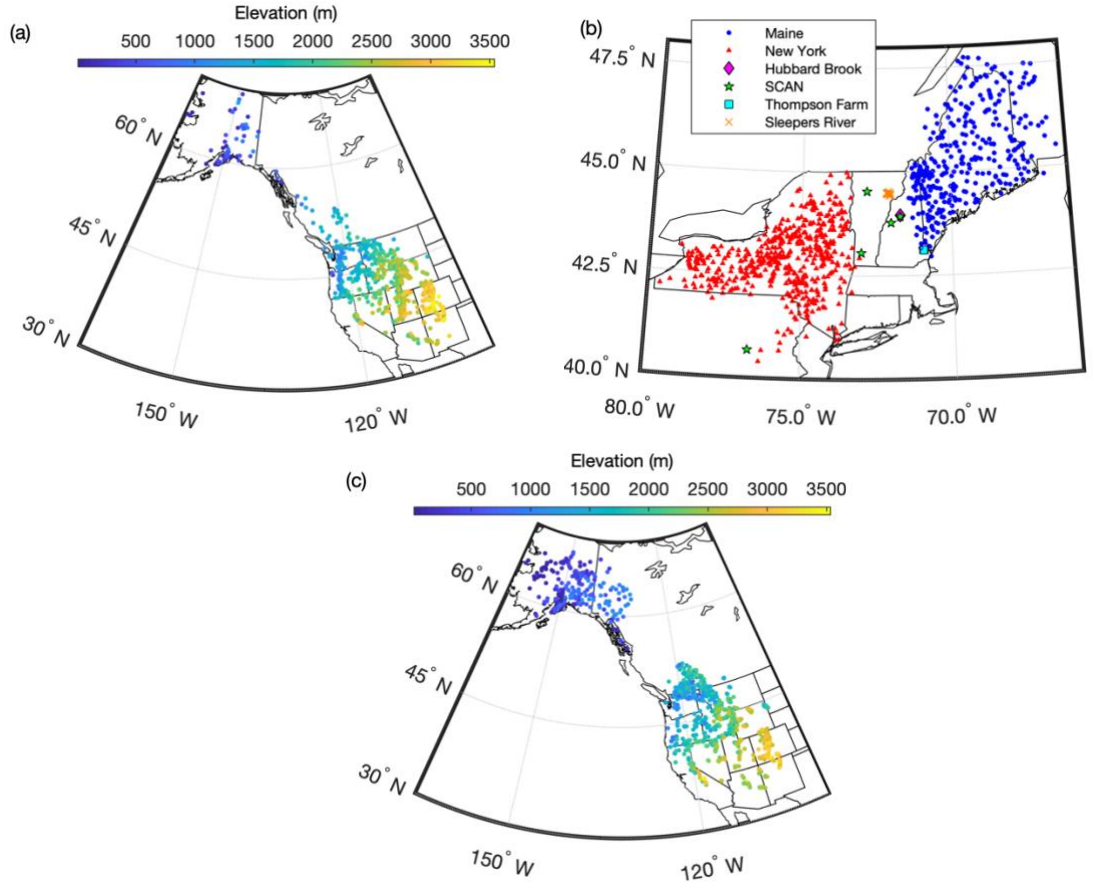
730  
731 Sturm, M., Taras, B., Liston, G.E., Derksen, C., Jonas, T., and Lea, J.: Estimating snow water equivalent using snow  
732 depth data and climate classes, *J. Hydrometeorol.*, 11, 1380-1394, <https://doi.org/10.1175/2010JHM1202.1>, 2010.  
733  
734 U.S. Army Corps of Engineers: Snow hydrology: Summary report of the snow investigations of the North Pacific  
735 Division, 437pp., 1956.  
736  
737 U.S. Department of Agriculture: The History of Snow Survey and Water Supply Forecasting. Interviews With U.S.  
738 Department of Agriculture Pioneers, D. Helms, S. Phillips and P. Reich (eds.), Natural Resources Conservation  
739 Service, 2008.  
740  
741 U.S. Department of Agriculture: Snow Survey and Water Supply Forecasting. National Engineering Handbook Part  
742 622, Water and Climate Center, Natural Resources Conservation Service, 2011.  
743  
744 Wang, T., Hamann, A., Spittlehouse, D.L., and Murdock, T.: ClimateWNA - High-Resolution Spatial Climate Data  
745 for Western North America, *J. Appl. Meteorol. Climatol.*, 51, 16-29, <https://doi.org/10.1175/JAMC-D-11-043.1>,  
746 2012.  
747  
748 Wang, T., Hamann, A., Spittlehouse, D.L., and Carroll, C: Locally downscaled and spatially customizable climate  
749 data for historical and future periods for North America, *PLoS One*, 11, DOI:10.1371/journal.pone.0156720.  
750  
751 Wigmosta, M.S., Vail, L., and Lettenmaier, D.: A distributed hydrology-vegetation model for complex  
752 terrain, *Water Resour. Res.*, 30, 1665-1679, <https://doi.org/10.1029/94WR00436>, 1994

753 Figure 1: Conceptual sketch of the evolution of snow water equivalent (SWE) over the course of a water year (black  
754 line). Also shown is the evolution of SWE with snowpack depth over a water year (red line). Note the hysteresis  
755 loop due to the densification of the snowpack.



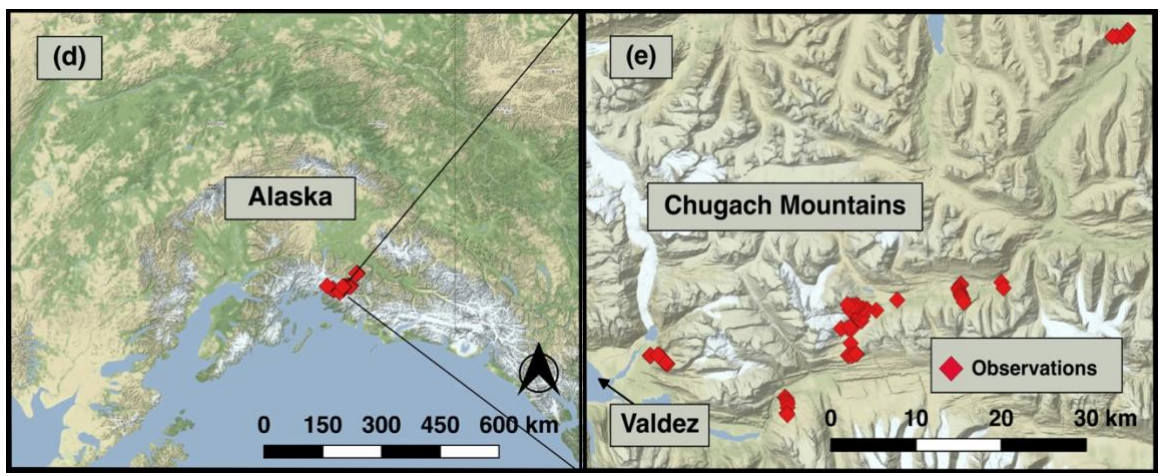
756

757 Figure 2: Distribution of measurement locations used in this study. (a) Western USA and Canada snow pillow  
 758 locations, with colors indicating station elevation in meters. (b) Northeast USA snow pillow and snow course  
 759 locations, with stations colored according to data source. (c) Western North America snow course and aerial marker  
 760 locations, with colors indicating station elevation in meters. (d, e) Measurement sites in the Chugach Mountains,  
 761 southcentral Alaska.  
 762



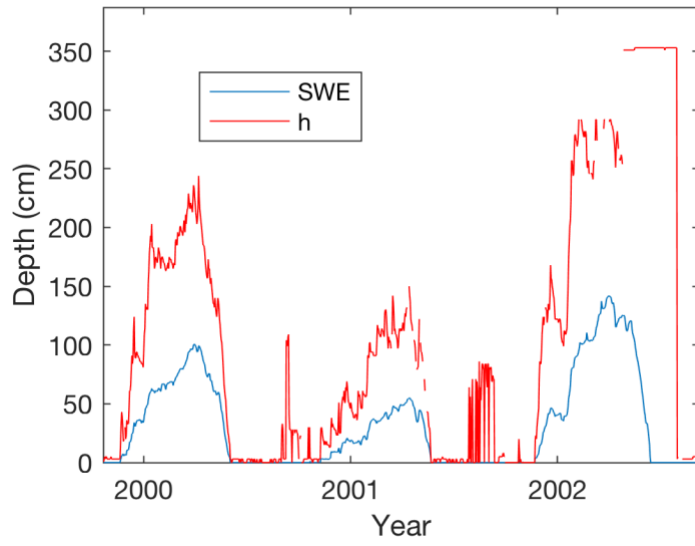
763

764



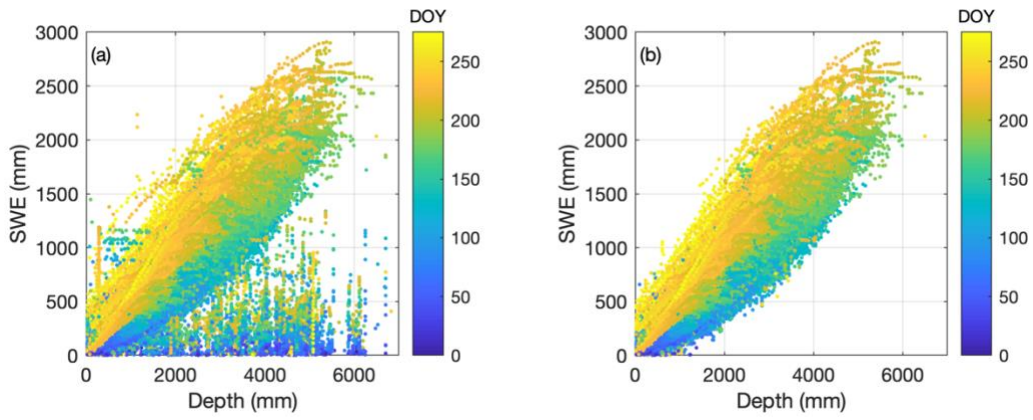
765

766 Figure 3: Sample time series of SWE and  $h$  from the Rex River (WA) SNOTEL station. Observations of  $h$  at times  
767 when SWE is zero are likely spurious.



768

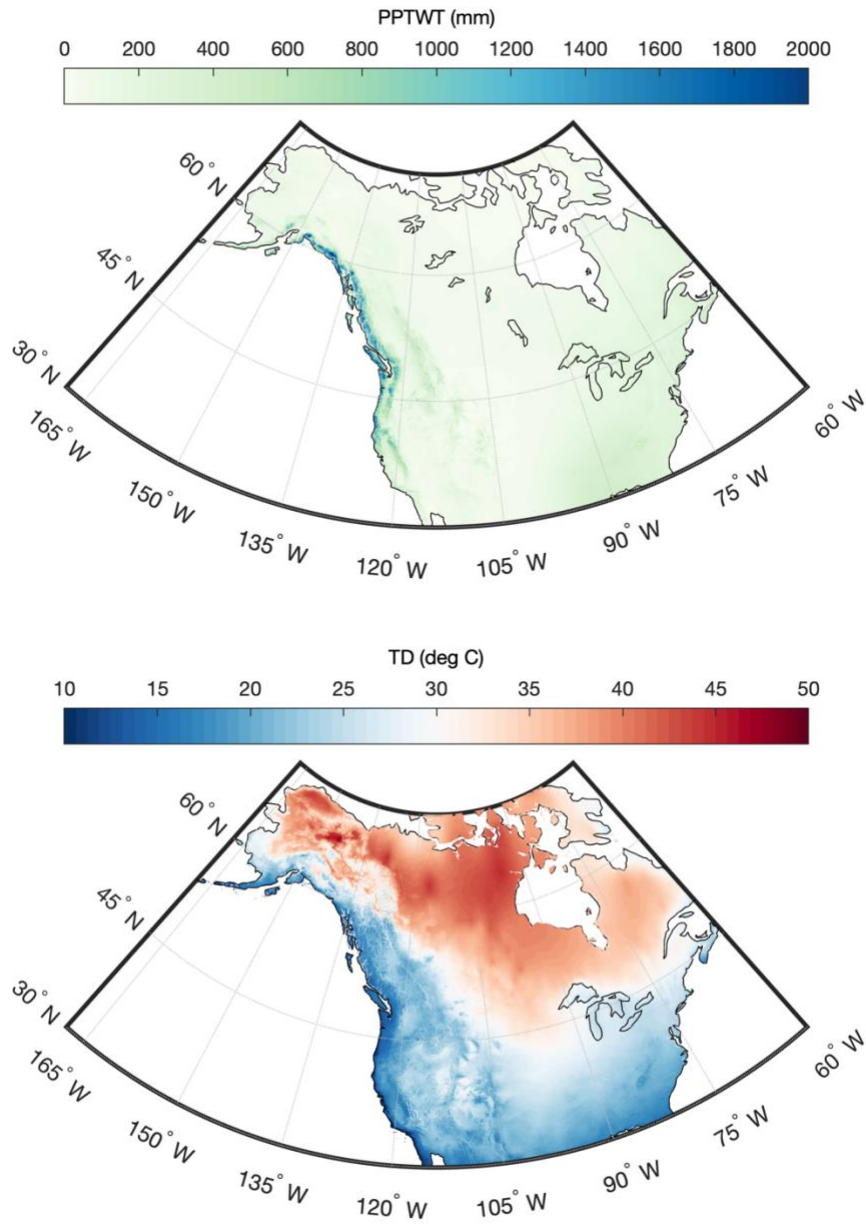
769 Figure 4: Scatter plot of SWE vs.  $h$  for the complete SNOTEL dataset before (a) and after (b) removing data points,  
770 following the method described in Section 2.1.1.5. Symbols are colored by 'day of water year' ( $DOY$ ; October 1 is  
771 the origin).  
772



773

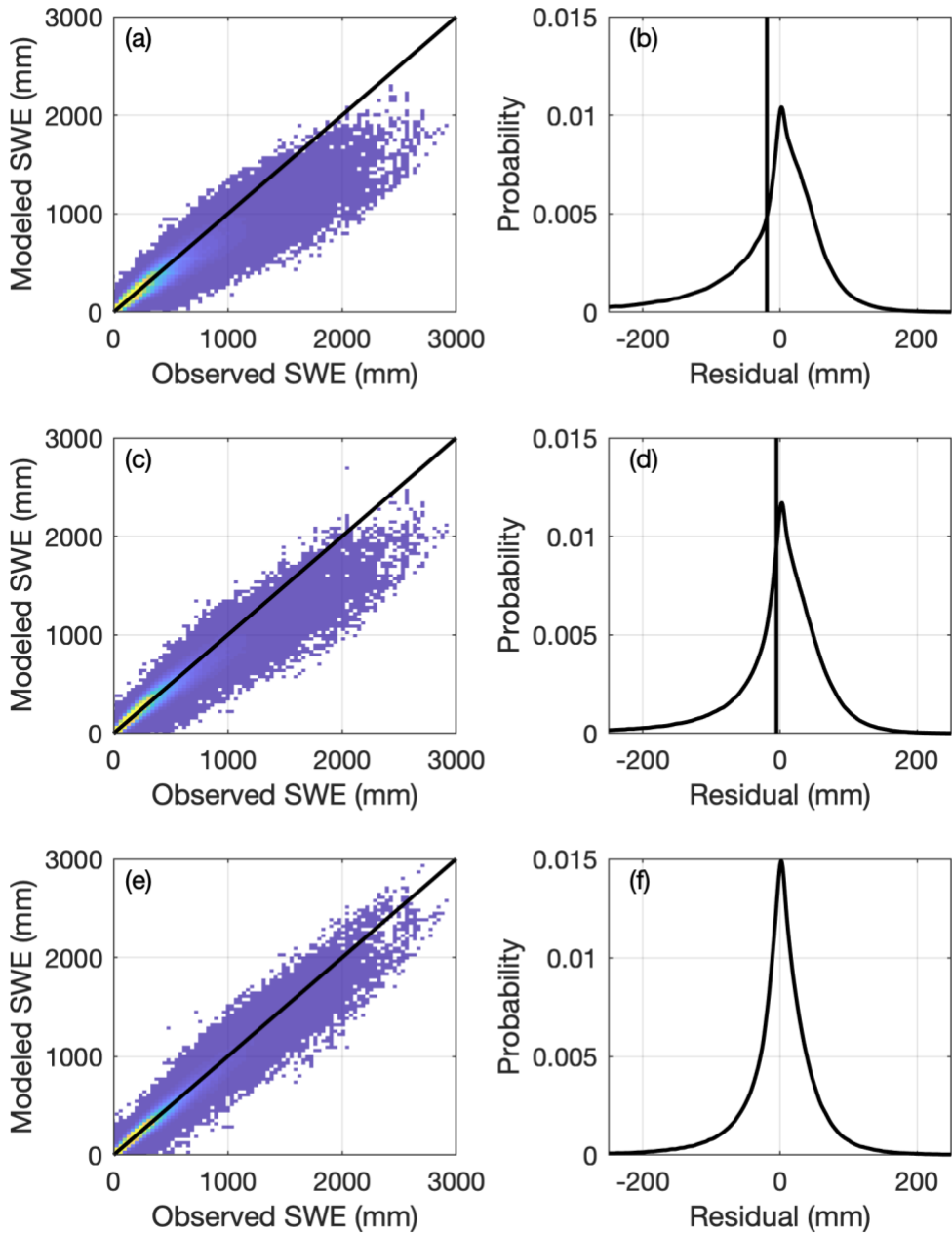


774 Figure 5: Gridded maps of winter (December, January, February) precipitation (PPTWT) and temperature difference  
775 (TD) between mean of warmest month and mean of coldest month) for North America. Maps are for the 1981-2010  
776 climatological period.



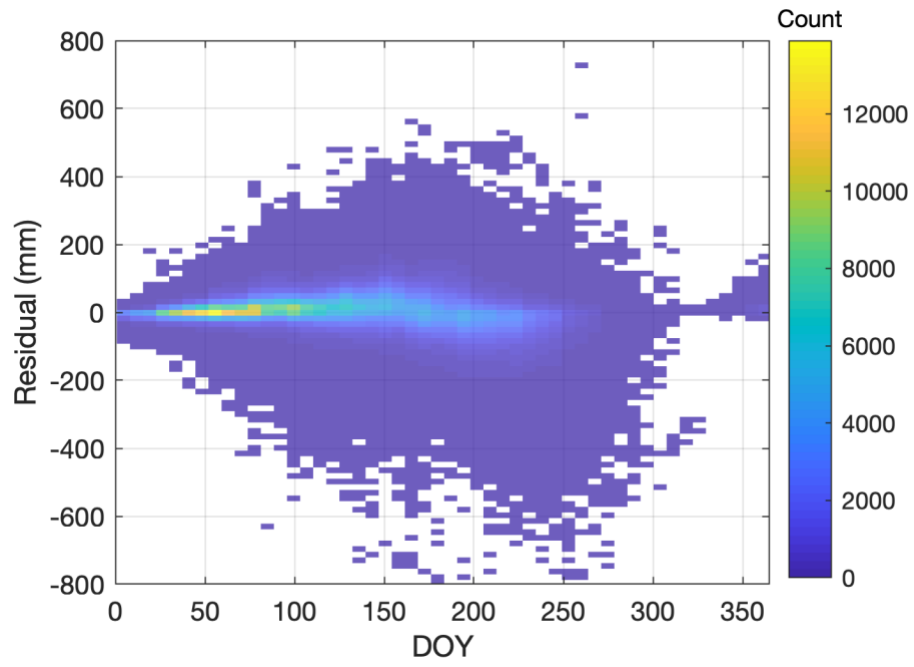
778  
779  
780  
781

782 Figure 6: Two-dimensional histograms (heat maps; left column) of modeled vs. observed SWE and probability  
 783 density functions (right column) of the residuals for three simple models applied to the CONUS, AK, and BC snow  
 784 pillow data. Warmer colors in the heat maps indicate greater density. The vertical lines in the right column indicate  
 785 the location of the mean residual, or bias. Top row (a-b): One-equation model (Section 2.2.1). Middle row (c-d):  
 786 Two-equation model (Section 2.2.2). Bottom row (e-f): Multi-variable two-equation model (Section 2.2.3).



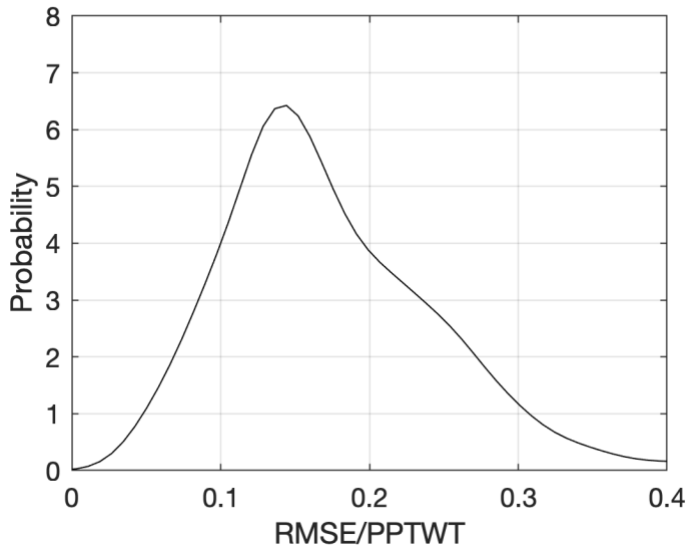
787  
 788

789 Figure 7: Heat map of SWE residuals as a function of *DOY*.  
790



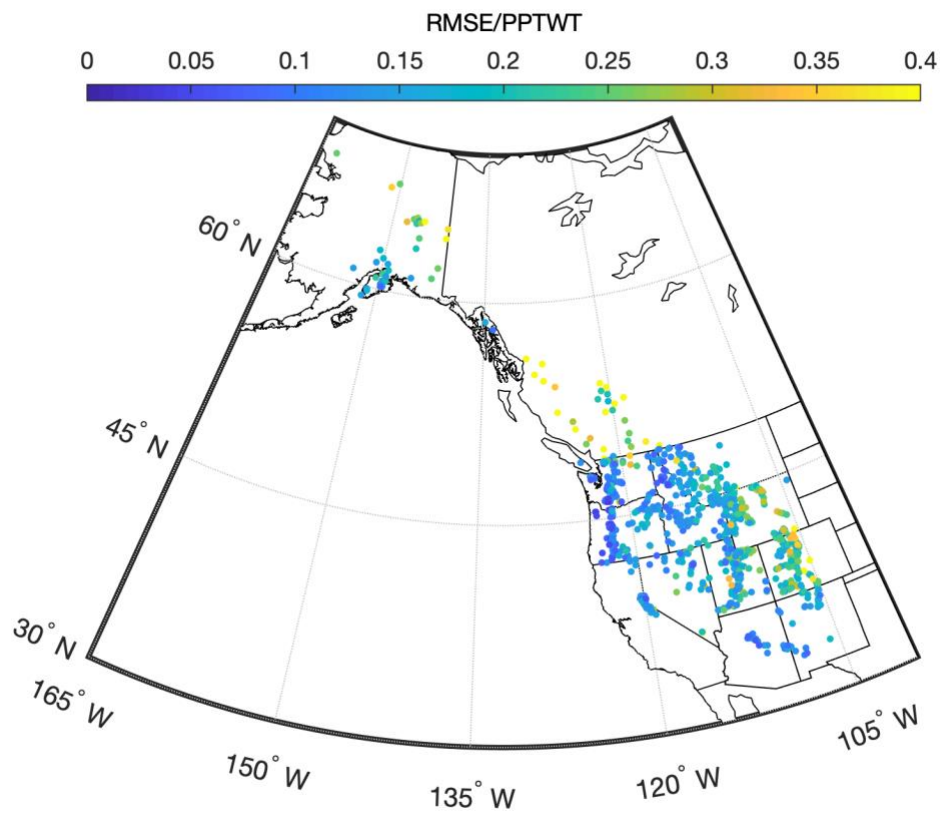
791  
792  
793

794 Figure 8: Probability density function of snow pillow station root-mean-square error (RMSE) normalized by station  
795 winter precipitation (*PPTWT*).



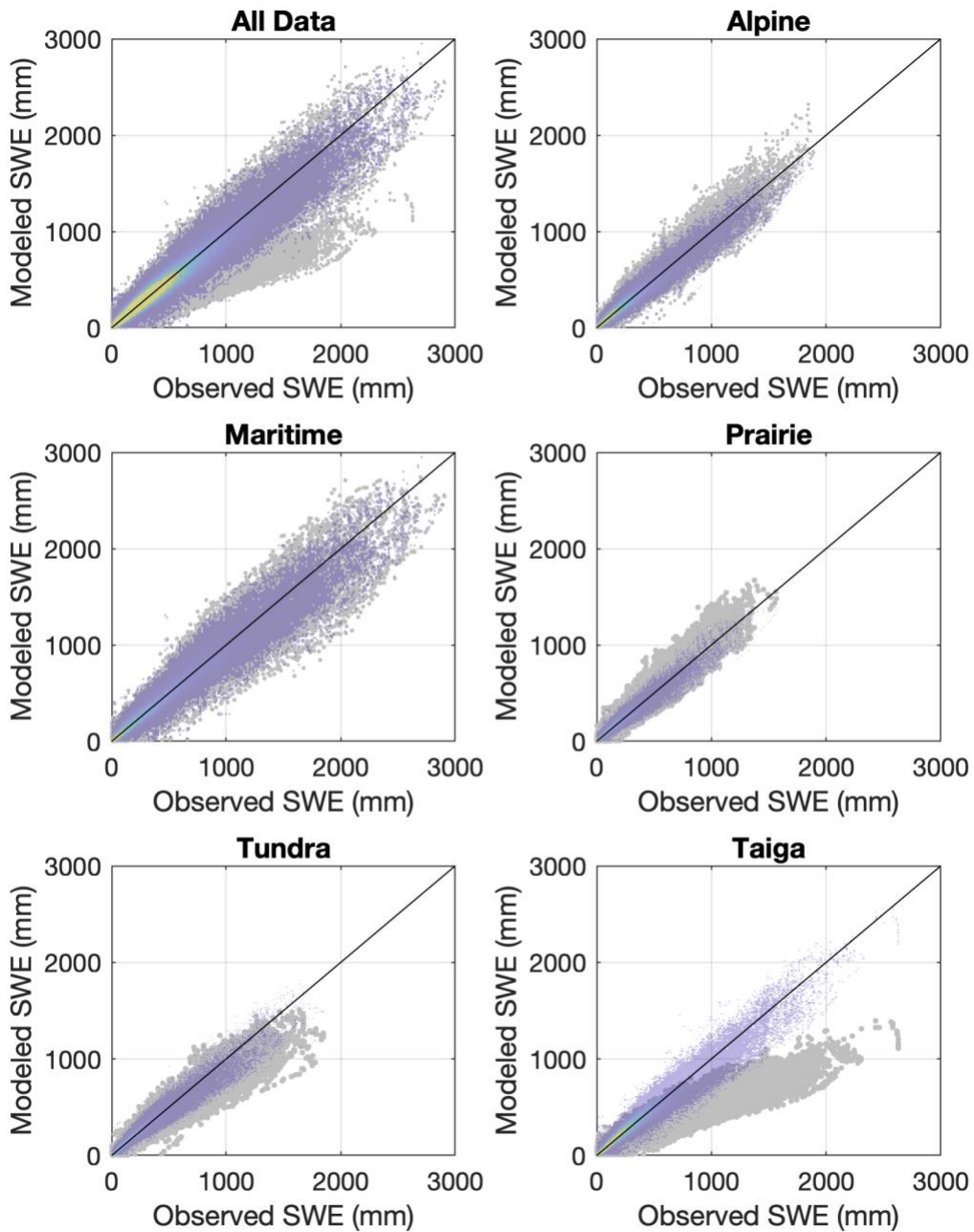
796

797 Figure 9: Spatial distribution of snow pillow station root-mean-square error (RMSE) normalized by station winter  
798 precipitation (PPTWT).



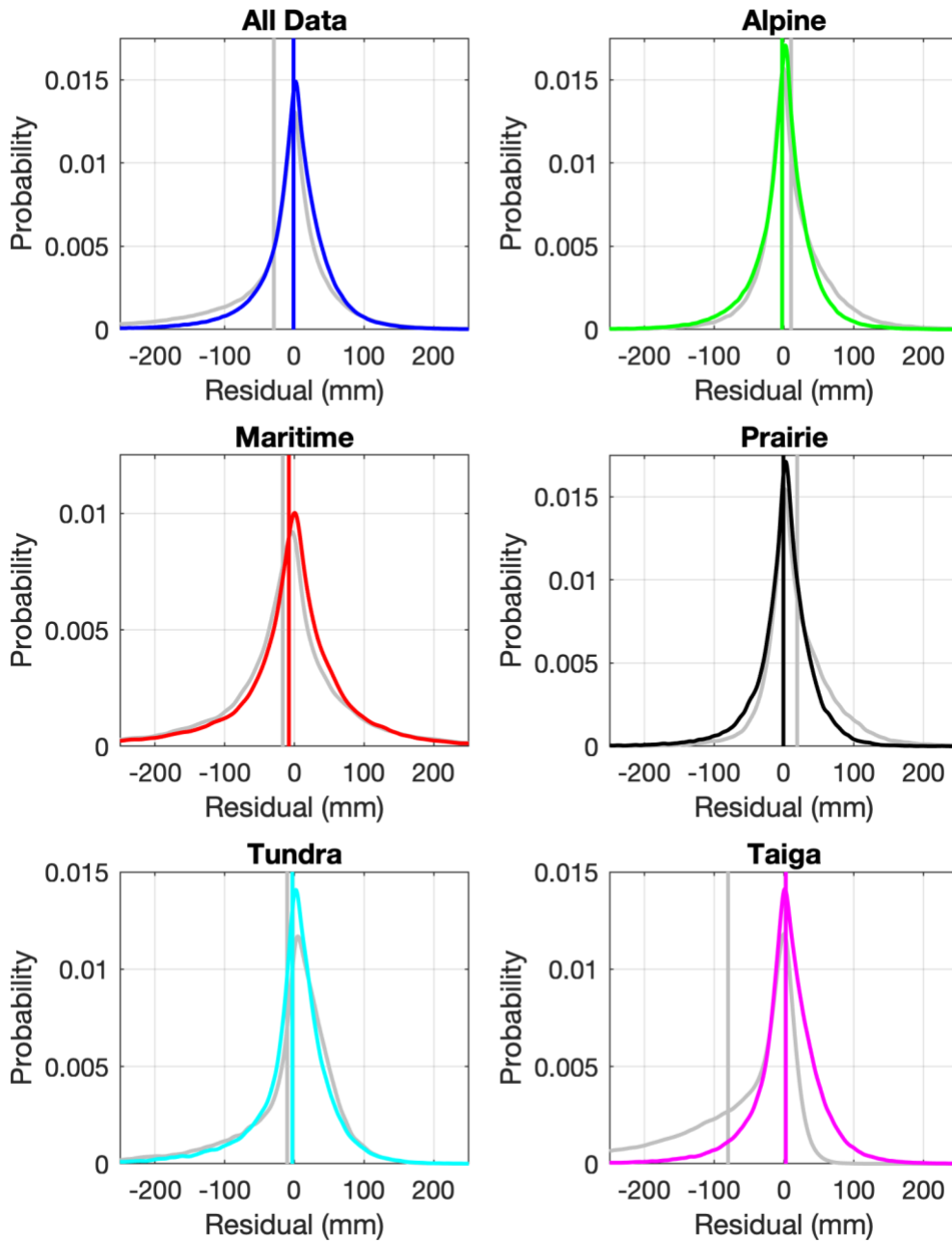
799  
800

801 Figure 10: Comparison of the multi-variable, two-equation model of the current study with the model of Sturm et al.  
802 (2010). The subpanels show modeled SWE vs. observed SWE for all of the data binned together, as well as for the  
803 data broken out by the snow classes identified by Sturm et al. (1995). The gray symbols show the Sturm result and  
804 the transparent heat maps (warmer colors indicate greater density) show the current result. The models are being  
805 applied to the validation data set (50% of the aggregated snow pillow data for CONUS, AK, and BC).  
806



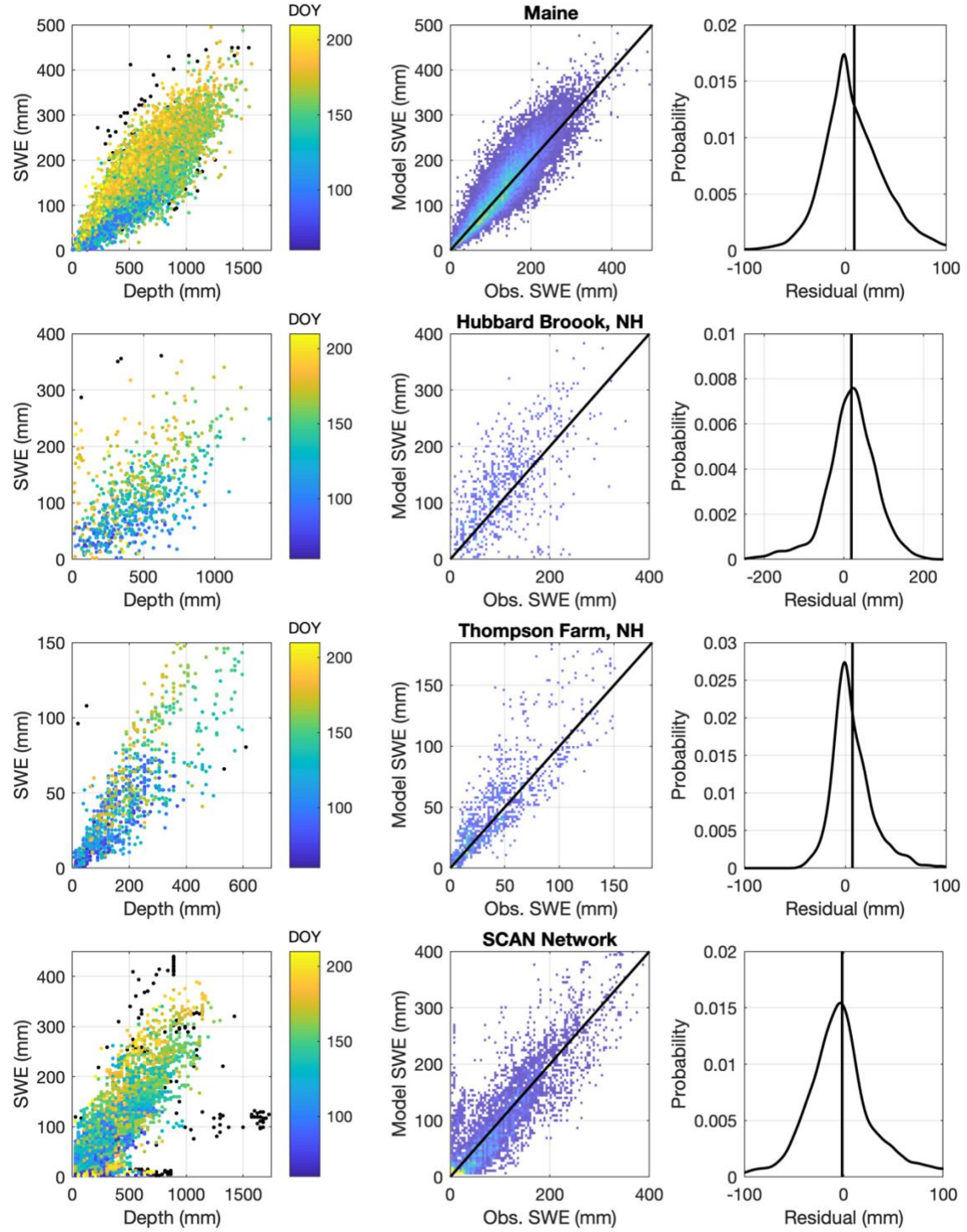
807

808 Figure 11: Comparison of the multi-variable, two-equation model of the current study with the model of Sturm et al.  
809 (2010). The subpanels show probability density functions of the residuals of the model fits for all of the data binned  
810 together, as well as for the data broken out by the snow classes identified by Sturm et al. (1995). The gray lines  
811 show the Sturm result and the colored lines show the current result. The vertical lines show the mean error, or the  
812 model bias, for both the Sturm and the current result. The models are being applied to the validation data set (50% of  
813 the aggregated snow pillow data for CONUS, AK, and BC).  
814



815

816 Figure 12: Results from application of the multi-variable, two-equation model to numerous east coast datasets. The  
 817 left column shows the SWE-*h* data for each dataset. Note that the black symbols are points removed by the outlier  
 818 detection procedure discussed in section 2.1.1.4. The remaining symbols are colored by *DOY*. The middle panel  
 819 plots heat maps of the model estimates of SWE against the observations of SWE with the 1:1 line included. Warmer  
 820 colors indicate higher densities. The right panel shows probability density functions of the model residuals, with the  
 821 vertical line indicating the mean error, or bias. Individual rows correspond to individual data sets and are labeled.



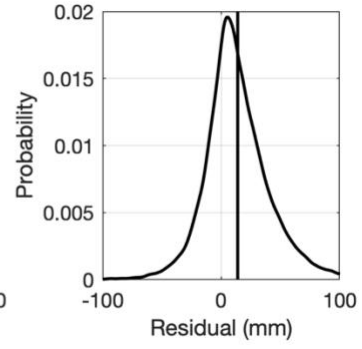
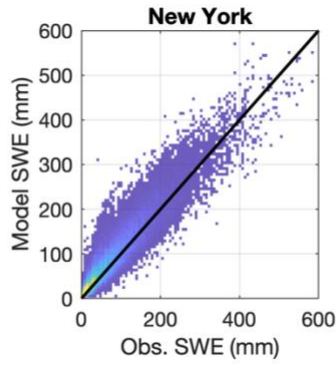
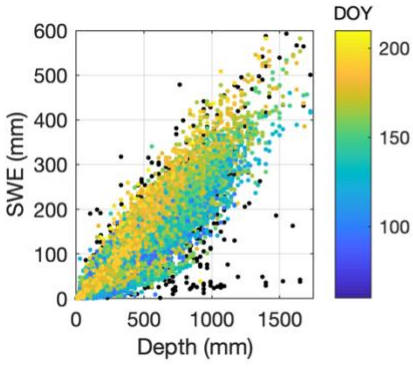
822

823

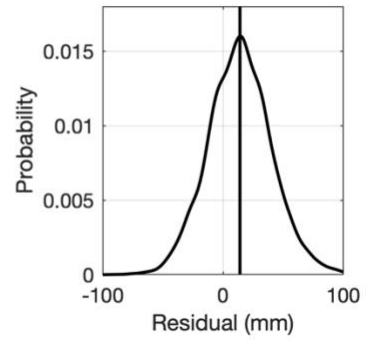
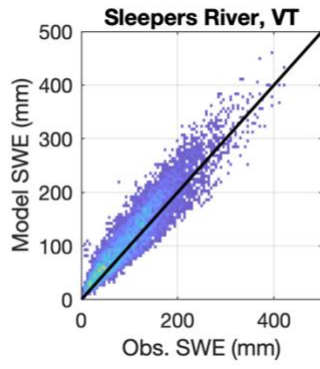
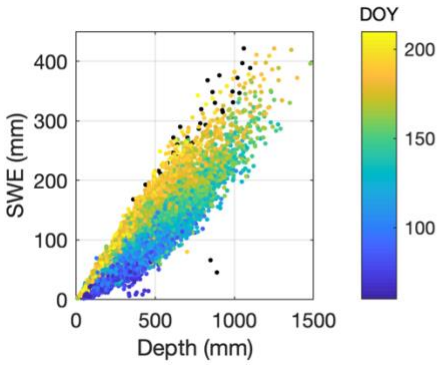
824

825





826

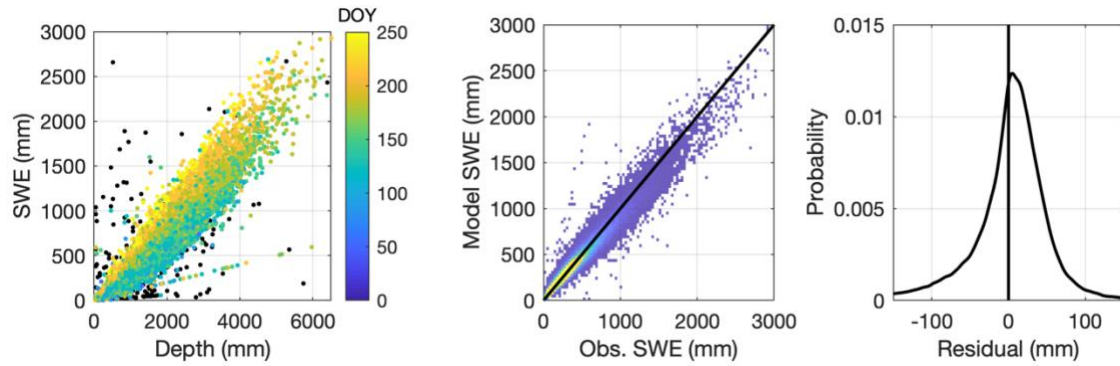


827

828

829

830 Figure 13: Results from application of the multi-variable, two-equation model to the NRCS snow course / aerial  
831 marker dataset. The left column shows the SWE-*h* data for each dataset. Note that the black symbols are points  
832 removed by the outlier detection procedure discussed in section 2.1.1.5. The remaining symbols are colored by  
833 *DOY*. The middle panel plots heat maps of the model estimates of SWE against the observations of SWE with the  
834 1:1 line included. Warmer colors indicate higher densities. The right panel shows probability the density function of  
835 the model residuals, with the vertical line indicating the mean error, or bias.  
836



837  
838

# 1 **Converting Snow Depth to Snow Water Equivalent Using** 2 **Climatological Variables**

3  
4 David F. Hill<sup>1</sup>, Elizabeth A. Burakowski<sup>2</sup>, Ryan L. Crumley<sup>3</sup>, Julia Keon<sup>4</sup>, J. Michelle Hu<sup>5</sup>,  
5 Anthony A. Arendt<sup>6</sup>, Katreen Wikstrom Jones<sup>7</sup>, Gabriel J. Wolken<sup>8</sup>

6  
7 <sup>1</sup>Civil and Construction Engineering, Oregon State University, OR, USA

8 <sup>2</sup>Institute for the Study of Earth, Oceans, and Space, University of New Hampshire, NH, USA

9 <sup>3</sup>Water Resources Graduate Program, Oregon State University, OR, USA

10 <sup>4</sup>Civil and Construction Engineering, Oregon State University, OR, USA

11 <sup>5</sup>Civil and Environmental Engineering, University of Washington

12 <sup>6</sup>Applied Physics Laboratory, University of Washington

13 <sup>7</sup>Alaska Division of Geological & Geophysical Surveys, Fairbanks, AK, USA

14 <sup>8</sup>Alaska Division of Geological & Geophysical Surveys, Fairbanks, AK, USA; International Arctic Research Center,  
15 University of Alaska Fairbanks, Fairbanks, AK, USA

16 *Correspondence to:* David F. Hill (david.hill@oregonstate.edu)

17  
18  
19 **Abstract.** We present a simple method that allows snow depth measurements to be converted to snow water  
20 equivalent (SWE) estimates. These estimates are useful to individuals interested in water resources, ecological  
21 function, and avalanche forecasting. They can also be assimilated into models to help improve predictions of total  
22 water volumes over large regions. The conversion of depth to SWE is particularly valuable since snow depth  
23 measurements are far more numerous than costlier and more complex SWE measurements. Our model regresses  
24 SWE against snow depth ( *$h$* ), day of water year (*DOY*) and climatological (30-year normal) values for *winter*  
25 (*December, January, February*) precipitation (*PPTWT*) and the difference (*TD*) between mean temperature of the  
26 *warmest month and mean temperature of the coldest month*, producing a power-law relationship. Relying on  
27 climatological normals rather than weather data for a given year allows our model to be applied at measurement  
28 sites lacking a weather station. Separate equations are obtained for the accumulation and the ablation phases of the  
29 snowpack. The model is validated against a large database of snow pillow measurements and yields a bias in SWE  
30 of less than *2* mm and a root-mean-squared-error (RMSE) in SWE of *less than 60* mm. The model is additionally  
31 validated against *two* completely independent sets of data: *one from western North America, and one* from the  
32 northeast United States. Finally, the results are compared with *three* other models for bulk density that have varying  
33 degrees of complexity and that were built in multiple geographic regions. The results show that the model described  
34 in this paper has the best performance for the validation data sets.

Formatted: Font: Italic

Deleted: mean annual

Formatted: Font: Italic

Deleted: MAP

Formatted: Font: Italic

Deleted: mean February temperature ( $\bar{T}_{mean}$ ),

Deleted: , which introduces 'day of water year' (DOY) as an additional variable

Deleted: 0.5

Deleted: approximately 65

Deleted: When the errors are investigated on a station-by-station basis, the average RMSE is about 5% of the MAP at each station.

Deleted: a

46 **1 Introduction**

47 In many parts of the world, snow plays a leading-order role in the hydrological cycle (USACE, 1956; Mote et al.,  
48 2018). Accurate information about the spatial and temporal distribution of snow water equivalent (SWE) is useful to  
49 many stakeholders (water resource planners, avalanche forecasters, aquatic ecologists, etc.), but can be time  
50 consuming and expensive to obtain.

51  
52 Snow pillows (Beaumont, 1965) are a well-established tool for measuring SWE at fixed locations. Figure 1 provides  
53 a conceptual sketch of the variation of SWE with time over a typical water year. A comparatively long accumulation  
54 phase is followed by a short ablation phase. While simple in operation, snow pillows are relatively large in size and  
55 they need to be installed prior to the onset of the season’s snowfall. This limits their ability to be rapidly or  
56 opportunistically deployed. Additionally, snow pillow installations tend to require vehicular access, limiting their  
57 locations to relatively simple topography. Finally, snow pillow sites are not representative of the lowest or highest  
58 elevation bands within mountainous regions (Molotch and Bales, 2005). In the western United States (USA), the  
59 Natural Resources Conservation Service (NRCS) operates a large network of Snow Telemetry (SNOTEL) sites,  
60 featuring snow pillows. The NRCS also operates the smaller Soil Climate Analysis Network (SCAN) which  
61 provides the only, and very limited, snow pillow SWE measurements in the eastern USA.

62  
63 SWE can also be measured manually, using a snow coring device that measures the weight of a known volume of  
64 snow to determine snow density (Church, 1933). These measurements are often one-off measurements, or in the  
65 case of ‘snow courses’ they are repeated weekly or monthly [as a transect of measurements](#) at a given location. The  
66 simplicity and portability of coring devices expand the range over which measurements can be collected, but it can  
67 be challenging to apply these methods to deep snowpacks due to the [limited](#) length of standard coring devices. Note  
68 that there are numerous different styles of coring devices, including the Adirondack sampler and the Mt. Rose /  
69 Federal sampler (Church and Marr, 1937). [The NRCS operates a large network of snow course sites \(USDA, 2011\)](#)  
70 [in the western United States.](#)

71  
72 There are a number of issues that affect the accuracy of both snow pillow and snow coring measurements. With  
73 coring measurements, if the coring device is not carefully extracted, a portion of the core may fall out of the device.  
74 Or, snow may become compressed in the coring device during insertion. These effects have led to varying  
75 conclusions, with some studies (e.g., Sturm et al., 2010) showing a low SWE bias and other studies (e.g., Goodison,  
76 1978) showing a high SWE bias. As noted by Johnson et al. (2015) a good rule of thumb is that coring devices are  
77 accurate to around  $\pm 10\%$ . Also, studies comparing different styles of snow samplers report statistically different  
78 results, suggesting that SWE measurements are sensitive to the design of the specific coring device, such as the  
79 presence of holes or slots, the device material, etc. (Beaumont and Work, 1963; Dixon and Boon, 2012). With snow  
80 pillows, some studies (e.g., Goodison et al., 1981) note that ice bridging can lead to low biases in measured SWE,  
81 with the snow surrounding the pillow partly supporting the snow over the pillow. Other studies (Johnson and Marks,  
82 2004; Dressler et al., 2006; Johnson et al., 2015) note a more complex situation with SWE under-reported at times,

83 but over-reported at other times. Note that when snow pillow data are evaluated, they are most commonly compared  
84 to coring measurements at the same location.

85

86 All methods of measuring SWE are challenged by the fact that SWE is a depth-integrated property of a snowpack.  
87 This is why the snowpack must be weighed, in the case of a snow pillow, or a core must be extracted from the  
88 surface to the ground. This measurement complexity makes it difficult to obtain SWE information with the spatial  
89 and temporal resolution desired for watershed-scale studies. Other snowpack properties, such as the depth  $h$ , are  
90 much easier to measure. For example, using a graduated device such as a meterstick or an avalanche probe to  
91 measure the depth takes only seconds. Automating depth measurements at a fixed location can easily be done using  
92 low-cost ultrasonic devices (Goodison et al., 1984; Ryan et al., 2008). High-spatial-resolution measurements of  
93 snowpack depth are commonly made with Light Detection and Ranging (LIDAR). One example of this is the  
94 Airborne Snow Observatory program (ASO; Painter et al., 2016). The comparatively high expense of airborne  
95 LIDAR surveys typical limits measurements geographically (to a few basins) and temporally (weekly to monthly  
96 interval).

97

98 Given the relative ease in obtaining depth measurements, it is common to use  $h$  as a proxy for SWE. Figure 1 shows  
99 a conceptual sketch of the variation of SWE with  $h$  over a typical water year. Noting the arrows on the curve, we see  
100 that SWE is multi-valued for each  $h$ . This is due to the fact that the snowpack increases in density throughout the  
101 water year, producing a hysteresis loop in the curve. A large body of literature exists on the topic of how to convert  
102  $h$  to SWE. It is beyond the scope of this paper to provide a full review of these ‘bulk density equations,’ where the  
103 density is given by  $\rho_b = \text{SWE}/h$ . Instead, we refer readers to the useful comparative review by Avanzi et al. (2015).  
104 Here, we prefer to discuss a limited number of previous studies that illustrate the spectrum of methodologies and  
105 complexities that can be used to determine  $\rho_b$  or SWE.

106

107 Many studies express  $\rho_b$  as an increasing function (often linear) of  $h$ . In some cases (e.g., Lundberg et al., 2006) a  
108 second equation is added where  $\rho_b$  attains a constant value when a threshold  $h$  is exceeded. A single linear equation  
109 captures the process of densification of the snowpack during the accumulation phase, but performs poorly during the  
110 ablation phase, where depths are decreasing but densities continue to increase or approach a constant value.

111 Other approaches choose to parameterize  $\rho_b$  in terms of time, rather than  $h$ . Pistocchi (2016) provides a single  
112 equation while Mizukami and Perica (2008) provide two sets of equations, one set each for early and late season.  
113 Each set contains four equations, each of which is applicable to a particular ‘cluster’ of stations. This clustering was  
114 driven by observed densification characteristics and the resulting clusters are relatively spatially discontinuous.

115 Jonas et al. (2009) take the idea of region- (or cluster-) specific equations and extend it further to provide  
116 coefficients that depend on time and elevation as well. They use a simple linear equation for  $\rho_b$  in terms of  $h$  and the  
117 slope and intercept of the equation are given as monthly values, with three elevation bins for each month (36 pairs of  
118 coefficients). There is an additional contribution to the intercept (or ‘offset’) which is region-specific (one of 7  
119 regions).

120

121 These classifications, whether based on region, elevation, or season, are valuable since they acknowledge that all  
122 snow is not equal. McKay and Findlay (1971) discuss the controls that climate and vegetation exert on snow density,  
123 and Sturm et al. (2010) address this directly by developing a snow density equation where the coefficients depend  
124 upon the 'snow class' (5 classes). Sturm et al. (1995) explain the decision tree, based on temperature, precipitation,  
125 and wind speed, that leads to the classification. The temperature metric is the 'cooling degree month' calculated  
126 during winter months only. Similarly, only precipitation falling during winter months was used in the classification.  
127 Finally, given the challenges in obtaining high quality, high-spatial-resolution wind information, vegetation  
128 classification was used as a proxy. Using climatological values (rather than values for a given year), Sturm et al.  
129 (1995) were able to develop a global map of snow classification.

130

131 There are many other formulations for snow density that increase in complexity and data requirements. Meloysund  
132 et al. (2007) express  $\rho_b$  in terms of sub-daily measurements of relative humidity, wind characteristics, air pressure,  
133 and rainfall, as well as  $h$  and estimates of solar exposure ('sun hours'). McCreight and Small (2014) use daily snow  
134 depth measurements to develop their regression equation. They demonstrate improved performance over both Sturm  
135 et al. (2010) and Jonas et al. (2009). However, a key difference between the McCreight and Small (2014) model and  
136 the others listed above is that the former cannot be applied to a single snow depth measurement. Instead, it requires a  
137 continuous time series of depth measurements at a fixed location. Further increases in complexity are found in  
138 energy-balance snowpack models (SnowModel, Liston and Elder, 2006; VIC, Liang et al., 1994, DHSVM,  
139 Wigmosta et al., 1994, others), many of which use multi-layer models to capture the vertical structure of the  
140 snowpack. While the particular details vary, these models generally require high temporal-resolution time series of  
141 many meteorological variables as input.

142

143 Despite the development of multi-layer energy-balance snow models, there is still a demonstrated need for bulk  
144 density formulations and for vertically integrated data products like SWE. Pagano et al. (2009) review the  
145 advantages and disadvantages of energy-balance models and statistical models and describe how the NRCS uses  
146 SWE (from SNOTEL stations) and accumulated precipitation in their statistical models to make daily water supply  
147 forecasts. If SWE information is desired at a location that does not have a SNOTEL station, and is not part of a  
148 modeling effort, then bulk density equations and depth measurements are an excellent choice.

149

150 The present paper seeks to generalize the ideas of Mizukami and Perica (2008), Jonas et al. (2009), and Sturm et al.,  
151 (2010). Specifically, our goal is to regress physical and environmental variables directly into the equations. In this  
152 way, environmental variability is handled in a continuous fashion rather than in a discrete way (model coefficients  
153 based on classes). The main motivation for this comes from evidence (e.g., Fig. 3 of Alford, 1967) that density can  
154 vary significantly over short distances on a given day. Bulk density equations that rely solely on time completely  
155 miss this variability and equations that have coarse (model coefficients varying over either vertical bins or horizontal  
156 grids) spatial resolution may not fully capture it either.

157  
158 Our approach is most similar to Mizukami and Perica (2008), Jonas et al. (2009), and Sturm et al., (2010) in that a  
159 minimum of information is needed for the calculations; we intentionally avoid approaches like Meloyund et al.  
160 (2007) and McCreight and Small (2014). This is because our interests are in converting  $h$  measurements to SWE  
161 estimates in areas lacking weather instrumentation. The following sections introduce the numerous data sets that  
162 were used in this study, outline the regression model adopted, and assess the performance of the model.

## 163 2 Methods

164

### 165 2.1 Data

166

#### 167 2.1.1 Snow Depth and Snow Water Equivalent

168 In this section, we list sources of 1970-present snow data utilized for this study (Table 1). With regards to snow  
169 coring devices, we refer to them using the terminology preferred in the references describing the datasets.

170

##### 171 2.1.1.1 USA NRCS Snow Telemetry and Soil Climate Analysis Networks

172 SNOTEL (Serreze et al., 1999; Dressler et al., 2006) and SCAN (Schaefer et al. 2007) stations in the contiguous  
173 United States (CONUS) and Alaska typically record sub-daily observations of  $h$ , SWE, and a variety of weather  
174 variables (Figure 2a). The periods of record are variable, but the vast majority of stations have a period of record in  
175 excess of 30 years. For this study, data from all SNOTEL sites in CONUS and Alaska and northeast USA SCAN  
176 sites (Figure 2b) were obtained with the exception of sites whose period of record data were unavailable online.  
177 Only stations with both SWE and  $h$  data were retained.

178

##### 179 2.1.1.2 Canada (British Columbia) Snow Survey Data

180 Goodison et al. (1987) note that Canada has no national digital archive of snow observations from the many  
181 independent agencies that collect snow data and that snow data are instead managed provincially. The quantity and  
182 availability of the data vary considerably among the provinces. The Water Management Branch of the British  
183 Columbia (BC) Ministry of the Environment manages a comparatively dense network of Automated Snow Weather  
184 Stations (ASWS) that measure SWE,  $h$ , accumulated precipitation, and other weather variables (Figure 2a). For this  
185 study, data from all British Columbia ASWS sites were initially obtained. As with the NRCS stations, only ASWS  
186 stations with both SWE and  $h$  data were retained.

187

##### 188 **2.1.1.3 USA NRCS Snow Course / Aerial Marker Data**

189 The snow survey program (USDA, 2008) dates to the 1930s and includes a large number of snow course and aerial  
190 marker sites (Figure 2c) in western North America. While the measurement frequency is variable, it is most  
191 commonly monthly. To generate a dataset for this study, data were extracted using the National Water and Climate

Deleted: -b

Formatted: Font: Bold

193 [Center Report Generator 2.0](#). This allows filtering by time period, elevation band, and other elements. All sites with  
194 data between 1980-2018 were included (Figure 2c).

#### 196 2.1.1.4 Northeast USA Data

197 In addition to the data from the SCAN sites, snow data for this project from the northeast US come from two  
198 networks and three research sites (Figure 2b). The Maine Cooperative Snow Survey (MCSS, 2018) network  
199 includes  $h$  and SWE data collected by the Maine Geological Survey, the United States Geological Survey, and  
200 numerous private contributors and contractors. MCSS snow data are collected using the Standard Federal or  
201 Adirondack snow sampling tubes typically on a weekly to bi-weekly schedule throughout the winter and spring,  
202 1951-present. The New York Snow Survey network data were obtained from the National Oceanic and Atmospheric  
203 Administration's Northeast Regional Climate Center at Cornell University (NYSS, 2018). Similar to the MCSS,  
204 NYSS data are collected using Standard Federal or Adirondack snow sampling tubes on weekly to bi-weekly  
205 schedules, 1938-present.

206  
207 The Sleepers River, Vermont Research Watershed in Danville, Vermont (Shanley and Chalmers, 1999) is a USGS  
208 site that includes 15 stations with long-term weekly records of  $h$  and SWE collected using Adirondack snow tubes.  
209 Most of the periods of record are 1981-present, with a few stations going back to the 1960s. The sites include  
210 topographically flat openings in conifer stands, old fields with shrub and grass, a hayfield, a pasture, and openings in  
211 mixed softwood-hardwood forests. The Hubbard Brook Experiment Forest (Campbell et al., 2010) has collected  
212 weekly snow observations at the Station 2 rain gauge site, 1959-present. Measurement protocol collects ten samples  
213 2 m apart along a 20 m transect in a hardwood forest opening about  $\frac{1}{4}$  hectare in size. At each sample location along  
214 the transect,  $h$  and SWE are measured using a Mt. Rose snow tube and the ten samples are averaged for each  
215 transect. Finally, the Thompson Farm Research site includes a mixed hardwood forest site and an open pasture site  
216 (Burakowski et al. 2013; Burakowski et al. 2015). Daily (from 2011-2018), at each site, a snow core is extracted  
217 with an aluminum tube and weighed (tube + snow) using a digital hanging scale. The net weight of the snow is  
218 combined with the depth and the tube diameter to determine  $\rho_b$ , similar to a Federal or Adirondack sampler.

#### 220 2.1.1.5 Chugach Mountains (Alaska) Data

221 In the spring of 2018, we conducted three weeks of fieldwork in the Chugach mountains in coastal Alaska, near the  
222 city of Valdez (Figure 2d-e). We measured  $h$  using an avalanche probe at 71 sites along elevational transects during  
223 March, April, and May. The elevational transects ranged between 250 and 1100 m (net change along transect) and  
224 were accessible by ski and snowshoe travel. At each site, we measured  $h$  in 8 locations within the surrounding 10  
225 m<sup>2</sup>, resulting in a total of 550+ snow depth measurements. These 71 sites were scattered across 8 regions in order to  
226 capture spatial gradients that exist in the Chugach mountains as the wetter, more-dense maritime snow near the coast  
227 gradually changes to drier, less dense snow on the interior side.

Deleted: 3

Deleted: 4

Deleted: c-d



232 **2.1.1.5 Data Pre-Processing**

233 Figure 3 demonstrates that it is not uncommon for automated snow pillow measurements to become noisy or non-  
234 physical, at times reporting large depths when there is no SWE reported. This is different from instances when  
235 physically plausible, but very low densities might be reported; say in response to early season dry, light snowfalls. It  
236 was therefore desirable to apply some objective, uniform procedure to each station's dataset in order to remove clear  
237 outlier points, while minimizing the removal of valid data points. We recognize that there is no accepted  
238 standardized method for cleaning bivariate SWE-*h* data sets. While Serreze et al. (1999) offer a procedure for  
239 SNOTEL data in their appendix, it is relevant only for precipitation and SWE values, not *h*. Given the strong  
240 correlation between *h* and SWE, we instead choose to use common outlier detection techniques for bivariate data.

241  
242 The Mahalanobis distance (MD; Maesschalck et al., 2000) quantifies how far a point lies from the mean of a  
243 bivariate distribution. The distances are in terms of the number of standard deviations along the respective principal  
244 component axes of the distribution. For highly correlated bivariate data, the MD can be qualitatively thought of as a  
245 measure of how far a given point deviates from an ellipse enclosing the bulk of the data. One problem is that the MD  
246 is based on the statistical properties of the bivariate data (mean, covariance) and these properties can be adversely  
247 affected by outlier values. Therefore, it has been suggested (e.g., Leys et al., 2018) that a 'robust' MD (RMD) be  
248 calculated. The RMD is essentially the MD calculated based on statistical properties of the distribution unaffected  
249 by the outliers. This can be done using the Minimum Covariance Determinant (MCD) method as first introduced by  
250 Rousseeuw (1984).

251  
252 Once RMDs have been calculated for a bivariate data set, there is the question of how large an RMD must be in  
253 order for the data point to be considered an outlier. For bivariate normal data, the distribution of the square of the  
254 RMD is  $\chi^2$  (Gnanadesikan and Kettenring, 1972), with *p* (the dimension of the dataset) degrees of freedom. So, a  
255 rule for identifying outliers could be implemented by selecting as a threshold some arbitrary quantile (say 0.99) of  
256  $\chi_p^2$ . For the current study, a threshold quantile of 0.999 was determined to be an appropriate compromise in terms of  
257 removing obviously outlier points, yet retaining physically plausible results.

258  
259 A scatter plot of SWE vs. *h* for the SNOTEL dataset from CONUS and AK reveals many non-physical points,  
260 mostly when a very large *h* is reported for a very low SWE (Figure 4a). Approximately 0.7% of the original data  
261 points were removed in the pre-processing described above, creating a more physically plausible scatter plot (Figure  
262 4b). Note that the outlier detection process was applied to each station individually. The distribution of 'day of year'  
263 (*DOY*) values of removed data points was broad, with a mean of 160 and a standard deviation of 65. Note that the  
264 *DOY* origin is 1 October. The same procedure was applied to the BC snow pillow, NRCS snow course, and  
265 northeast USA data sets as well (not shown). Table 1 summarizes useful information about the numerous data sets  
266 described above and indicates the final number of data points retained for each. We acknowledge that our process  
267 inevitably removes some valid data points, but, as a small percentage of an already small 0.7% removal rate, we  
268 judged this to be acceptable.

Deleted: depth

Deleted: source

Deleted:

272

273 Table 1: Summary of information about the datasets used in this study. Datasets in bold font were used to construct  
274 the regression model. The numbers of stations and data points reflect the post-processed data.

Dataset Name	Dataset Type	Number of retained stations	Number and percentage of retained data points	Precision ( <i>h</i> / SWE)
<b>NRCS SNOTEL</b>	<b>Snow pillow (SWE), ultrasonic (<i>h</i>)</b>	<b>791</b>	<b>1,900,000 (99.3%)</b>	<b>(0.5 in / 0.1 in)</b>
NRCS SCAN	Snow pillow (SWE), ultrasonic ( <i>h</i> )	5	7094 (97.8%)	(0.5 in / 0.1 in)
<b>British Columbia Snow Survey</b>	<b>Snow pillow (SWE), ultrasonic (<i>h</i>)</b>	<b>31</b>	<b>61,000 (97.5%)</b>	<b>(1 cm / 1 mm)</b>
<del>NRCS Snow Survey</del>	<del>Federal sampler / Aerial marker</del>	<del>1085</del>	<del>116,000 (99.6%)</del>	<del>(0.5 in / 0.1 in) for manual sampler (2 in / n/a) for aerial marker</del>
Maine Geological Survey	Adirondack or Federal sampler (SWE and <i>h</i> )	431	28,000 (99.3%)	(0.5 in / 0.5 in)
Hubbard Brook (Station 2), NH	Mount Rose sampler (SWE and <i>h</i> )	1	704 (99.4%)	(0.1 in / 0.1 in)
Thompson Farm, NH	Snow core (SWE and <i>h</i> )	2	988 (99.4%)	0.5 in / 0.5 in)
Sleepers River, VT	Adirondack sampler	14	7214 (99.4%)	(0.5 in / 0.5 in)
New York Snow Survey	Adirondack or Federal sampler (SWE and <i>h</i> )	523	44,614 (98.2%)	(0.5 in / 0.5 in)
Chugach Mountains, AK	Avalanche probe ( <i>h</i> )	71	71 (100%)	(1 cm)

- Formatted: Font: Not Bold
- Formatted: Font: Not Bold
- Formatted: Not Highlight
- Formatted: Font: Not Bold
- Formatted: Not Highlight
- Formatted: Font: Not Bold
- Formatted: Font: Not Bold

275

### 276 2.1.2 Climatological Variables

277 30-year climate normals at 1 km resolution for North America were obtained from the ClimateNA project (Wang et al., 2016). This project provides grids for minimum, maximum, and mean temperature, and total precipitation for a given month. These grids are based on the PRISM normals (Daly et al., 1994) and are available for the periods 1961-1990 and 1981-2010. For this study, the more recent climatology was used. The ClimateNA project also provides a wide array of derived bioclimatic variables, such as precipitation as snow (PAS), frost-free-period (FFP), mean annual relative humidity (RH) and others. Wang et al. (2012) summarize these additional variables and how they are derived. Figure 5 shows gridded maps of winter (sum of December, January, February) precipitation (PPTWT) and the temperature difference (TD) between the mean temperature of the warmest month and the mean temperature of the coldest month. The latter variable (TD) is a measure of continentality.

- Deleted: 800
- Deleted: (nominal)
- Deleted: CONUS
- Deleted: and for the period 1981-2010
- Formatted: Font: Italic
- Formatted: Font: Italic
- Formatted: Font: Italic
- Formatted: Font: Italic
- Formatted: Font: Italic
- Formatted: Font: Italic

### 287 2.2 Regression Model

288 In order to demonstrate the varying degrees of influence of explanatory variables, several regression models were  
289 constructed. In each case, the model was built by randomly selecting 50% of the paired SWE-*h* measurements from  
290 the aggregated CONUS, AK, and BC snow pillow datasets. The model was then validated by applying it to the

- Deleted: PRISM website (Daly et al., 1994). PRISM normals for British Columbia (BC), Canada, were obtained from the ClimateBC project (Wang et al., 2012), also for the 1981-2010 period. Finally, PRISM normals for Alaska (AK) were obtained from the Integrated Resource Management Applications (IRMA) Portal run by the National Park Service. The AK normals are for the 1971-2000 period and have a slightly coarser resolution (approximately 1.5 km). Figure 5 shows gridded maps of mean annual precipitation (MAP) and mean February Temperature (T<sub>F</sub>) for these three climate products, plotted together. Other temperature products (max and min temperatures; other months) were obtained as well, but are not shown.

308 remaining 50% of the dataset and comparing the modeled SWE to the observed SWE for those points. We  
309 constructed a second version of the regression models by randomly selecting 50% of the snow pillow stations and  
310 using all of the data from those stations. The model was then validated by applying it to the data from the remaining  
311 50% of the stations. These two methods provided identical results, likely due to the very large sample size (N) of our  
312 dataset. In all cases, the p values from the linear regression were 0, again due to the large sample size. Additional  
313 validation was done with the northeast USA datasets (SCAN snow pillow and various snow coring datasets) and the  
314 NRCS snow course dataset, which were completely left out of the model building process.

### 316 2.2.1 One-Equation Model

317 The simplest equation, and one that is supported by the strong correlation seen in the portions of Figure 3 when  
318 SWE is present, is one that expresses SWE as a function of  $h$ . A linear model is attractive in terms of simplicity, but  
319 this limits the snowpack to a constant density. An alternative is to express SWE as a power law, i.e.,

$$321 (1) \quad SWE = Ah^{a_1}.$$

322 This equation can be log-transformed into

$$325 (2) \quad \log_{10}(SWE) = \log_{10}(A) + a_1 \log_{10}(h)$$

326 which immediately allows for simple linear regression methods to be applied. With both  $h$  and SWE expressed in  
327 units of mm, the obtained coefficients are  $(A, a_1) = (0.146, 1.102)$ . Information on the performance of the model  
328 will be deferred until the results section.

### 331 2.2.2 Two-Equation Model

332 Recall from Figures 1 and 4 that there is a hysteresis loop in the SWE- $h$  relationship. During the accumulation  
333 phase, snow densities are relatively low. During the ablation phase, the densities are relatively high. So, the same  
334 snowpack depth is associated with two different SWEs, depending upon the time of year. The regression equation  
335 given above does not resolve this difference. This can be addressed by developing two separate regression  
336 equations, one for the accumulation (*acc*) and one for the ablation (*abl*) phase. This approach takes the form

$$338 (3) \quad SWE_{acc} = Ah^{a_1}; \quad DOY < DOY^*$$

$$340 (4) \quad SWE_{abl} = Bh^{b_1}; \quad DOY \geq DOY^*$$

341 where  $DOY$  is the number of days from the start of the water-year, and  $DOY^*$  is the critical or dividing day-of-water-  
342 year separating the two phases. Put another way,  $DOY^*$  is the day of peak SWE. Interannual variability results in a  
343 range of  $DOY^*$  for a given site. Additionally, some sites, particularly the SCAN sites in the northeast USA,

Deleted: (October 1 is the origin),

346 demonstrate multi-peak SWE profiles in some years. To reduce model complexity, however, we investigated the use  
 347 of a simple climatological (long term average) value of  $DOY^*$  at each site. For each snow pillow station, the average  
 348  $DOY^*$  was computed over the period of record of that station. Analysis of all of the stations revealed that this  
 349 average  $DOY^*$  was relatively well correlated with the climatological mean April maximum temperature (the average  
 350 of the daily maximums recorded in April;  $R^2 = 0.7$ ). However, subsequent regression analysis demonstrated that the  
 351 SWE estimates were relatively insensitive to  $DOY^*$  and the best results were actually obtained when  $DOY^*$  was  
 352 uniformly set to 180 for all stations. Again, with both SWE and  $h$  in units of mm, the regression coefficients turn out  
 353 to be  $(A, a_1) = (0.150, 1.082)$  and  $(B, b_1) = (0.239, 1.069)$ .

354  
 355 As these two equations are discontinuous at  $DOY^*$ , they are blended smoothly together to produce the final two-  
 356 equation model

357  
 358 (5) 
$$SWE = SWE_{acc} \frac{1}{2} (1 - \tanh[0.01\{DOY - DOY^*\}]) +$$
  
 359 
$$SWE_{abl} \frac{1}{2} (1 + \tanh[0.01\{DOY - DOY^*\}])$$

360  
 361 The coefficient 0.01 in the tanh function controls the width of the blending window and was selected to minimize  
 362 the root mean square error of the model estimates.

363  
 364 **2.2.3 Two-Equation Model with Climate Parameters**

365 A final model was constructed by incorporating climatological variables. Again, the emphasis in this study is on  
 366 methods that can be implemented at locations lacking the time series of weather variables that might be available at  
 367 a weather or SNOTEL station. Climatological normals are unable to account for interannual variability, but they do  
 368 preserve the high spatial gradients in climate that can lead to spatial gradients in snowpack characteristics. Stepwise  
 369 linear regression was used to determine which variables to include in the regression. The initial list of potential  
 370 variables included was

371  
 372 (6) 
$$SWE = f(h, z, PPTWT, PAS, TWT, TD, DOY, RH)$$

373  
 374 where  $z$  is the elevation (m),  $PPTWT$  is the winter (sum of December, January, February) precipitation (mm),  $PAS$  is  
 375 mean annual precipitation as snow (mm),  $TWT$  is the winter (December, January, February) mean temperature ( $^{\circ}C$ ),  
 376  $TD$  is the difference between the mean temperature of the warmest month and the mean temperature of the coldest  
 377 month ( $^{\circ}C$ ),  $DOY$  is the day of water year, and  $RH$  is the relative humidity (%). In the stepwise regression,  
 378 explanatory variables were accepted only if they improved the adjusted  $R^2$  value by 0.001. The result of the  
 379 regression yielded

380  
 381 (7) 
$$SWE_{acc} = Ah^{a_1} PPTWT^{a_2} TD^{a_3} DOY^{a_4}; \quad DOY < DOY^*$$

Deleted: is

Deleted: , MAP,

Deleted:  $\bar{T}_{Jmin}, \bar{T}_{Jmean}, \bar{T}_{Jmax}, \bar{T}_{Fmin}, \bar{T}_{Fmean}, \bar{T}_{Fmax}, \bar{T}_{Mmin}, \bar{T}_{Mmean}$

Deleted: , MAP is the mean annual precipitation (mm)

Formatted: Font: Italic

Formatted: Font: Italic

Deleted: and the

Deleted: s

Formatted: Font: Italic

Formatted: Font: Italic

Formatted: Font: Italic

Formatted: Font: Italic

Deleted:

Deleted: represent the mean of minimum, mean, and maximum daily values for the months January through April (J, F, M, A). For example,  $\bar{T}_{Jmin}$  is the climatological normal of the average of the daily minimum temperatures observed in January.

394

395 (8)  $SWE_{abl} = Bh^{b_1}PPTWT^{b_2}TD^{b_3}DOY^{b_4}; DOY \geq DOY^*$

396

397 or, in log-transformed format,

398

399 (9)  $log_{10}(SWE_{acc}) = log_{10}(A) + a_1 log_{10}(h) + a_2 log_{10}(PPTWT) +$   
400  $a_3 log_{10}(TD) + a_4 log_{10}(DOY); DOY < DOY^*$

401

402 (10)  $log_{10}(SWE_{abl}) = log_{10}(B) + b_1 log_{10}(h) + b_2 log_{10}(PPTWT) +$   
403  $b_3 log_{10}(TD) + b_4 log_{10}(DOY); DOY \geq DOY^*$

404

405 indicating that only snow depth, winter precipitation, temperature difference, and day of water year were relevant.  
406 Manual tests of model construction with other variables included confirmed that Eqns. (7-8) yielded the best results.

407 These two SWE estimates for the individual (acc and abl) phases of the snowpack were then blended with Eqn. (5)  
408 to produce a single equation for SWE spanning the entire water year. The obtained regression coefficients were

409  $(A, a_1, a_2, a_3, a_4) = (0.0533, 0.9480, 0.1701, -0.1314, 0.2922)$  and  $(B, b_1, b_2, b_3, b_4) = (0.0481, 1.0395,$   
410  $0.1699, -0.0461, 0.1804)$ . The physical interpretation of these coefficients is straightforward. For example, both  $a_2$

411 and  $b_2$  are greater than zero. So, for two locations with equal  $h, DOY,$  and  $TD,$  the location with greater  $PPTWT$  will  
412 have a greater SWE and therefore density. These locations are typically maritime climates with wetter, denser snow.

413 In contrast, both  $a_3$  and  $b_3$  are less than zero. Therefore, for two locations with equal  $h, DOY,$  and  $PPTWT,$  the  
414 location with greater  $TD$  (a more continental climate) will have a lower density, which is again an expected result.

415 These trends are similar in concept to Sturm et al. (2010), whose discrete snow classes (based on climate classes)  
416 indicate which snow will densify more rapidly.

### 417 3 Results

418 A comparison of the three regression models (one-equation model, Eq. (2); two-equation model, Eqs. (3-5); multi-  
419 variable two-equation model, Eqs. (5, 7-8)) is provided in Figure 6. The left column shows scatter plots of modeled  
420 SWE to observed SWE for the validation data set with the 1:1 line shown in black. The right column shows  
421 distributions of the model residuals. The vertical lines in the right column show the mean error, or model bias.

422 Visually, it is clear that the one-equation model performs relatively poorly with a large negative bias. This large  
423 negative bias is partially overcome by the two-equation model (middle row, Figure 6). The cloud of points is closer  
424 to the 1:1 line and the vertical black line indicating the mean error is closer to zero. In the final row of Figure 6, we  
425 see that the multi-variable two-equation model yields the best result by far. The residuals are now evenly distributed  
426 with a small bias. Several metrics of performance for the three models, including  $R^2$  (Pearson coefficient), bias, and  
427 root-mean-square-error (RMSE), are provided in Table 2. Figure 7 shows the distribution of model residuals for the  
428 multi-variable two-equation model as a function of DOY.

429

Deleted: mean annual precipitation

Deleted: and mean February temperature

Deleted: In the above equations, note that an offset is added to the temperature in order to avoid taking the log of a negative number.

Deleted: are

Deleted: 128

Deleted: 1.070

Deleted: 0.132

Deleted: 0.506

Deleted: 271

Deleted: 8

Deleted: 201

Deleted: 310

Deleted: If  $a_1$  and  $b_1$  were equal to unity, then the density, given by  $(SWE/h)$ , would be a constant at a given location. Since they are greater than unity, they capture the effect that snow density increases as depth increases. Turning to the coefficients on the climate variables,

Formatted: Font: Italic

Formatted: Font: Italic

Formatted: Font: Italic

Formatted: Font: Italic

Deleted: equal depth, equal temperature characteristics, but different precipitation characteristics, the regression model predicts that the wetter location (larger  $MAP$ ) will have a greater density

Deleted: Finally

Deleted: , regarding temperature

Deleted: greater

Formatted: Font: Italic

Formatted: Font: Italic

Formatted: Font: Italic

Deleted: equal depth, equal precipitation characteristics, but different temperature characteristics, the regression model predicts that the warmer location (larger  $T_{F_{mean}}$ ) will have a greater density.

Deleted: histograms

Deleted: negligible

462 Table 2: Summary of performance metrics for the three regression models presented in Section 2.2.

Model	R <sup>2</sup>	Bias (mm)	RMSE (mm)
One-equation	0.946	-19.5	102
Two-equation	0.962	-5.1	81
Multi-variable two-equation	0.978	-1.2	59

463  
 464 It is useful to also consider the model errors in a non-dimensional way. Therefore, an RMSE was computed at each  
 465 station location and normalized by the **winter precipitation (PPTWT)** at that location. Figure 8 shows the probability  
 466 density function of these normalized errors. The average RMSE is approximately 15% of **PPTWT** with most values  
 467 falling into the range of 5-30%. The spatial distribution of these normalized errors is shown in Figure 9. For the  
 468 SNOTEL stations, it appears there is a slight regional trend, in terms of stations in continental climates (**Rockies**)  
 469 having **larger** relative errors than stations in maritime climates (Cascades). The British Columbia stations also show  
 470 higher relative errors.  
 471

- Deleted: 2
- Deleted: 0.5
- Deleted: 67
- Deleted: mean annual maximum SWE ( $SWE_{max}$ )
- Formatted: Font: Italic
- Deleted: 1
- Deleted:  $SWE_{max}$ .
- Deleted: 25
- Deleted: northern
- Deleted: smaller

472 **3.1 Results for Snow Classes**

473 A key objective of this study is to regress climatological information in a continuous rather than a discrete way. The  
 474 work by Sturm et al. (2010) therefore provides a valuable point of comparison. In that study, the authors developed  
 475 the following equation for density  $\rho_b$

476  
 477 (11)  $\rho_b = (\rho_{max} - \rho_0)[1 - e^{(-k_1 t - k_2 DOY)}] + \rho_0$   
 478

479 where  $\rho_0$  is the initial density,  $\rho_{max}$  is the maximum or ‘final’ density (end of water year),  $k_1$  and  $k_2$  are coefficients,  
 480 and  $DOY$  in this case begins on January 1. This means that their  $DOY$  for October 1 is -92. The coefficients vary  
 481 with snow class and the values determined by Sturm et al. (2010) are shown in Table 3.  
 482

- Formatted: Font: Italic
- Formatted: Font: Italic

483 Table 3: Model parameters by snow class for Sturm et al. (2010).

Snow Class	$\rho_{max}$	$\rho_0$	$k_1$	$k_2$
Alpine	0.5975	0.2237	0.0012	0.0038
Maritime	0.5979	0.2578	0.0010	0.0038
Prairie	0.5941	0.2332	0.0016	0.0031
Tundra	0.3630	0.2425	0.0029	0.0049
Taiga	0.2170	0.2170	0.0000	0.0000

484  
 485 To make a comparison, the snow class for each SNOTEL and British Columbia snow survey (Rows 1 and 3 of Table  
 486 1) site was determined using a 1-km snow class grid (Sturm et al., 2010). The aggregated dataset from these stations  
 487 was made up of 27% Alpine, 14% Maritime, 10% Prairie, 11% Tundra, and 38% Taiga data points. Equation (11)  
 488 was then used to estimate snow density (and then SWE) for every point in the validation dataset described in Section  
 489 2.2. Figure 10 compares the SWE estimates from the Sturm model and from the **current** multi-variable, two-equation  
 490 model (Equations 5, 7-8). The upper left panel of Figure 10 shows all of the data, and the remaining panels show the  
 491 results for each snow class. In all cases, the current model provides better estimates (**narrow cloud of points: closer**

- Deleted: present

502 to the 1:1 line). Plots of the residuals by snow class are provided in Figure 11, giving an indication of the bias of  
 503 each model for each snow class. Summaries of the model performance, broken out by snow class, are given in Table  
 504 4. The current model has smaller biases and RMSEs for each snow class.  
 505

506 Table 4: Comparison of model performance by Sturm et al. (2010) and the current study.

Model	Sturm et al. (2010)			Multi-variable two-equation model		
	R <sup>2</sup>	Bias (mm)	RMSE (mm)	R <sup>2</sup>	Bias (mm)	RMSE (mm)
All Data	0.928	-29.2	111	0.978	-1.2	59
Alpine	0.973	10.1	55	0.978	-2.7	48
Maritime	0.968	-16.8	109	0.975	-7.8	95
Prairie	0.967	18.7	56	0.971	-0.7	45
Tundra	0.956	-10.5	82	0.974	-2.9	59
Taiga	0.943	-80.0	151	0.978	2.6	54

507  
 508 **3.2 Comparison to Pistocchi (2016)**

509 In order to provide an additional comparison, the simple model of Pistocchi (2016) was also applied to the validation  
 510 dataset. His model calculates the bulk density as

511  
 512 (12)  $\rho_b = \rho_0 + K(DOY + 61),$

513  
 514 where  $\rho_0$  has a value of 200 kg m<sup>-3</sup> and  $K$  has a value of 1 kg m<sup>-3</sup>. The  $DOY$  for this model has its origin at  
 515 November 1. Application of this model to the validation dataset yields a bias of 55 mm and an RMSE of 94 mm.  
 516 These results are comparable to the Sturm et al. (2010) model, with a larger bias but smaller RMSE.

517  
 518 **3.3 Comparison to Jonas et al. (2009)**

519 A final point of comparison can be provided by the model of Jonas et al. (2009). The full version of that model  
 520 contains region-specific offset parameters that are not relevant to North America, so the following partial version of  
 521 the model is used (their Eq. 4):

522  
 523 (13)  $\rho_b = ah + b,$

524  
 525 where the parameters ( $a, b$ ) vary with elevation and month, as given by Table 5. Note that coefficients are not given  
 526 for every month. Application of the Jonas et al. (2009) model to the snow pillow dataset yields a bias of -5 mm and  
 527 an RMSE of 69 mm. These results are not directly comparable to those of the current model (Table 2, row 3) since  
 528 the Jonas et al. (2009) model is unable to compute results for several months of the year. To make a direct  
 529 comparison to the current model, it is necessary to first remove those data points (about 5%). When this is done, the  
 530 current model yields a bias of -0.3 mm and an RMSE of 59 mm.

531  
 532 Table 5: Model coefficients ( $a, b$ ) for the Jonas et al. (2009) model.

Deleted: present

Deleted: 2

Deleted: -0.5

Deleted: 67

Deleted: 1

Deleted: 0.3

Deleted: 55

Deleted: 0

Deleted: 4.5

Deleted: 105

Deleted: 65

Deleted: 2

Deleted: 51

Deleted: 69

Deleted: 6.1

Deleted: 67

Formatted Table

Deleted: 1

Deleted: 4

Deleted: 62

Deleted: one

Formatted: Font: Italic

Formatted: Font: 12 pt, Font color: Auto

Formatted: Normal

Formatted: Font: 10 pt, Bold

Formatted: Not Highlight

Formatted: Normal, Line spacing: single

Month	$z > 2000\text{ m}$	$2000\text{ m} > z > 1400\text{ m}$	$1400\text{ m} > z$
January	(206, 52)	(208, 47)	(235, 31)
February	(217, 46)	(218, 52)	(279, 9)
March	(272, 26)	(281, 31)	(333, 3)
April	(331, 9)	(354, 15)	(347, 25)
May	(378, 21)	(409, 29)	(413, 19)
June	(452, 8)	n/a	n/a
July	(470, 15)	n/a	n/a
August	n/a	n/a	n/a
September	n/a	n/a	n/a
October	n/a	n/a	n/a
November	(206, 47)	(183, 35)	(149, 37)
December	(203, 52)	(190, 47)	(201, 26)

Formatted Table

Formatted: Centered

Formatted: Centered

Formatted: Centered

Formatted: Centered

Formatted: Centered

Deleted: ¶

Formatted: Font color: Auto

Formatted: Line spacing: 1.5 lines

Deleted: 3

Deleted: SNOTEL

Deleted: are

Deleted: ,

Deleted: present

### 3.4 Results for Northeast USA

The regression equations in this study were developed using a large collection of snow pillow sites in CONUS, AK, and BC. The snow pillow sites are limited to locations west of approximately W 105° (Figure 2a). By design, the data sets from the northeastern USA (Section 2.1.1.3) were left as an entirely independent validation set. These northeastern sites are geographically distant from the training data sets, subject to a very different climate, largely use different methods (snow coring, with the exception of the SCAN network) and are generally at much lower elevations than the western sites, providing an interesting opportunity to test how robust the current model is.

Figure 12 graphically summarizes the datasets and the performance of the multi-variable two-equation model of the current study. The RMSE values are comparable to those found for the western stations, but, given the comparatively thinner snowpacks in the northeast, represent a larger relative error (Table 5). The bias of the model is consistently positive, in contrast to the western stations where the bias was negligible. Note that Table 5 also includes results from the application of the other three models discussed. Sturm et al. (2010) cannot be applied to several of the datasets since their available 1 km snowclass dataset cuts off at -71.6° longitude. The current model and the Jonas et al. (2009) model perform better than the other two models, with the current model generally outperforming the Jonas et al. (2009) model. The two datasets where the Jonas et al. (2009) model has a slightly better performance are the two smallest datasets (less than 1000 measurements; see Table 1).

Formatted: Font: Not Italic

Formatted: Font: Not Italic

Table 5: Performance metrics for various models applied to the northeastern USA datasets. Bold font is used to highlight the model with the best performance for each dataset.

Dataset Name	Multi-variable, two-equation model		Sturm et al. (2010)		Jonas et al. (2009)		Pistocchi (2015)	
	Bias (mm)	RMSE (mm)	Bias (mm)	RMSE (mm)	Bias (mm)	RMSE (mm)	Bias (mm)	RMSE (mm)

Deleted: the multi-variable two-equation model

Deleted: various



Maine Geological Survey, ME	<b>13.1</b>	<b>34.0</b>	n/a	n/a	25.1	46.0	59.2	77.1
Hubbard Brook (Station 2), NH	21.8	66.6	34.2	76.9	<b>19.4</b>	<b>65.4</b>	52.0	90.8
Thompson Farm, NH	7.1	<b>20.2</b>	n/a	n/a	<b>5.6</b>	<b>19.9</b>	<b>20.4</b>	<b>32.3</b>
NRCS SCAN	<b>1.2</b>	<b>39.2</b>	8.4	45.0	-2.8	40.6	23.4	56.9
Sleepers River, VT	<b>14.4</b>	<b>28.2</b>	36.5	48.9	20.4	33.5	55.8	67.1
New York Snow Survey	<b>14.8</b>	<b>31.2</b>	21.0	49.3	16.3	33.0	41.3	56.1

### 3.5 Results for NRCS Snow Course / Aerial Marker Data

The NRCS snow course and aerial marker data were also left out of the model building process so they provide an additional and completely independent comparison of the various models considered. Recall that these data come from snow course (coring measurements) and aerial surveys, which are different measurement methods than the snow pillows which provided the data for construction of the current regression model. Table 6 shows the results and demonstrates that the current model has the best performance.

Table 6: Performance metrics for various models applied to the NRCS snow course and aerial marker dataset. Bold font is used to highlight the model with the best performance.

	Multi-variable, two-equation model		Sturm et al. (2010)		Jonas et al. (2009)		Pistocchi (2015)	
Dataset Name	Bias (mm)	RMSE (mm)	Bias (mm)	RMSE (mm)	Bias (mm)	RMSE (mm)	Bias (mm)	RMSE (mm)
NRCS Snow Course / Aerial Marker	<b>0</b>	<b>59</b>	-24	123	24	72	71	99

## 4 Discussion

The results presented in this study show that the regression equation described by equations (5, 7-8) is an improvement (lower bias and RMSE) over other widely used bulk density equations. The key advantage is that the current method regresses in relevant parameters directly, rather than using discrete bins (for snow class, elevation, month of year, etc.), each with its own set of model coefficients. The comparison (Figs. 10-11; Table 4) to the model of Sturm et al. (2010) reveals a peculiar behavior of that model for the Taiga snow class, with a large negative bias in the Sturm estimates. Inspection of the coefficients provided for that class (Table 3) shows that the model simply predicts that  $\rho_b = \rho_{max} = 0.217$  for all conditions.

When our multi-variable two-equation model, developed solely from western North American data, is applied to northeast USA locations, it produces SWE estimates with smaller RSME values and larger biases than the western stations. When comparing the SWE- $h$  scatter plots of the SNOTEL data (Figure 4b) to those of the east coast data sets (left column; Figure 12), it is clear that the northeast data generally have more scatter. This is confirmed by computing the correlation coefficients between SWE and  $h$  for each dataset. It is unclear if this disparity in correlation is related to measurement methodology or is instead a 'signal to noise' issue. Comparing Figures 4 and 12 shows the considerable difference in snowpack depth between the western and northeastern data sets. When the western dataset is filtered to include only measurement pairs where  $h < 1.5$  m, the correlation coefficient is reduced to a value consistent with the northeast datasets. This suggests that the performance of the current (or other) regression model is not as good at shallow snowpack depths. This is also suggested upon examination of the time

Deleted: 8.9

Formatted: Font: Bold

Deleted: 3.3

Deleted: 18.9

Deleted: 64.2

Formatted: Font: Bold

Deleted: 21.6

Formatted: Font: Bold

Formatted: Font: Bold

Deleted: 1.8

Deleted: 8.7

Deleted: 14

Formatted: Font: Bold

Deleted: .0

Deleted: 29.7

Formatted: Font: Not Bold

Formatted: Font: Not Bold

Formatted: Font: Bold

Deleted: 3

Formatted: Font: (Default) Times New Roman, Not Italic, Font color: Text 1

Formatted Table

Deleted: ¶

Deleted: present

Deleted: physical

Deleted: curves

626 series of observed  $\rho_b = SWE/h$  for a given season at a snow pillow site. Very early in the season, when the depths  
627 are small, the density curve has a lot of variability. Later in the season, when depths are greater, the density curve  
628 becomes much smoother. Very late in the season, when depths are low again, the density curve becomes highly  
629 variable again.

630

631 Measurement precision and accuracy affect the construction and use of a regression model. Upon inspection of the  
632 snow pillow data, it was observed that the precision of the depth measurements was approximately 25 mm and that  
633 of the SWE measurements was approximately 2.5 mm. To test the sensitivity of the model coefficients to the  
634 measurement precision, the depth values in the training dataset were randomly perturbed by +/- 25 mm and the SWE  
635 values were randomly perturbed by +/- 2.5 mm and the regression coefficients were recomputed. This process was  
636 repeated numerous times and the mean values of the perturbed coefficients were obtained. These adjusted  
637 coefficients were then used to recompute the SWE values for the validation data set and the bias and RMSE were  
638 found to be -10.5 mm and 72.7 mm. This represents a roughly 10% increase in RMSE, but a considerable increase in  
639 bias magnitude (see Table 4 for the original values). This sensitivity of the regression analysis to measurement  
640 precision underscores the need to have high-precision measurements for the training data set. Regarding accuracy,  
641 random and systematic errors in the paired SWE -  $h$  data used to construct the regression model will lead to  
642 uncertainties in SWE values predicted by the model. As noted in the introduction, snow pillow errors in SWE  
643 estimates do not follow a simple pattern. Additionally, they are complicated by the fact that the errors are often  
644 computed by comparing snow pillow data to coring data, which itself is subject to error. Lacking quantitative  
645 information on the distribution of snow pillow errors, we are unable to quantify the uncertainty in the SWE  
646 estimates.

647

648 Another important consideration has to do with the uncertainty of depth measurements that the model is applied to.  
649 For context, one application of this study is to crowd-sourced, opportunistic snow depth measurements from  
650 programs like the Community Snow Observations (CSO; Hill et al., 2018) project. In the CSO program,  
651 backcountry recreational users submit depth measurements, typically taken with an avalanche probe, using a  
652 smartphone in the field. The measurements are then converted to SWE estimates which are assimilated into  
653 snowpack models. These depth measurements are 'any time, any place' in contrast to repeated measurements from  
654 the same location, like snow pillows or snow courses. Most avalanche probes have cm-scale graduated markings, so  
655 measurement precision is not a major issue. A larger problem is the considerable variability in snowpack depth that  
656 can exist over short (meter scale) distances. The variability of the Chugach avalanche probe measurements was  
657 assessed by taking the standard deviation of 8  $h$  measurements per site. The average of this standard deviation over  
658 the sites was 22 cm and the average coefficient of variation (standard deviation normalized by the mean) over the  
659 sites was 15%. This variability is a function of the surface roughness of the underlying terrain, and also a function of  
660 wind redistribution of snow. Propagating this uncertainty through the regression equations yields a slightly higher  
661 (16%) uncertainty in the SWE estimates. CSO participants can do three things to ensure that their recorded depth  
662 measurements are as representative as possible. First, avoid measurements in areas of significant wind scour or

663 deposition. Second, avoid measurements in terrain likely to have significant surface roughness (rocks, fallen logs,  
664 etc.). Third, take several measurements and average them.

665

666 Expansion of CSO measurements in areas lacking SWE measurements can increase our understanding of the  
667 extreme spatial variability in snow distribution and the inherent uncertainties associated with modeling SWE in  
668 these regions. It could also prove useful for estimating watershed-scale SWE in regions like the northeastern USA,  
669 which is currently limited to five automated SCAN sites with historical SWE measurements for only the past two  
670 decades. Additionally, historical snow depth measurements are more widely available in the Global Historical  
671 Climatology Network (GHCN-Daily; Menne et al. 2012), with several records extending back to the late 1800s.  
672 While many of the GHCN stations are confined to lower elevations with shallower snow depths, the broader  
673 network of quality-controlled snow depth data paired with daily GHCN temperature and precipitation measurements  
674 could potentially be used to reconstruct SWE in the eastern US given additional model development and refinement.

## 675 **5 Conclusions**

676 We have developed a new, easy to use method for converting snow depth measurements to snow water equivalent  
677 estimates. The key difference between our approach and previous approaches is that we directly regress in  
678 climatological variables in a continuous fashion, rather than a discrete one. Given the abundance of freely available  
679 climatological norms, a depth measurement tagged with coordinates (latitude and longitude) and a time stamp is  
680 easily and immediately converted into SWE.

681

682 We developed this model with data from paired SWE-*h* measurements from the western United States and British  
683 Columbia. The model was tested against entirely independent data (primarily snow course; some snow pillow) from  
684 the northeastern United States and was found to perform well, albeit with larger biases and root-mean-squared-  
685 errors. The model was tested against other well-known regression equations and was found to perform better. [The](#)  
686 [model was also tested against a large dataset of independent snow course and aerial marker measurements from](#)  
687 [western North America. For this second independent test, the current model outperformed the other models](#)  
688 [considered.](#)

689

690 This model is not a replacement for more sophisticated snow models that evolve the snowpack based on high  
691 frequency (e.g., daily or sub-daily) weather data inputs. The intended purpose of this model is to constrain SWE  
692 estimates in circumstances where snow depth is known, but weather variables are not, a common issue in sparsely  
693 instrumented areas in North America.

## 694 **6 Acknowledgements**

695 Support for this project was provided by NASA (NNX17AG67A). R. Crumley acknowledges support from the  
696 CUAHSI Pathfinder Fellowship. E. Burakowski acknowledges support from NSF (MSB-ECA #1802726). We thank  
697 M. Sturm, A. Winstral and a third anonymous referee for their careful and thoughtful reviews of this manuscript.

698 **7 Data Access**

699 Numerous online datasets were used for this project and were obtained from the following locations:

- 700 1. NRCS Snow Telemetry: <https://www.wcc.nrcs.usda.gov/snow/SNOTEL-wedata.html>
- 701 2. NRCS Soil Climate Analysis Network: <https://www.wcc.nrcs.usda.gov/scan/>
- 702 3. British Columbia Automated Snow Weather Stations:  
703 [https://www2.gov.bc.ca/gov/content/environment/air-land-water/water/water-science-data/water-data-  
705 tools/snow-survey-data/automated-snow-weather-station-data](https://www2.gov.bc.ca/gov/content/environment/air-land-water/water/water-science-data/water-data-<br/>704 tools/snow-survey-data/automated-snow-weather-station-data)
- 705 4. Maine Cooperative Snow Survey: <https://mgs-maine.opendata.arcgis.com/datasets/maine-snow-survey-data>
- 706 5. New York Snow Survey: <http://www.nrec.cornell.edu/regional/snowsurvey/snowsurvey.html>
- 707 6. Sleepers River Research Watershed. Snow data not available online; request data from contact at:  
708 <https://nh.water.usgs.gov/project/sleepers/index.htm>
- 709 7. Hubbard Brook Experimental Forest: <https://hubbardbrook.org/d/hubbard-brook-data-catalog>
- 710 8. Climatological Data: <https://adaptwest.databasin.org/pages/adaptwest-climatena>
- 711 9. NRCS Snow Course / Aerial Marker Data: <https://wcc.sc.egov.usda.gov/reportGenerator/>

712  
713  
714 A Matlab function for calculating SWE based on the results is this paper [has been](https://github.com/communitysnowobs/snowdensity) made publicly available at Github  
715 (<https://github.com/communitysnowobs/snowdensity>)  
716

Formatted: Default Paragraph Font, Font: (Default) +Body (Calibri), 12 pt

Formatted: Default Paragraph Font, Font: (Default) +Body (Calibri), 12 pt

Formatted: Default Paragraph Font, Font: (Default) +Body (Calibri), 12 pt

Formatted: No underline, Font color: Auto

Formatted: Default Paragraph Font, Font: (Default) +Body (Calibri), 12 pt

Formatted: No underline, Font color: Auto

Formatted: Default Paragraph Font, Font: (Default) +Body (Calibri), 12 pt

Formatted: Default Paragraph Font, Font: (Default) +Body (Calibri), 12 pt

Formatted: No underline, Font color: Auto

Formatted: Default Paragraph Font, Font: 12 pt

Deleted: ¶

Formatted: Font: (Default) Times New Roman, No underline, Font color: Auto

Deleted: CONUS PRISM Data:  
<http://www.prism.oregonstate.edu/>

Formatted: Font: 10 pt

Formatted: Font: 10 pt

Deleted: ¶

Formatted: Font: 10 pt

Formatted: Default Paragraph Font, Font: 12 pt

Formatted: Font:

Formatted: No underline, Font color: Auto

Formatted: Font: (Default) Times New Roman

Formatted: Font: (Default) Times New Roman

Formatted: Font: 10 pt

Formatted: List Paragraph, Line spacing: single

Deleted: British Columbia PRISM Data:  
<http://climatebcdata.climatewna.com/>

Alaska PRISM Data: <https://irma.nps.gov/Portal/>

Deleted: has been

Deleted: (<https://github.com/communitysnowobs/snowdensity>).

Formatted: Default Paragraph Font, Font: 12 pt

727 **References**

728

729 Alford, D.: Density variations in alpine snow, *J. Glaciol.*, 6(46), 495-503,

730 <https://doi.org/10.3189/S0022143000019717>, 1967.

731

732 Avanzi, F., De Michele, C., and Ghezzi, A.: On the performances of empirical regressions for the estimation of bulk

733 snow density, *Geogr. Fis. Dinam. Quat.*, 38, 105-112, doi:10.4461/GFDQ.2015.38.10, 2015.

734

735 Beaumont, R.: Mt. Hood pressure pillow snow gage, *J. Appl. Meteorol.*, 4, 626-631, [https://doi.org/10.1175/1520-](https://doi.org/10.1175/1520-0450(1965)004<0626:MHPPSG>2.0.CO;2)

736 [0450\(1965\)004<0626:MHPPSG>2.0.CO;2](https://doi.org/10.1175/1520-0450(1965)004<0626:MHPPSG>2.0.CO;2), 1965.

737

738 Beaumont, R., and Work, R.: Snow sampling results from three samplers, *Hydrol. Sci. J.*, 8(4), 74-78,

739 <https://doi.org/10.1080/02626666309493359>, 1963.

740

741 Burakowski, E.A., Ollinger, S., Lepine, L., Schaaf, C.B., Wang, Z., Dibb, J.E., Hollinger, D.Y., Kim, J.-H., Erb, A.,

742 and Martin, M.E.: Spatial scaling of reflectance and surface albedo over a mixed-use, temperate forest landscape

743 during snow-covered periods, *Remote Sens. Environ.*, 158, 465-477, <https://doi.org/10.1016/j.rse.2014.11.023>,

744 2015.

745

746 Burakowski, E.A., Wake, C.P., Stampone, M., and Dibb, J.: Putting the Capital 'A' in CoCoRAHS: An

747 Experimental Program to Measure Albedo using the Community Collaborative Rain Hail and Snow (CoCoRaHS)

748 Network, *Hydrol. Process.*, 27(21), 3024-3034, <https://doi.org/10.1002/hyp.9825>, 2013.

749

750 Campbell, J., Ollinger, S., Flerchinger, G., Wicklein, H., Hayhoe, K., and Bailey, A.: Past and projected future

751 changes in snowpack and soil frost at the Hubbard Brook Experimental Forest, New Hampshire, USA, *Hydrol.*

752 *Process.*, 24, 2465-2480, <https://doi.org/10.1002/hyp.7666>, 2010.

753

754 Church, J.E.: Snow surveying: its principles and possibilities, *Geogr. Rev.*, 23(4), 529-563, DOI: 10.2307/209242,

755 1933.

756

757 Church, J.E., and Marr, J.C.: Further improvement of snow-survey apparatus, *Transactions of the American*

758 *Geophysical Union*, 18(2), 607-617, [10.1029/TR018i002p00607](https://doi.org/10.1029/TR018i002p00607), 1937.

759

760 Daly, C., Neilson, R., and Phillips, D.: A statistical-topographic model for mapping climatological precipitation over

761 mountainous terrain, *J. Appl. Meteorol.*, 33, 140-158, [https://doi.org/10.1175/1520-](https://doi.org/10.1175/1520-0450(1994)033<0140:ASTMFM>2.0.CO;2)

762 [0450\(1994\)033<0140:ASTMFM>2.0.CO;2](https://doi.org/10.1175/1520-0450(1994)033<0140:ASTMFM>2.0.CO;2), 1994.

763

Formatted: Default Paragraph Font, Font: 12 pt

Deleted: ¶

Deeb, E., Marshall, H.-P., Forster, R., Jones, C., Hiemstra, C., and Siqueira, P.: Supporting NASA SnowEx remote sensing strategies and requirements for L-band interferometric snow depth and snow water equivalent estimation, *Proceedings of the 2017 IEEE International Geoscience and Remote Sensing Symposium*, Fort Worth, TX, 1395-1396, DOI: 10.1109/IGARSS.2017.8127224, 2017.¶

773 Dixon, D., and Boon, S.: Comparison of the SnowHydro sampler with existing snow tube designs, *Hydrol. Process.*,  
774 26(17), 2555-2562, <https://doi.org/10.1002/hyp.9317>, 2012.

775

776 Dressler, K., Fassnacht, S., and Bales, R.: A comparison of snow telemetry and snow course measurements in the  
777 Colorado River basin, *J. Hydrometeorol.*, 7, 705-712, <https://doi.org/10.1175/JHM506.1>, 2006.

778

779 Goodison, B.: Accuracy of snow samplers for measuring shallow snowpacks: An update, *Proceedings of the 35<sup>th</sup>*  
780 *Annual Eastern Snow Conference*, Hanover, NH, 36-49, 1978.

781

782 Goodison, B., Ferguson, H., and McKay, G.: Measurement and data analysis. *The Handbook of Snow: Principles,*  
783 *Processes, Management, and Use*, D. Gray and D. Male, Eds., Pergamon Press, 191-274, 1981.

784

785 Goodison, B., Wilson, B., Wu., K., and Metcalfé, J.: An inexpensive remote snow-depth gauge: An assessment,  
786 *Proceedings of the 52<sup>nd</sup> Annual Western Snow Conference*, Sun Valley, ID, 188-191, 1984.

787

788 Goodison, B., Glynn, J., Harvey, K., and Slater, J.: Snow Surveying in Canada: A Perspective, *Can. Water Resour.*  
789 *J.*, 12(2), 27-42, <https://doi.org/10.4296/cwrj1202027>, 1987.

790

791 Gnanadesikan, R., and Kettenring, J.: Robust estimates, residuals, and outlier detection with multiresponse data,  
792 *Biometrics*, 28, 81-124, DOI: 10.2307/2528963, 1972.

793

794 Hill, D.F., Wolken, G. J., Wikstrom Jones, K., Crumley, R., and Arendt, A.: Crowdsourcing snow depth data with  
795 citizen scientists, *Eos*, 99, <https://doi.org/10.1029/2018EO108991>, 2018.

796

797 Johnson, J., and Marks, D.: The detection and correction of snow water equivalent pressure sensor errors, *Hydrol.*  
798 *Proc.*, <https://doi.org/10.1002/hyp.5795>, 2004.

799

800 Johnson, J., Gelvin, A., Duvoy, P., Schaefer G., Poole, G., and Horton, G.: Performance characteristics of a new  
801 electronic snow water equivalent sensor in different climates, *Hydrol. Proc.*, DOI: 10.1002/hyp.10211, 2015.


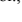
802


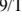
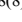
803 Jonas, T., Marty, C., and Magnusson, M.: Estimating the snow water equivalent from snow depth measurements, *J.*  
804 *Hydrol.*, 378, 161-167, <https://doi.org/10.1016/j.jhydrol.2009.09.021>, 2009.

805

806 Leys, C., Klein, O., Dominicy, Y., and Ley, C.: Detecting multivariate outliers: use a robust variant of the  
807 Mahalanobis distance, *J. Exp. Soc. Psychol.*, 74, 150-156, <https://doi.org/10.1016/j.jesp.2017.09.011>, 2018.

808



**Deleted:**   
Fick, S., and Hijmans, R.: WorldClim2: new 1-km spatial resolution climate surfaces for global land areas, *Int. J. Climatol.*, 37, 4302-4315, <https://doi.org/10.1002/joc.5086>, 2017. 

**Deleted:**   
Kang, D.H., and Barros, A.P.: Full-system testing in laboratory conditions of an L-band snow sensor system for in situ monitoring of snow-water content, *IEEE Trans. Geosci. Remote Sens.*, 49(3), 908-919, [10.1109/TGRS.2010.2072786](https://doi.org/10.1109/TGRS.2010.2072786), 2011.   
Leinss, S., Wiesmann, A., Lemmetyinen, J., and Hajnsek, I.: Snow water equivalent measured by differential interferometry, *IEEE J. Sel. Top. Appl. Earth Obs. Remote Sens.*, 8(8), 3773-3790, [10.1109/JSTARS.2015.2432031](https://doi.org/10.1109/JSTARS.2015.2432031), 2015. 

826 Liang, X., Lettermaier, D., Wood, E., and Burges, S.: A simple hydrologically based model of land surface water  
827 and energy fluxes for general circulation models, *J. Geophys. Res. Atmos.*, 99(D7), 14,415-14,428,  
828 <https://doi.org/10.1029/94JD00483>, 1994.  
829  
830 Liston, G., and Elder, K.: A distributed snow evolution modeling system (SnowModel), *J. Hydrometeorol.*, 7, 1259-  
831 1276, <https://doi.org/10.1175/JHM548.1>, 2006.  
832  
833 Lundberg, A., Richardson-Naslund, C., and Andersson, C.: Snow density variations: consequences for ground  
834 penetrating radar, *Hydrol. Process.*, 20, 1483-1495, <https://doi.org/10.1002/hyp.5944>, 2006.  
835  
836 Maine Geological Survey: Maine Cooperative Snow Survey Dataset,  
837 [https://www.maine.gov/dacf/mgs/hazards/snow\\_survey/](https://www.maine.gov/dacf/mgs/hazards/snow_survey/), 2018.  
838  
839 McKay, G., and Findlay, B., 1971: Variation of snow resources with climate and vegetation in Canada, *Proceedings*  
840 *of the 39<sup>th</sup> Western Snow Conference*, Billings, MT, 17-26, 1971.  
841  
842 De Maesschalck, R., Jouan-Rimbaud, D., and Massart, D.: The Mahalanobis distance, *Chemometr. Intell. Lab. Syst.*,  
843 50(1), 1-18, [https://doi.org/10.1016/S0169-7439\(99\)00047-7](https://doi.org/10.1016/S0169-7439(99)00047-7), 2000.  
844  
845 McCreight, J., and Small, E.: Modeling bulk density and snow water equivalent using daily snow depth  
846 observations, *The Cryosphere*, 8, 521-536, <https://doi.org/10.5194/tc-8-521-2014>, 2014.  
847  
848 Meloyund, V., Leira, B., Hoiseth, K., and Liso, K.: Predicting snow density using meteorological data, *Meteorol.*  
849 *Appl.*, 14, 413-423, <https://doi.org/10.1002/met.40>, 2007.  
850  
851 Menne, M.J., I. Durre, R.S. Vose, B.E. Gleason, and Houston, T.G.: An overview  
852 of the Global Historical Climatology Network-Daily Database, *J. Atmos. Ocean. Technol.*, 29, 97-910,  
853 [doi:10.1175/JTECH-D-11-00103.1](https://doi.org/10.1175/JTECH-D-11-00103.1), 2012.  
854  
855 Molotch, N.P., and Bales, R.C.: SNOTEL representativeness in the Rio Grande headwaters on the basis of  
856 physiographics and remotely sensed snow cover persistence, *Hydrol. Process.*, 20(4), 723-739,  
857 <https://doi.org/10.1002/hyp.6128>, 2006.  
858  
859 Mote, P., Li, S., Lettermaier, D., Xiao, M., and Engel, R.: Dramatic declines in snowpack in the western US,” *npj*  
860 *Clim. Atmos. Sci.*, 1(2), 1-6, [doi:10.1038/s41612-018-0012-1](https://doi.org/10.1038/s41612-018-0012-1), 2018.  
861

Formatted: No underline, Font color: Auto

862 Mizukami, N., and Perica, S.: Spatiotemporal characteristics of snowpack density in the mountainous regions of the  
863 western United States, *J. Hydrometeorol.*, 9, 1416-1426, <https://doi.org/10.1175/2008JHM981.1>, 2008.  
864  
865 New York Snow Survey, NOAA, Northeast Regional Climate Center at Cornell University, 2018.  
866  
867 Pagano, T., Garen, D., Perkins, T., and Pasteris, P.: Daily updating of operational statistical seasonal water supply  
868 forecasts for the western U.S., *J. Am. Water Resour. Assoc.*, 45(3), 767-778, <https://doi.org/10.1111/j.1752->  
869 [1688.2009.00321.x](https://doi.org/10.1111/j.1752-1688.2009.00321.x), 2009.  
870  
871 Painter, T., Berisford, D., Boardman, J., Bormann, K., Deems, J., Gehrke, F., Hedrick, A., Joyce, M., Laidlaw, R.,  
872 Marks, D., Mattmann, C., McGurk, B., Ramirez, P., Richardson, M., Skiles, S., Seidel, F., and Winstral, A.: The  
873 Airborne Snow Observatory: fusion of scanning lidar, imaging spectrometer, and physically-based modeling for  
874 mapping snow water equivalent and snow albedo, *Remote Sens. Environ.*, 184, 139-152,  
875 [doi:10.1016/j.rse.2016.06.018](https://doi.org/10.1016/j.rse.2016.06.018), 2016.  
876  
877 Pistocchi, A.: Simple estimation of snow density in an Alpine region, *J. Hydrol. Reg. Stud.*, 6, 82-89,  
878 <http://dx.doi.org/10.1016/j.ejrh.2016.03.004>, 2016.  
879  
880 Rousseeuw, P.: Least Median of Squares Regression, *J. Am. Stat. Assoc.*, 79, 871-880, DOI:  
881 [10.1080/01621459.1984.10477105](https://doi.org/10.1080/01621459.1984.10477105), 1984.  
882  
883 Ryan, W., Doesken, N., and Fassnacht, S.: Evaluation of Ultrasonic Snow Depth Sensors for U.S. Snow  
884 Measurements, *J. Atmos. Ocean. Technol.*, 25, 667-684, <https://doi.org/10.1175/2007JTECHA947.1>, 2008.  
885  
886 Schaefer, G., Cosh, M., and Jackson, T.: The USDA Natural Resources Conservation Service Soil Climate Analysis  
887 Network (SCAN), *J. Atmos. Ocean. Technol.*, 24, 2073-2077, <https://doi.org/10.1175/2007JTECHA930.1>, 2007.  
888  
889 Serreze, M., Clark, M., Armstrong, R., McGinnis, D., and Pulwarty, R.: Characteristics of the western United States  
890 snowpack from snowpack telemetry (SNOTEL) data, *Water Resour. Res.*, 35(7), 2145-2160,  
891 <https://doi.org/10.1029/1999WR900090>, 1999.  
892  
893 Shanley, J., and Chalmers, A.: The effect of frozen soil on snowmelt runoff at Sleepers River, Vermont, *Hydrol.*  
894 *Process.*, 13(12-13), 1843-1857, [https://doi.org/10.1002/\(SICI\)1099-1085\(199909\)13:12/13<1843::AID-](https://doi.org/10.1002/(SICI)1099-1085(199909)13:12/13<1843::AID-)  
895 [HYP879>3.0.CO;2-G](https://doi.org/10.1002/(SICI)1099-1085(199909)13:12/13<1843::AID-HYP879>3.0.CO;2-G), 1999.  
896  
897 Sturm, M., Holmgren, J., and Liston, G.: A seasonal snow cover classification system for local to global  
898 applications, *J. Clim.*, 8, 1261-1283, [https://doi.org/10.1175/1520-0442\(1995\)008<1261:ASSCCS>2.0.CO;2](https://doi.org/10.1175/1520-0442(1995)008<1261:ASSCCS>2.0.CO;2), 1995.

**Deleted:**  Sokol, J., Pultz, T., and Walker, A.: Passive and active airborne microwave remote sensing of snow cover," *Int. J. Remote. Sens.*, 24, 5327-5344, <https://doi.org/10.1080/0143116031000115076>, 2003. 



904

905 Sturm, M., Taras, B., Liston, G.E., Derksen, C., Jonas, T., and Lea, J.: Estimating snow water equivalent using snow  
 906 depth data and climate classes, *J. Hydrometeorol.*, 11, 1380-1394, <https://doi.org/10.1175/2010JHM1202.1>, 2010.

907

908 U.S. Army Corps of Engineers: Snow hydrology: Summary report of the snow investigations of the North Pacific  
 909 Division, 437pp., 1956.

910

911 [U.S. Department of Agriculture: The History of Snow Survey and Water Supply Forecasting. Interviews With U.S.](#)  
 912 [Department of Agriculture Pioneers, D. Helms, S. Phillips and P. Reich \(eds.\), Natural Resources Conservation](#)  
 913 [Service, 2008.](#)

914

915 [U.S. Department of Agriculture: Snow Survey and Water Supply Forecasting. National Engineering Handbook Part](#)  
 916 [622, Water and Climate Center, Natural Resources Conservation Service, 2011.](#)

917 ▼

918 Wang, T., Hamann, A., Spittlehouse, D.L., and Murdock, T.: ClimateWNA - High-Resolution Spatial Climate Data  
 919 for Western North America, *J. Appl. Meteorol. Climatol.*, 51, 16-29, <https://doi.org/10.1175/JAMC-D-11-043.1>,  
 920 2012.

921

922 [Wang, T., Hamann, A., Spittlehouse, D.L., and Carroll, C: Locally downscaled and spatially customizable climate](#)  
 923 [data for historical and future periods for North America, PLoS One, 11, DOI:10.1371/journal.pone.0156720.](#)

924 ▼

925 Wigmosta, M.S., Vail, L., and Lettenmaier, D.: A distributed hydrology-vegetation model for complex  
 926 terrain, *Water Resour. Res.*, 30, 1665-1679, <https://doi.org/10.1029/94WR00436>, 1994

**Deleted:** ¶  
 Vuyovich, C., Jacobs, J., and Daly, S.: Comparison of passive microwave and modeled estimates of total watershed SWE in the continental United States, *Water Resour. Res.*, 50(11), 9088-9012, <https://doi.org/10.1002/2013WR014734>, 2014.¶

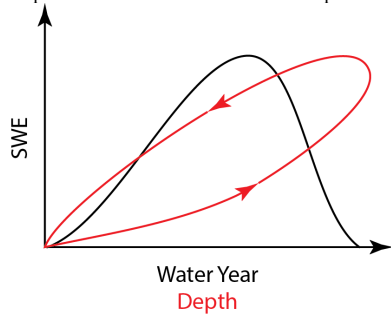
**Formatted:** Space After: 5 pt

**Deleted:** ¶

934  
935  
936

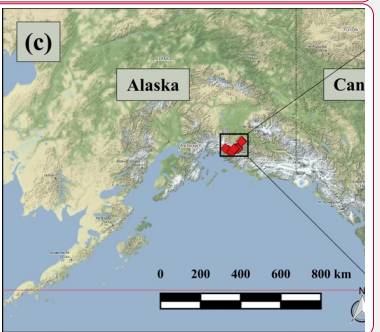
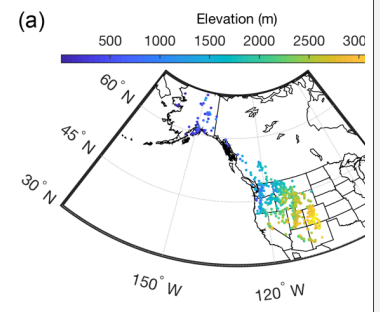
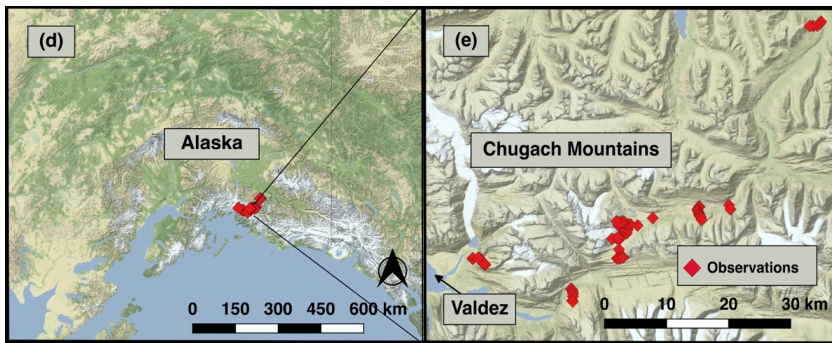
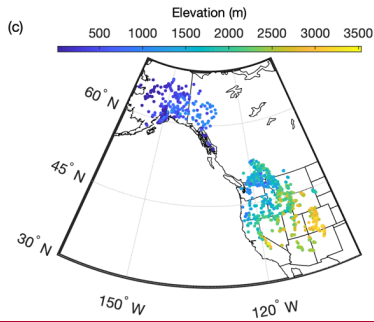
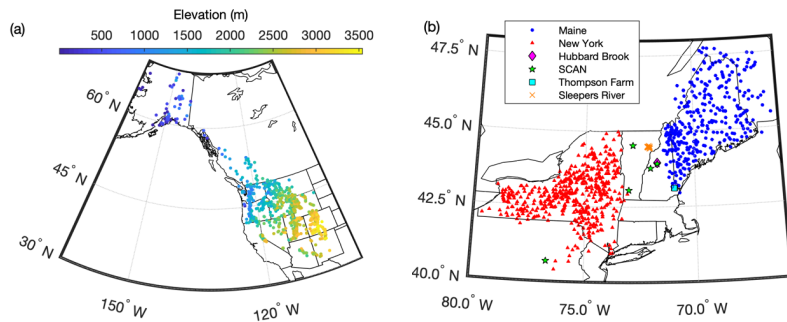
Figure 1: Conceptual sketch of the evolution of snow water equivalent (SWE) over the course of a water year (black line). Also shown is the evolution of SWE with snowpack depth over a water year (red line). Note the hysteresis loop due to the densification of the snowpack.

Formatted: Line spacing: single



937

938 Figure 2: Distribution of measurement locations used in this study. (a) Western USA and Canada snow pillow  
 939 locations, with colors indicating station elevation in meters. (b) Northeast USA snow pillow and snow course  
 940 locations, with stations colored according to data source. (c) Western North America snow course and aerial marker  
 941 locations, with colors indicating station elevation in meters. (d, e) Measurement sites in the Chugach Mountains,  
 942 southcentral Alaska.  
 943



Formatted: Line spacing: single  
 Deleted: station  
 Deleted: c  
 Deleted: d

Formatted: Font: 10 pt

Deleted:

Formatted: Font: 10 pt

Formatted: Centered

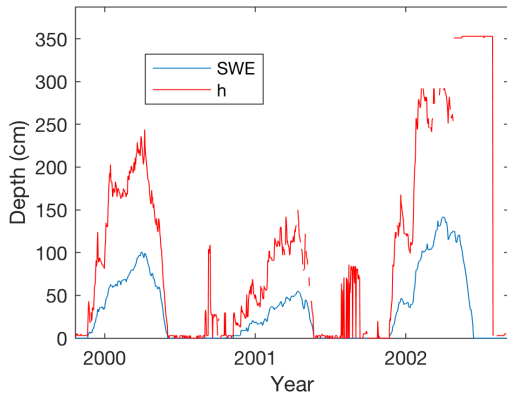
Deleted:

Deleted:

955  
956

Figure 3: Sample time series of SWE and  $h$  from the Rex River (WA) SNOTEL station. Observations of  $h$  at times when SWE is zero are likely spurious.

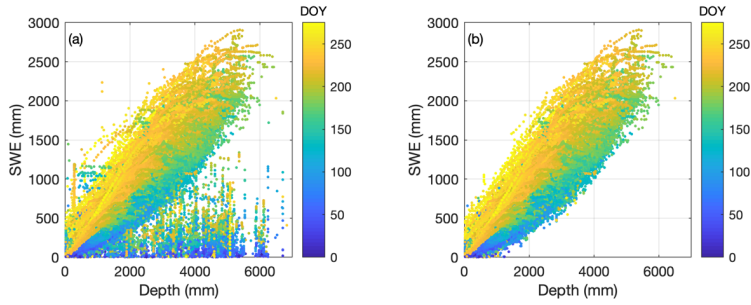
Formatted: Line spacing: single



957

958  
959  
960  
961

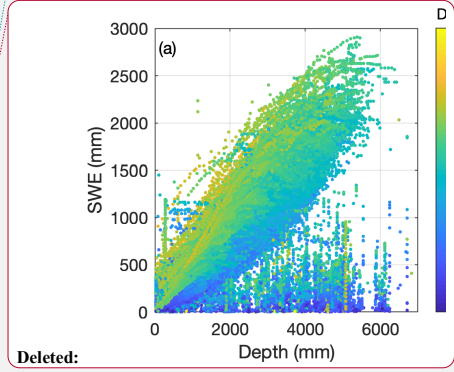
Figure 4: Scatter plot of SWE vs.  $h$  for the complete SNOTEL dataset before (a) and after (b) removing data points, following the method described in Section 2.1.1.5. Symbols are colored by 'day of water year' (DOY; October 1 is the origin).



962

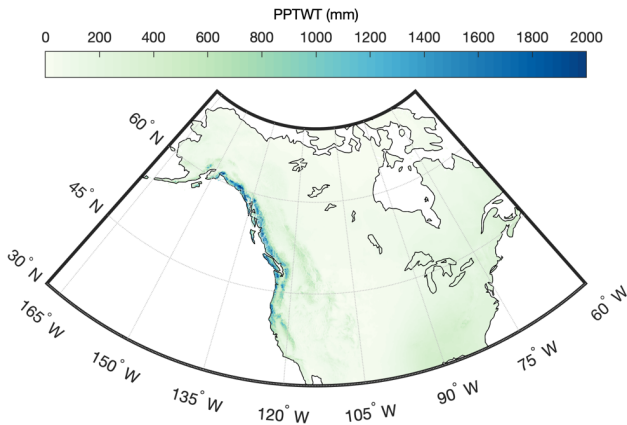
Formatted: Line spacing: single

Formatted: Font: 10 pt

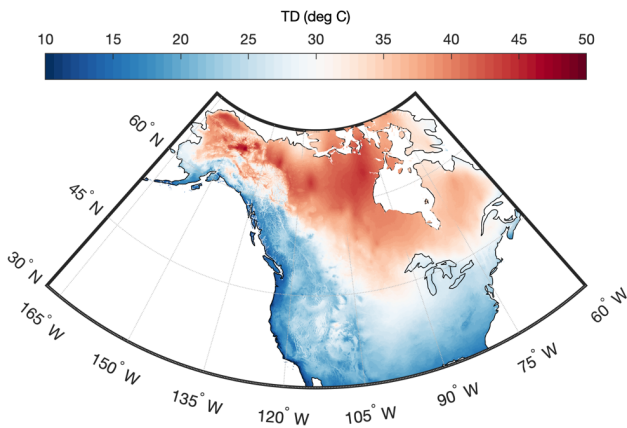


964  
965  
966

Figure 5: Gridded maps of winter (December, January, February) precipitation (PPTWT) and temperature difference (TD) between mean of warmest month and mean of coldest month for North America. Maps are for the 1981-2010 climatological period.



967



968  
969  
970  
971

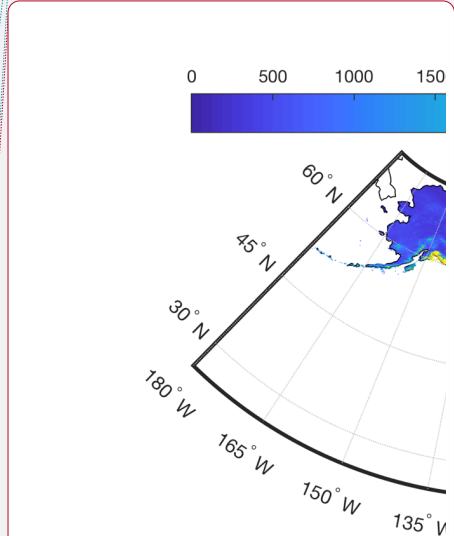
Formatted: Line spacing: single

Deleted: mean annual precipitation...inter (December, January, February) (MAP)...recipitation (PPTWT) and temperature difference (TD) between mean of warmest month and mean of coldest month and mean February temperature ( $T_{r,mean}$ ) for the study regions ... [2]

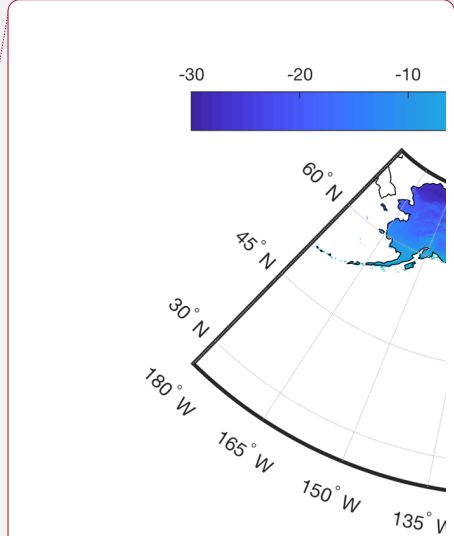
Deleted: Climate normals are from the PRISM data set (1981-2010 for CONUS and British Columbia; 1971-2000 for Alaska).

Formatted: Font:

Formatted: Font:



Deleted:



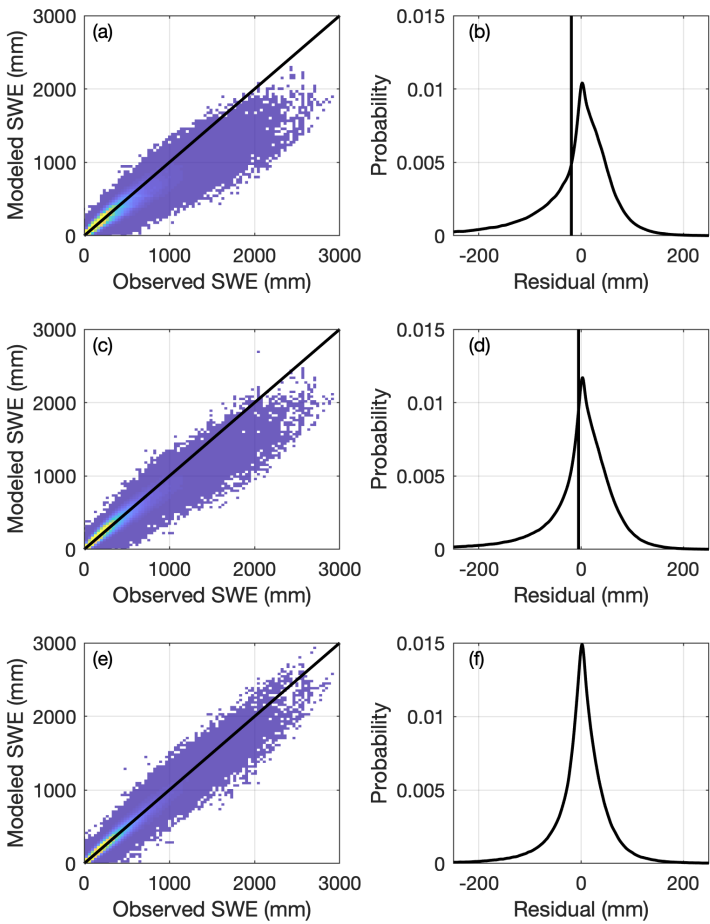
Deleted:

Formatted: Font:

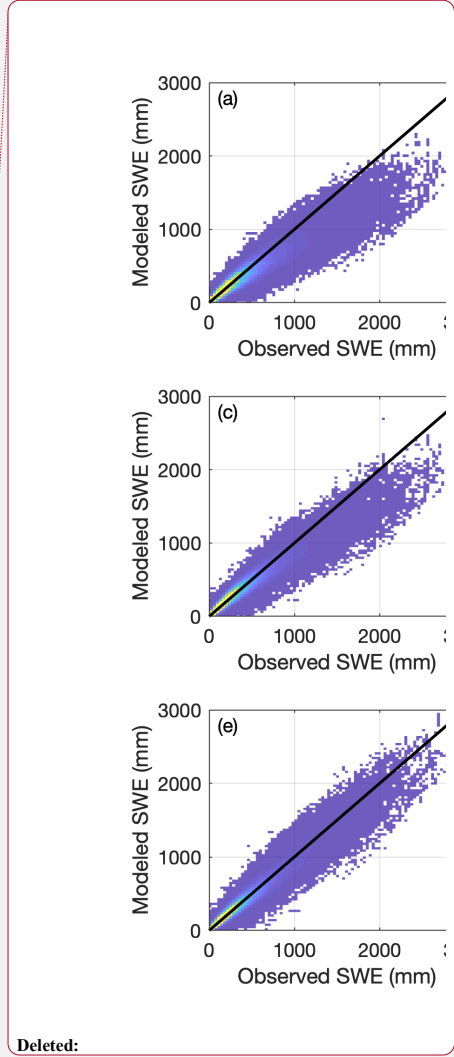
991  
992  
993  
994  
995

Figure 6: Two-dimensional histograms (heat maps; left column) of modeled vs. observed SWE and probability density functions (right column) of the residuals for three simple models applied to the CONUS, AK, and BC snow pillow data. Warmer colors in the heat maps indicate greater density. The vertical lines in the right column indicate the location of the mean residual, or bias. Top row (a-b): One-equation model (Section 2.2.1). Middle row (c-d): Two-equation model (Section 2.2.2). Bottom row (e-f): Multi-variable two-equation model (Section 2.2.3).

Commented [Office2]: FIX (F)  
Formatted: Line spacing: single

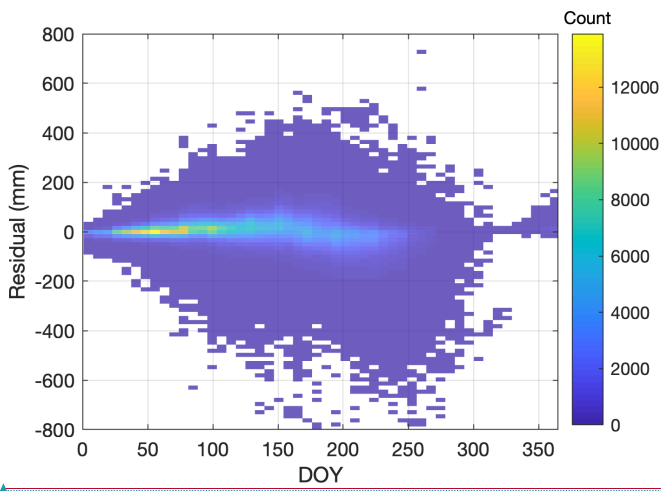


996  
997



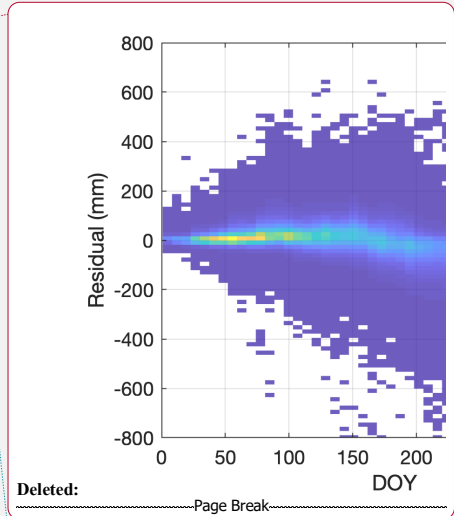
999  
1000

Figure 7: Heat map of SWE residuals as a function of *DOY*.



1001  
1002  
1003

Formatted: Font: 10 pt



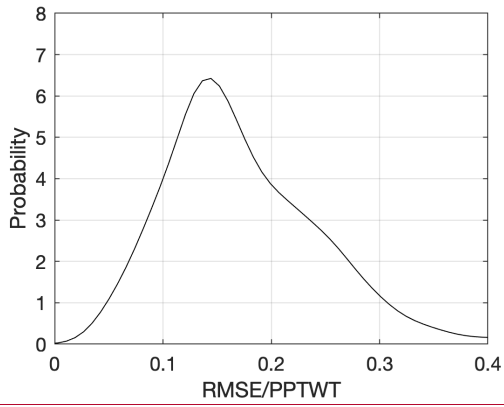
Deleted: Page Break

Formatted: Font: 10 pt



1006  
1007

Figure 8: Probability density function of snow pillow station root-mean-square error (RMSE) normalized by station winter precipitation (*PPTWT*).

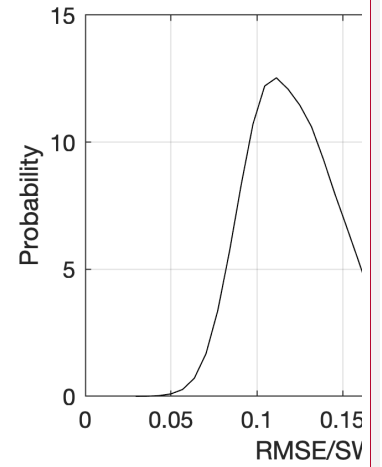


1008

Formatted: Line spacing: single

Deleted: mean annual maximum SWE

Formatted: Font: Italic

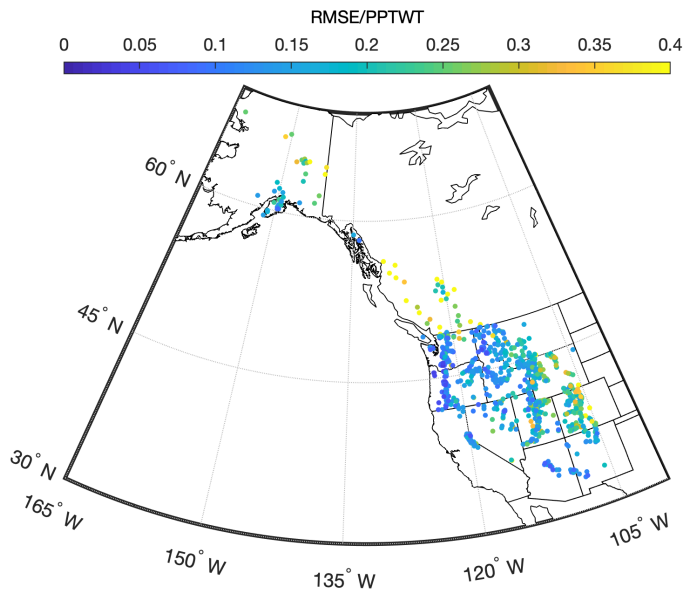


Deleted:

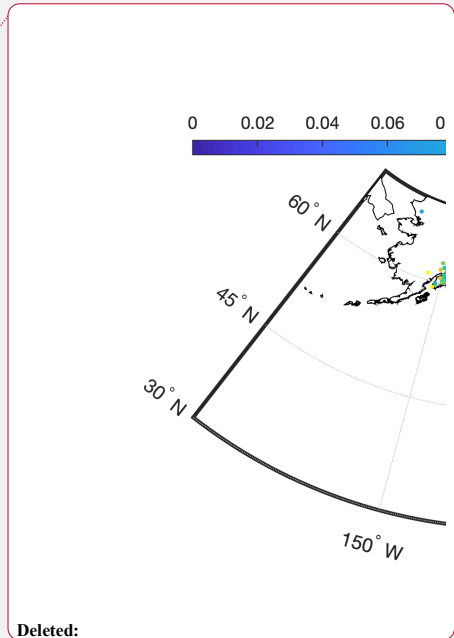
1011  
1012

Figure 9: Spatial distribution of snow pillow station root-mean-square error (RMSE) normalized by station ~~winter~~ precipitation (PPTWT).

Formatted: Line spacing: single  
Deleted: mean annual maximum SWE



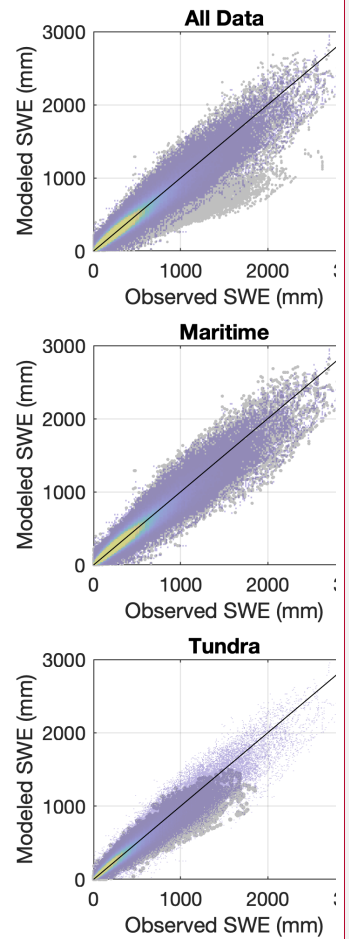
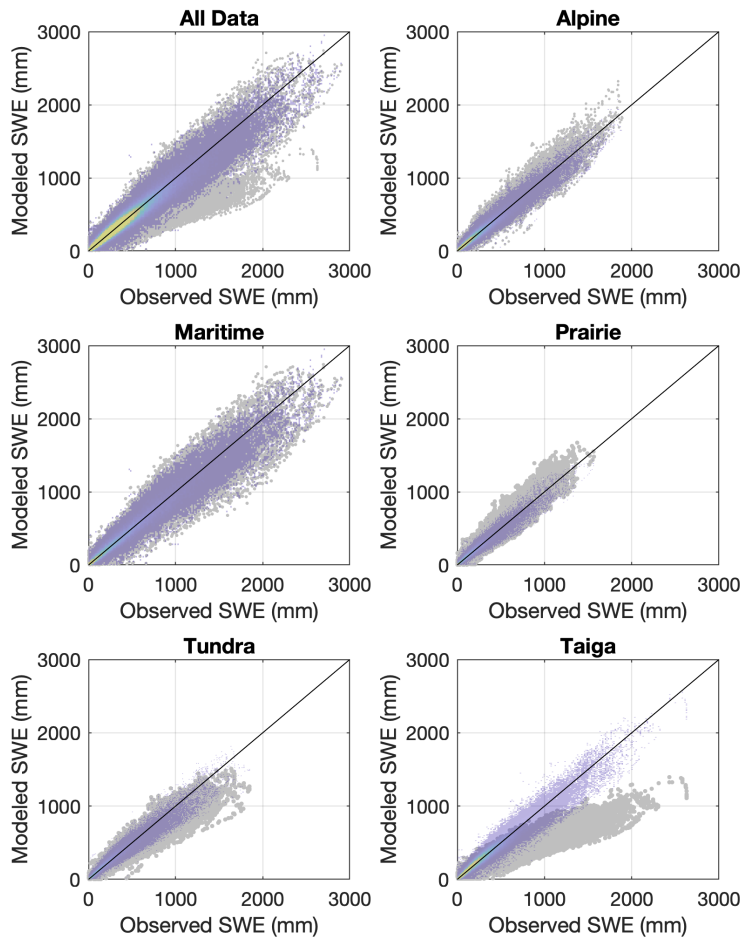
1013  
1014



1017  
1018  
1019  
1020  
1021  
1022

Figure 10: Comparison of the multi-variable, two-equation model of the **current** study with the model of Sturm et al. (2010). The subpanels show modeled SWE vs. observed SWE for all of the data binned together, as well as for the data broken out by the snow classes identified by Sturm et al. (1995). The gray symbols show the Sturm result and the transparent heat maps (warmer colors indicate greater density) show the current result. The models are being applied to the validation data set (50% of the aggregated snow pillow data for CONUS, AK, and BC).

Formatted: Line spacing: single  
Deleted: present



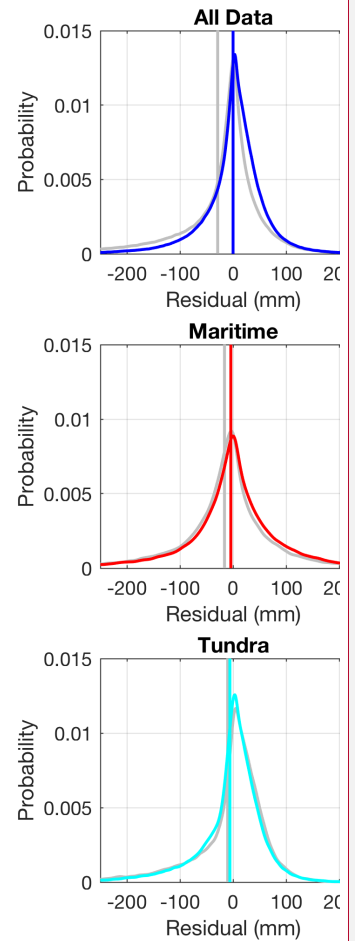
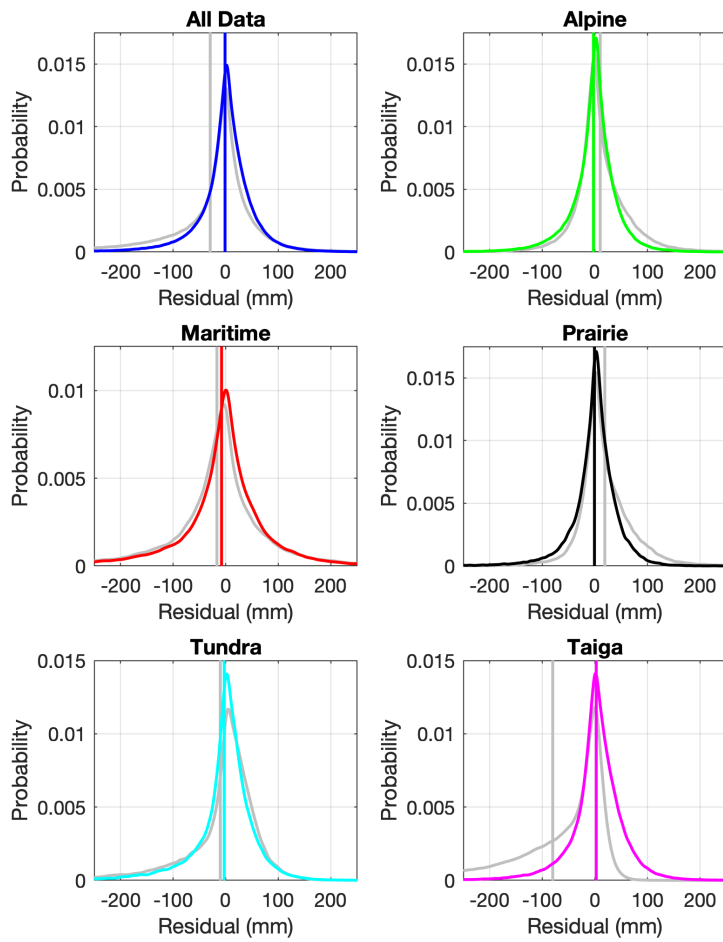
Deleted:  
Formatted: Font: 10 pt

1023

1026  
1027  
1028  
1029  
1030  
1031  
1032

Figure 11: Comparison of the multi-variable, two-equation model of the **current** study with the model of Sturm et al. (2010). The subpanels show probability density functions of the residuals of the model fits for all of the data binned together, as well as for the data broken out by the snow classes identified by Sturm et al. (1995). The gray lines show the Sturm result and the colored lines show the current result. The vertical lines show the mean error, or the model bias, for both the Sturm and the current result. The models are being applied to the validation data set (50% of the aggregated snow pillow data for CONUS, AK, and BC).

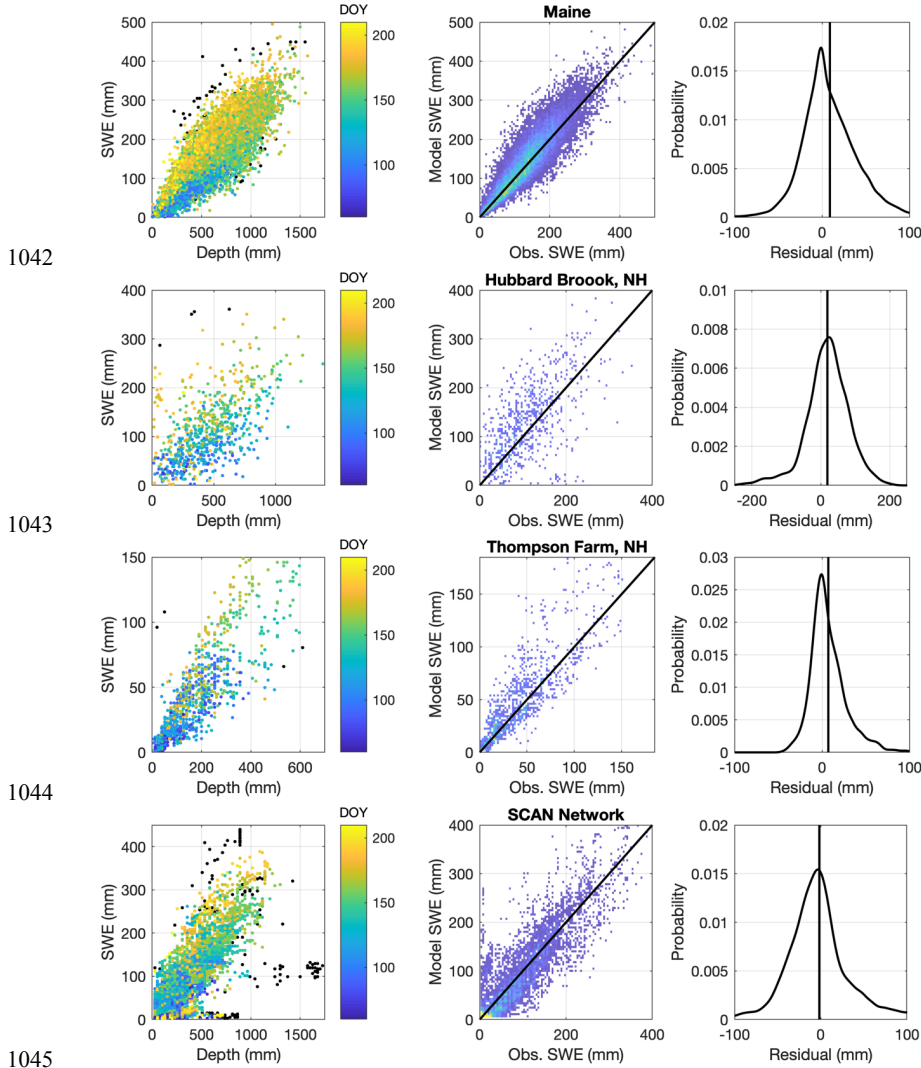
Formatted: Line spacing: single  
Deleted: present



Deleted:  
Formatted: Font: 10 pt

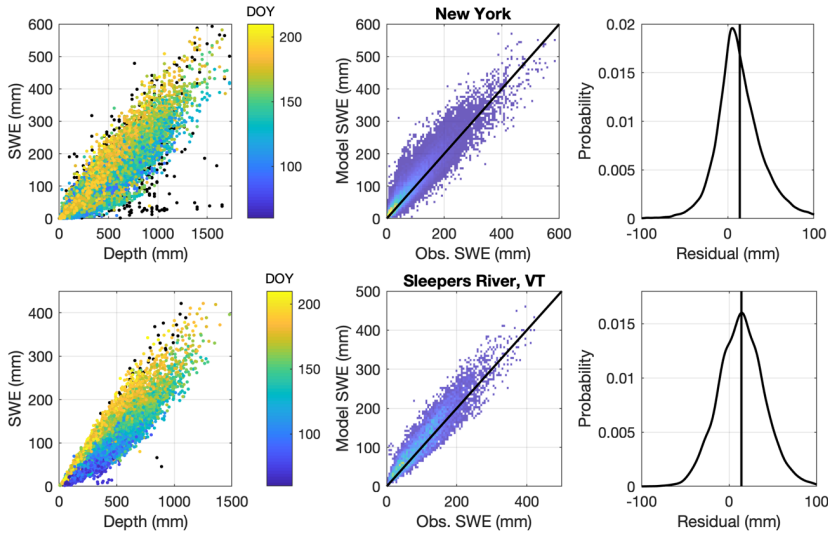
1033

1036 Figure 12: Results from application of the multi-variable, two-equation model to numerous east coast datasets. The  
 1037 left column shows the SWE-*h* data for each dataset. Note that the black symbols are points removed by the outlier  
 1038 detection procedure discussed in section 2.1.1.4. The remaining symbols are colored by *DOY*. The middle panel  
 1039 plots heat maps of the model estimates of SWE against the observations of SWE with the 1:1 line included. Warmer  
 1040 colors indicate higher densities. The right panel shows probability density functions of the model residuals, with the  
 1041 vertical line indicating the mean error, or bias. Individual rows correspond to individual data sets and are labeled.



Formatted: Line spacing: single

Formatted: Font: Italic

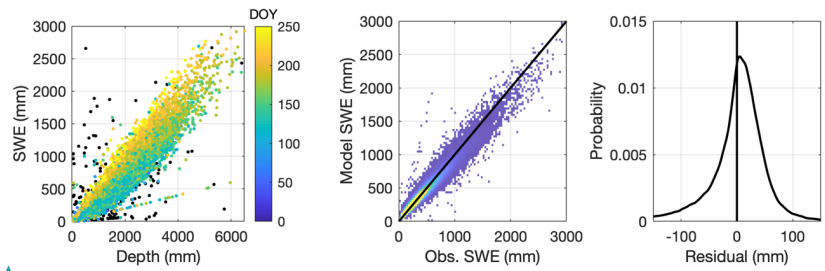


1046

1047  
1048  
1049

1050  
1051  
1052  
1053  
1054  
1055  
1056  
  
1057  
1058

Figure 13: Results from application of the multi-variable, two-equation model to the NRCS snow course / aerial marker dataset. The left column shows the SWE-*h* data for each dataset. Note that the black symbols are points removed by the outlier detection procedure discussed in section 2.1.1.5. The remaining symbols are colored by DOY. The middle panel plots heat maps of the model estimates of SWE against the observations of SWE with the 1:1 line included. Warmer colors indicate higher densities. The right panel shows probability the density function of the model residuals, with the vertical line indicating the mean error, or bias.



Formatted: Font: Italic

Formatted: Font: 10 pt

<b>Page 25: [1] Deleted</b>	<b>Microsoft Office User</b>	<b>5/28/19 11:05:00 AM</b>
-----------------------------	------------------------------	----------------------------



<b>Page 28: [2] Deleted</b>	<b>Microsoft Office User</b>	<b>5/21/19 1:48:00 PM</b>
-----------------------------	------------------------------	---------------------------



<b>Page 28: [2] Deleted</b>	<b>Microsoft Office User</b>	<b>5/21/19 1:48:00 PM</b>
-----------------------------	------------------------------	---------------------------

<b>Page 28: [2] Deleted</b>	<b>Microsoft Office User</b>	<b>5/21/19 1:48:00 PM</b>
-----------------------------	------------------------------	---------------------------

